Effects of Lubricant Viscosity and Surface Texturing on Ring-pack Performance in Internal Combustion Engines

by

Rosalind Takata

S.B., Mechanical Engineering
Massachusetts Institute of Technology, 2001

Submitted to the Department of Mechanical Engineering
in Partial Fulfillment of the Requirements of the Degree of
Master of Science in Mechanical Engineering

at the

Massachusetts Institute of Technology

June 2006

Signature of Author: _____
Department of Mechanical Engineering
May 12, 2006

Certified by: _____
Dr. Victor W. Wong
Lecturer, Department of Mechanical Engineering
Thesis Supervisor

Accepted by: _____
Lallit Anand
Chairman, Department Committee on Graduate Studies
Department of Mechanical Engineering

(This page was intentionally left blank)

Effects of Lubricant Viscosity and Surface Texturing on Ring-pack Performance in Internal Combustion Engines

by

Rosalind Takata

Submitted to the Department of Mechanical Engineering on May 12, 2006 in Partial Fulfillment of the Requirements for the Degree of Master of Science in Mechanical Engineering

Abstract

The piston ring-pack contributes approximately 25% of the mechanical losses in an internal combustion engine. Both lubricant viscosity and surface texturing were investigated in an effort to reduce this ring-pack friction and increase engine efficiency. While both optimizing viscosity and surface texturing are predicted to cause a reduction in ring/liner friction individually, a combined approach may cause an even greater friction reduction while mitigating unwanted side-effects such as oil consumption and wear.

Existing MIT models, with some modifications and supplementary programs to allow investigation of the parameters of interest, were used to conduct this research. A ring-pack model based on average flow-factor Reynolds analysis was used for both studies, with a modified form of this program, along with a supplementary deterministic model for surface analysis, used for the study of surface texturing. Although these advanced models are applicable in a wide range of cases, the surface textures studied in this research are very different than a typical cylinder liner surface, and can be represented only approximately by the averaged Reynolds analysis upon which the ring simulation is based. For this reason, the analysis of surface features has focused on a parametric study, whose goal is to analyze trends relating ring/liner friction to surface parameters, and to make a general evaluation of the potential of surface texturing to reduce ring-pack losses.

Study of lubricant viscosity effects throughout the engine cycle indicated that conditions in the mid-stroke region have the main influence (compared to the end-strokes) on friction power losses, and that reducing viscosity here could lead to a reduction in ring-pack FMEP of ~7%. Changes in cylinder liner surface texturing, also, can lead to significant friction reductions. Patterns of both grooves and round dimples were shown to reduce ring/liner friction by increasing hydrodynamic pressure in the lubricant, thus increasing oil film thickness and reducing both asperity contact and hydrodynamic friction. Also, because the effect of reducing viscosity is to decrease oil film thickness, and that of the surface texturing considered is to increase it, these two parameters can be optimized together, and balanced so that oil film thickness remains constant. Then, negative side-effects such as wear (due to decrease in film thickness) and oil consumption (resulting from an increase in film thickness) can be negated, even as friction is reduced even further than is possible using viscosity or surface effects alone.

Thesis Supervisor:
Dr. Victor W. Wong (Lecturer, Department of Mechanical Engineering)

(This page was intentionally left blank)

Acknowledgements

I would like to thank everyone, both at MIT and elsewhere, who helped to make my time here both enjoyable and constructive. First, I would like to recognize my advisor, Dr. Victor Wong. I am grateful to him for allowing me a good deal of independence in my work, encouraging me to become more of a critical thinker and to trust my own instincts. Dr. Wong has also shown me the value of good leadership and management, in addition to academic considerations.

There are many other individuals from the Sloan Automotive Lab who also deserve acknowledgement. I would like to thank my office-mates and office-neighbors Alex Sappok, Luke Moughon, Sean McGrogan, Fiona McClure and others, for making my time in the lab a pleasant experience, and, in particular, I would like to thank Sean for entertaining conversations, and for asking enough research questions to make me feel useful. I would also like to thank Jeff Jocsak, Yong Li, Dr. Tian Tian and Dr. Liang Liu for their advice and the use of many of the products of their own hard work. Thanks should also go to Nancy Cook and Janet Maslow, who manage to stay helpful and friendly despite all of the demands placed on them by the lab.

I would also like to thank several people outside of MIT who worked in cooperation with myself and others on this ongoing project. Rick Donahue and Ed Reinbold at Waukesha Engine Dresser, Inc., contributed valuable advice from the point of view of engine designers and manufacturers, as well as supplying hardware and expertise for testing of low-friction designs. Several people at the Engines and Energy Conversion Laboratory at Colorado State University also deserve thanks for carrying out the experimental testing, including Rudy Stanglmaier, Ted Bestor, Kirk Evans and Kris Quillen. I would also like to thank the U.S. Department of Energy for their financial support of this program, with special thanks to Ron Fiskum and Raj Sekar.

Finally, I would like to thank my apartment-mate Eric Smith and my boyfriend, Bayard Wenzel, for doing their best to keep me from getting any work done, and my parents, for allowing me to make my own decisions and always encouraging me wherever those decisions lead.

(This page was intentionally left blank)

Table of Contents

List of Figures

(This page was intentionally left blank)

List of Tables

(This page was intentionally left blank)

1. Introduction

Since the invention of the four-stroke cycle in the mid-19th century, internal combustion engines have been evolving, becoming more specialized to be used in different applications, and increasing in their level of performance. In recent years, growing concern over pollutants and greenhouse gases has driven increasingly stringent emissions regulations, while a desire to reduce energy usage, and particularly dependence on fossil fuels, has led to an interest in increasing engine efficiency. Together, these drives towards increased performance and efficiency and decreased emissions have put a high demand on the engine components, particularly the piston rings, which are exposed to the high cylinder temperatures and pressures that exist in high-performance engines. In addition, increasing engine efficiency requires reductions in engine friction, of which a large component is contributed by the ring-pack.

This study focuses on the latter concern, as part of an ongoing study evaluating various strategies for reducing ring/liner friction. The current effort considers the effects of lubricant and the cylinder liner surface structure on ring-pack friction (previous studies have included ring design and geometry), and ways in which lubricant and surface parameters can be optimized to minimize mechanical losses. While the analyses presented here are based on a specific engine – the Waukesha VGF 18GL – it is believed that the results will be relevant for other engines as well, with potential for wide-ranging applicability towards increasing engine efficiency.

1.1 The need to reduce engine friction

For the last century, consumption of energy both in the United States and worldwide has been increasing rapidly, as shown in Figure 1-1. Growing populations as well as the emergence and increasing popularity of technologies such as automobiles and the wide use of electricity has driven this increase. Not only is energy usage increasing, but the source of the energy has become concentrated in a few natural resources: coal, oil and natural gas. This situation presents several issues: these non-renewable resources will eventually be eliminated as they are used up to create power (although the timetable for such an event is widely disputed); and their usage also creates carbon dioxide, which enters the atmosphere and leads to global warming – a change in the earth's atmosphere that may lead to disastrous effects.

While "alternative" energy sources are being investigated to mitigate these issues, it is also necessary to reduce energy usage, at least partially through increasing the efficiency of devices currently in use. Internal combustion engines are very widely used, not only in automobiles but also in power generation and other applications. Thus, an increase in efficiency of these devices could lead to a real change in energy usage and CO_2 emissions.

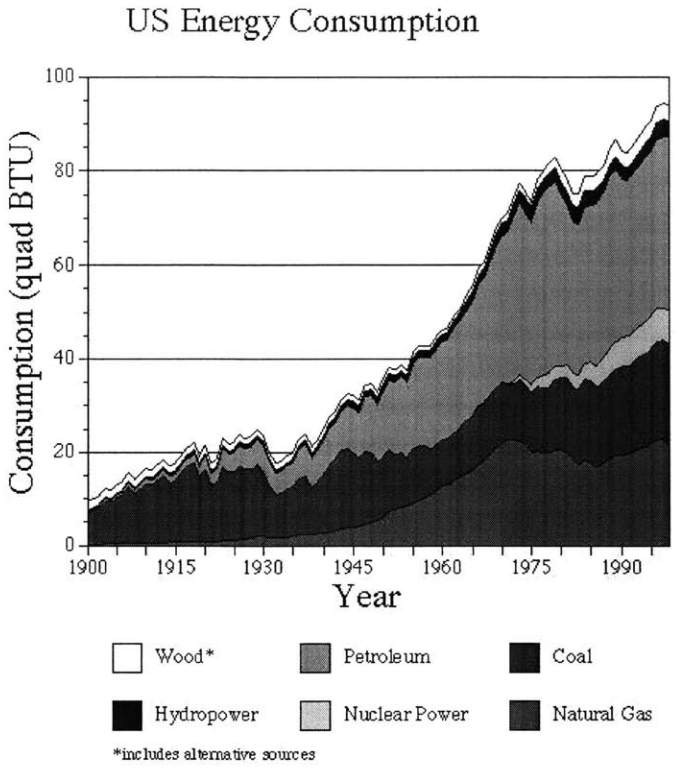

Figure 1-1: US energy consumption from 1900-2000, in quadrillions of BTU's. [1]

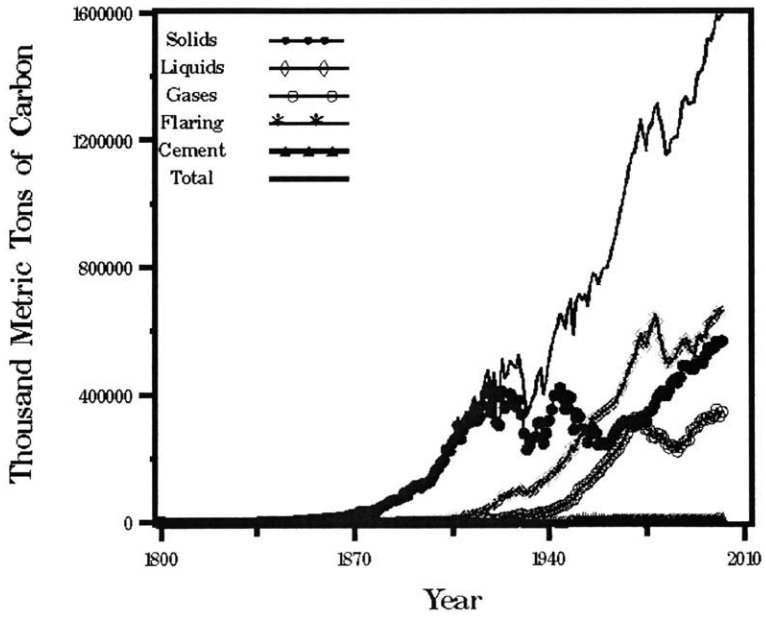

Figure 1-2: Carbon emissions grow along with energy consumption [2]

As Figure 1-1 shows, energy consumption in the U.S. has been increasing rapidly over the past century. This climb in energy usage corresponds closely with a climb in carbon dioxide

emissions, shown by a comparison of Figure 1-1 and Figure 1-2. While the correspondence between energy usage and CO_2 emissions is clear, it is argued that the increase in emissions of this "greenhouse gas" may not have a major effect on the environment. Figure 1-3 shows the global average temperature over the past 650,000 years, along with atmospheric concentrations of various gases, as measured with ice-core data. Levels of atmospheric gases are measured from samples in tiny gas bubbles in ice cores, while the temperature is estimated from the ratio of deuterium to hydrogen gas in the ice[3].

As the figure shows, there is a close correspondence between atmospheric levels of carbon dioxide and methane and the mean earth temperature. This evidence suggests that high levels of CO_2 in the atmosphere will correspond to a high mean temperature, and should be cause for concern, although the exact nature of the atmospheric and weather-related changes that will occur due to an overall temperature increase are not well understood. Additionally, CO_2 levels shown in this figure are notably lower than levels today – current greenhouse gas concentrations are higher than they have been in this measured history [3] – indicating that the situation today is unusual and deserves some attention.

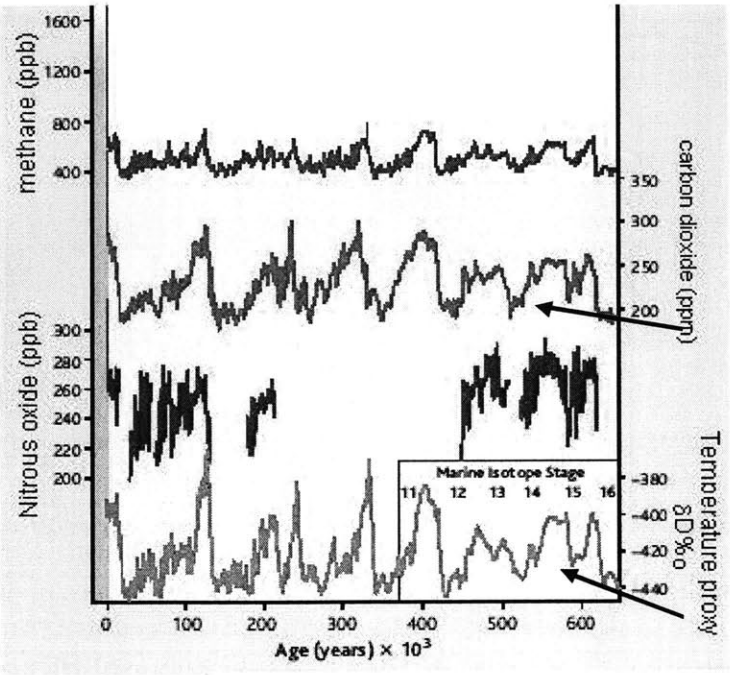

Figure 1-3: Correspondence of global temperatures with presence of atmospheric species, ice-core data[3]

While the likelihood that high greenhouse gas concentrations in the atmosphere will cause undesired environmental changes seems high, this issue is still under dispute. It is clear, however, that popular fuels such as oil and natural gas will eventually become depleted (although the timing of this occurrence is arguable), and that even those sources that exist today are non-ideal, as many of them are in regions that may be unstable or unfriendly, and from which a steady supply of material is not guaranteed. Thus it is desirable to reduce fuel use, while still

searching for alternative sources. While internal combustion engines are only one of many types of fuel-consumers, they represent a relatively large fraction of energy usage (in automobiles, electricity generation, etc.), so that increasing engine efficiency should be considered an important step towards this goal.

1.2 Sources of friction in large internal combustion engines

Friction in internal combustion engines comes from many sources, including the power cylinder (piston, rings, rods), bearings, valve-train, various pumps (coolant, water) and other components. The relative magnitudes of the contributions from each source vary greatly from engine to engine, as well as for different operating conditions. For a large ICE, the contribution of each component has been measured in a firing test engine and estimated to be in the ranges shown in Figure 1-4. As the figure shows, total mechanical friction for the engine may not be large, between 4-15%. However, in a widely used engine even a small increase in efficiency can result in a large net reduction in overall fuel use and carbon release.

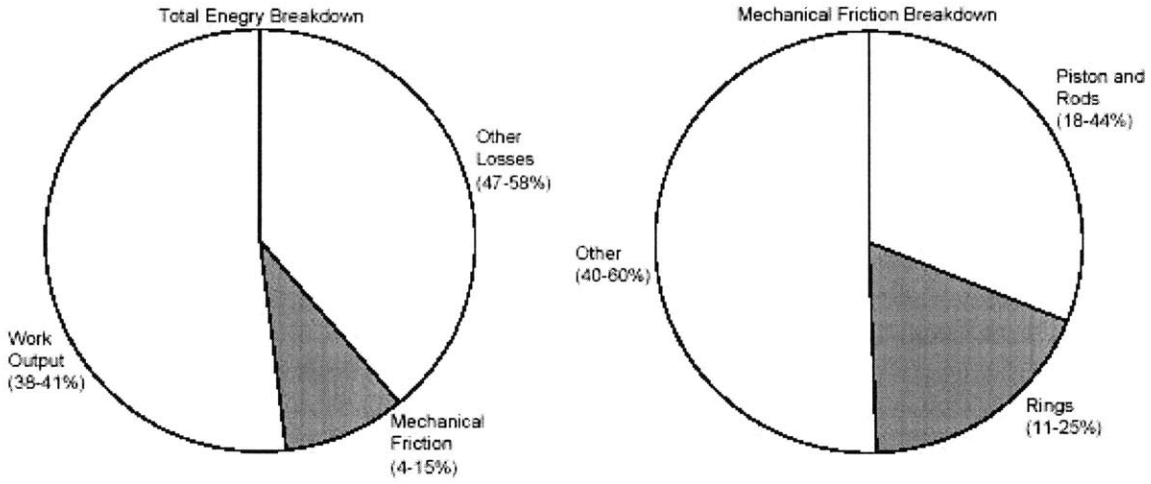

Figure 1-4: Component contributions to total engine friction, for a large diesel engine, firing[4]

As indicated in Figure 1-4, the power cylinder contributes approximately half of the total mechanical friction losses of the engine, where the ring-pack accounts for up to half of power cylinder losses, or a quarter of the total. Although the distribution of frictional losses within the engine varies between engines and operating conditions, in general the piston assembly is a major source of engine rubbing friction, and the rings make up a large fraction of this power-cylinder friction[5].

Within the ring-pack, the distribution of frictional losses can be further broken down into the contributions from each individual ring. Figure 1-5 shows the predicted contributions from each ring for the standard ring-pack in the Waukesha VGF 18GL engine, which is the subject of this study (more detail about this engine and engine specifications are given in section 5.1). Model results indicate that the majority of frictional losses come from the oil control ring, with

the top ring contributing most of the remainder. Further, most of the oil control ring losses are incurred in the hydrodynamic regime, while most of the top ring losses occur during one regime in the engine cycle – near the top-dead-center position of the piston, following combustion, where high gas pressures and poor lubricant availability result in very high boundary contact pressures. These phenomena are discussed further below.

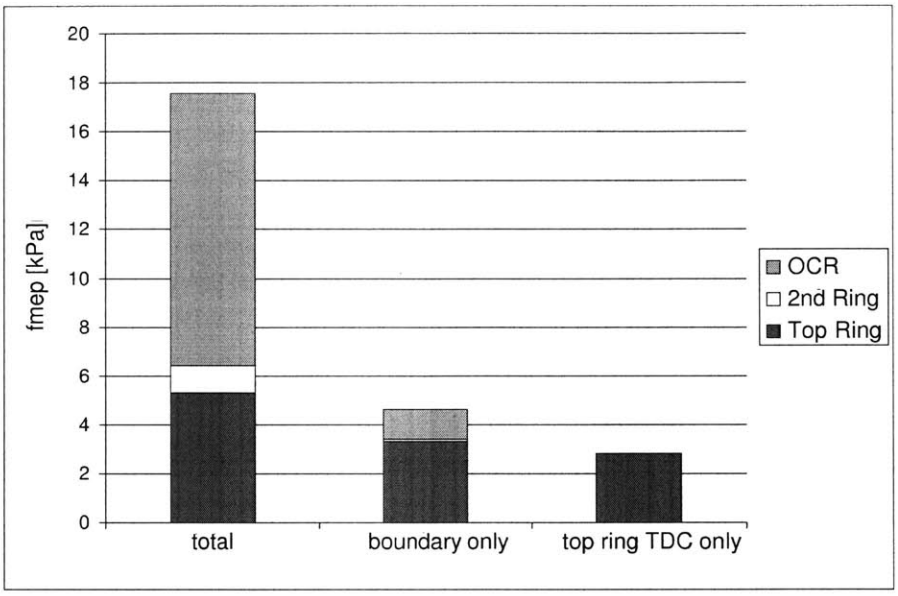

Figure 1-5: Contributions to ring-pack friction in Waukesha engine

1.3 Overview of the piston ring/liner system

1.3.1 Description of a typical piston ring/liner system

The piston ring pack in an internal combustion engine typically consists of three rings located in grooves in the piston, as shown in Figure 1-6. The primary purpose of the ring pack is to prevent high-pressure gases from leaking out of the combustion chamber, which would result in power losses. The rings must also prevent excessive leakage of oil from the crank case to the combustion chamber, while themselves remaining sufficiently lubricated. A third function of the piston rings, particularly for the top ring, is dissipation of heat from the piston to the cylinder liner. The rings should perform all of these functions without introducing excessive frictional losses into the system, and while keeping wear of both the rings and the cylinder liner to a minimum.

The system achieves these three objectives by using three specialized piston rings, each with a specific function. The top ring seals the ring-liner interface in order to prevent high-pressure gas from escaping from the cylinder into the lower parts of the ring pack. The top ring also dissipates heat from the piston to the cylinder liner. The oil control ring controls the amount of oil that flows towards the combustion chamber to lubricate the upper rings, regulating both the lubrication of the top two rings and oil consumption (oil that reaches the combustion chamber

evaporates or is burned away, resulting in oil loss). The second ring scrapes down any excessive oil that passes the oil control ring, further controlling oil consumption while maintaining adequate lubrication. In some cases the second ring is deemed unnecessary, as in racing engines, where light weight is more important than oil consumption, while in others extra scraper rings are added, as in large diesel engines with long life and stringent oil consumption requirements.

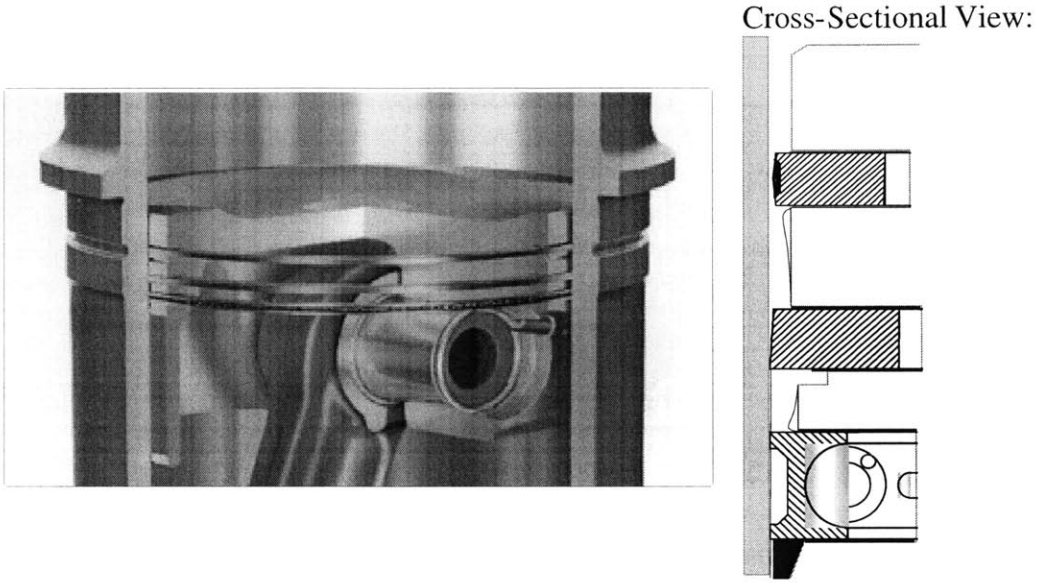

Figure 1-6: The Piston Ring Pack

1.3.2 Typical Piston Ring Designs

The designs of the three piston rings reflect their different purposes. The top ring, both far from the lubricant supply and exposed to harsh conditions, is designed to retain, and use to maximum effect, any available oil, while performing its main job of sealing combustion chamber gases. The second ring, also called the scraper ring, is designed to scrape excess oil down the liner (towards the crank case) on down-strokes, but not transport oil back up the liner, which can increase oil consumption. The oil control ring is the main element that controls oil flow into the power cylinder, and thus must conform well to the liner to prevent excessive oil flow under all engine conditions.

The top ring is the closest to the combustion chamber, so that it is exposed to very harsh conditions and rapidly changing loads. High combustion chamber gas pressures, in particular, can put high radial loads on the top ring, causing the ring to push into the liner at high force. While this high force effectively ensures that the ring conforms well to the liner and thus prevents gas leakage, it also causes high ring/liner friction and wear. Friction and wear are further exacerbated by poor oil supply to the top ring in parts of the cycle. To reduce these losses as much as possible, the top ring is designed to retain oil for lubrication. A barrel-shaped profile, which is commonly used, has been shown to aid in lubricant retention[6], and can also accommodate rotation due to piston secondary motion[5].

The second ring typically has a tapered face that very effectively accumulates oil on its lower edge (and may have a "hook" or other geometrical feature specifically designed for downward oil scraping) , but it cannot accumulate oil on its upper edge to scrape upward towards the combustion chamber. This allows the second ring to reduce oil consumption and act as a secondary control on oil flow. The scraper ring's unidirectional scraping profile is illustrated in Figure 1-7.

The oil control ring's purpose is to control the supply of oil traveling to the top two rings, and subsequently to the combustion chamber where it is consumed, making conformability to the liner a key design criteria. Several different oil control ring designs are in use, for different engine types. The focus of this study was the twin-land oil control ring (TLOCR). The TLOCR consists of a spring mounted inside two rails, where the circumferential length of the spring determines the ring tension that pushes the rails into the liner. The tension provided by the spring must be high enough to produce adequate ring-liner conformability for at least one of the lands, accommodating the thermal and mechanical deformation of the cylinder bore that occurs during engine operation. This high tension results in the high frictional losses associated with the oil control ring.

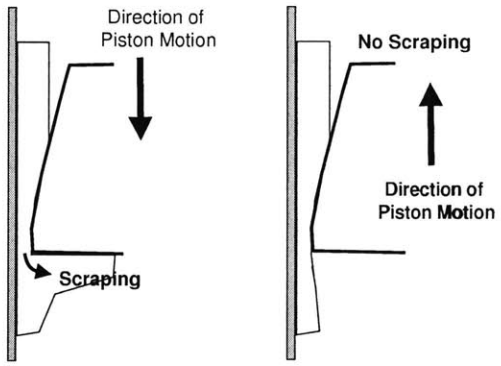

Figure 1-7: Effect of Taper Face Profile on Oil Transport

.

1.4 Overview of lubricant properties and requirements

Modern engine lubricant must perform many different functions, and fulfill many requirements. To this end, the typical lubricant contains a number of components and additives, designed to control viscosity, reduce boundary friction and wear, control lubricant degradation, and perform numerous other functions. While the lubricant viscosity is the focus of this study, other requirements should be taken into consideration in the design of an engine lubricant.

One of the main lubricant requirements is stability. The oil must maintain a stable state at all temperatures and conditions, so that it does not either react to create corrosive elements or form deposits that can reduce engine performance. The lubricant must also be able to mitigate the effects of any compounds that are formed in the engine or enter via intake air. Detergents

and dispersive additives allow the oil to keep such components in suspension – preventing them from being deposited on surfaces or creating wear - and to inhibit reactions that lead to undesirable products such as acidic compounds.[5]

In addition to these functions, the lubricant often also contains compounds that reduce wear and control viscosity. Anti-wear additives can be used to reduce wear due to metal-to-metal contact, while other additives are used to control attack on piston, cylinder and ring surfaces by acidic combustion products. The viscosity must also be controlled so that it maintains an acceptable value at both cold-start and running temperatures. Viscosity index improvers (VII's) can be used to reduce the variation of viscosity with temperature, so that the oil can be thin enough at start-up to lubricate the engine but not too thin at high temperatures to allow excessive boundary contact at running conditions.[5] One side effect of these VII's is to make the oil viscosity depend not only upon temperature but upon the shear rate in the oil. Not all lubricants contain VII's (those that do not are termed "straight" weight oils), but for those that do this viscosity variation must be taken into account.

1.5 Overview of liner surface structure

While they may appear smooth to the naked eye, the surfaces of both the rings and the cylinder walls are rough on the scale of interest – the thickness of the oil film separating the two. The texture of these surfaces can greatly affect both the amount of contact that occurs among asperities and the flow of oil between them. Understanding the effect of surface texturing on the interaction between the surfaces, and between the lubricant and the surfaces, is essential in understanding the lubrication of components currently in use and designing new surfaces to reduce friction.

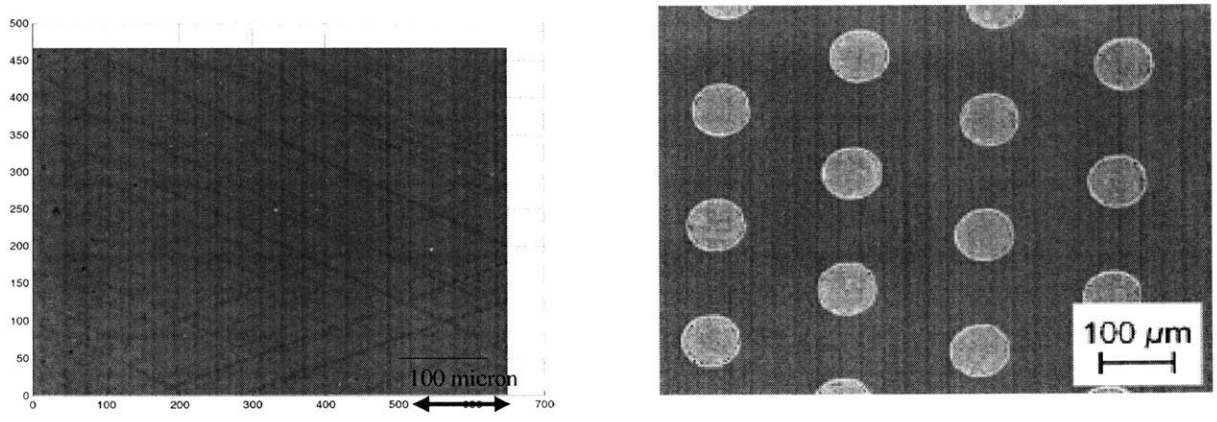

a) typical honed surface (slide-honed, WLI measurement) **b) Example of a "dimpled" surface.[7]**

Figure 1-8: Typical examples of honed and laser-textured surfaces

Two examples of surface finishes are shown in Figure 1-8. Figure 1-8a shows an example of a surface commonly found on cylinder liners today – a plateau finish clearly showing the

cross-hatch marks that result from the honing process. Figure 1-8b shows a less common texture, the surface has a dimpled pattern created by laser machining. While very uncommon at present, such designed surfaces are the subject of numerous studies and may be a key part of decreasing sliding friction and wear between the rings and liner.

1.5.1 Current production cylinder liner finishes

Today, most cylinder liner surfaces have a honed finish whose properties are stochastically controlled. That is, statistical parameters such as the surface roughness and skewness (see Figure 4-3a) are determined by the honing process, but the placement of specific features in specific locations is not possible. A typical honed surface, of which an example profile is shown in Figure 1-9 and a surface view in Figure 1-8a, has a negative skewness and a cross-hatch pattern of grooves, both created by the honing procedure.

Figure 1-9: Typical plateau honed profile

A typical honing tool is shown in Figure 1-10. The tool consists of a head with honing sticks or stones that are covered with abrasive particles, and are held outward radially by springs. The head is spun and at the same time moved axially in and out of the cylinder. The honing sticks are pressed outward into the bore and polish the surface. The process generally proceeds from a coarse grit to a fine one, so that deep grooves and large ridges are made during the initial rough honing passes. Then, the ridges are worn down to a relatively smooth finish by the subsequent fine passes, while the deep valleys remain. Such a process generally results in a plateau finish – a surface with negative skewness - in which the surface is relatively flat with many deep valleys. Such negatively skewed surfaces are thought to reduce friction by effectively breaking in the liner before actual engine use, and thus reducing actual breaking–in time, as well as by reducing asperity contact between ring and liner in a mixed lubrication regime [8,9,10].

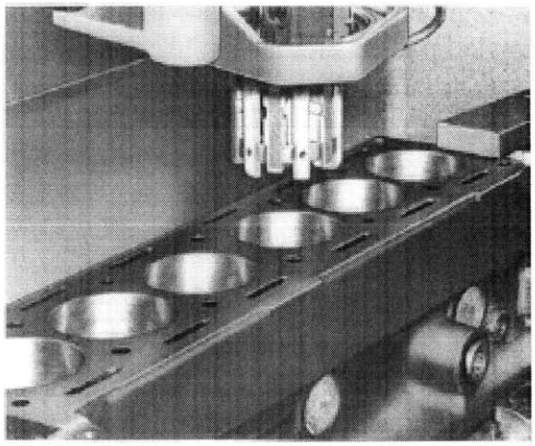

Figure 1-10: Typical cylinder bore honing tool [11]

In addition to creating a plateau surface, the combination of the rotating and axial feeding movements of the honing machine creates angled grooves on the surface, as shown in Figure 1-11. The relation between the rotation and feeding rates determines the angle of the cross-hatch grooves. The size and angle of these grooves has an influence on friction as well as oil consumption and wear. Several studies have predicted an increase in oil film thickness and decrease in friction for more transverse (relative to the cylinder axis) textures [8,12], although concerns about oil consumption and scuffing wear prevent very shallow-angle cross-hatch grooves from being implemented in production cylinder liners.

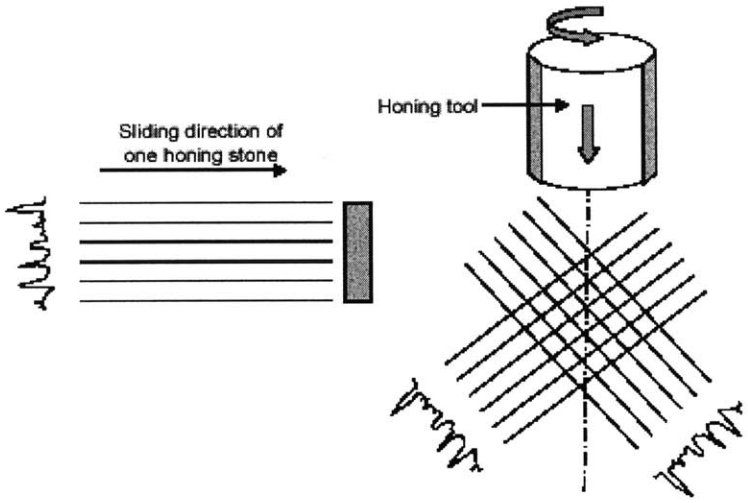

Figure 1-11: Schematic of honing process [10

1.5.2 Advanced finishes and textures

Deterministically controlled textures, in which individual features, such as the dimples shown in Figure 1-8b, are added to a surface, are already in use in some industries and show promise for friction and wear reduction in engine applications. For example, very small "micro-texturing" has been added to the "landing" sections of magnetic storage media for several years, to prevent stiction when recording heads contact the surface[13]. Although the mechanism for friction reduction here is different than that encountered in the case of the piston ring/liner interface, the success of this technique has encouraged other investigations into the possibility of engineering the surface structure.

Numerous studies, both analytical and experimental, have considered the effect of advanced textured surfaces on friction, wear, and other parameters in sliding applications. Research on face-seals, where loads and speeds are approximately constant during service, has shown great potential for increasing load capacity and lifetime with the addition of micro-texturing. Some experimental prototypes have been successfully field-tested in pumps, where they showed increased load capacity and greatly decreased wear over standard seals[14]. Studies of reciprocating sliding conditions have also indicated that friction may be reduced, although there is a lack of agreement over the mechanism for this effect. Still, both analytical and experimental results have shown potential for friction reduction, and laser-textured cylinder liners that promise low wear and oil consumption have been made commercially available by Gehring GmbH[15] in Germany.

Several methods are available for creating micro-textured surfaces, including chemical etching, machining, abrasive-jet machining, and laser texturing. Each method has advantages and disadvantages, and some may be more appropriate for use in a given application than others. Etching, for example, is versatile in the shapes it can produce, but the process is time-consuming and the profiles of the features are determined by the chemical erosion process and cannot be controlled (i.e., round-profiled dimples cannot be produced). Regular and abrasive-jet machining also have some limitations on profile shape, and may not be appropriate for cylinder liner texturing if machining heads are too large to access the inner liner surface. Laser texturing technology is currently believed to be a very promising technique based on its flexibility and speed [14]. A possible drawback is that the laser technique may create "burrs" of melted and re-deposited material around the edges of features so that surfaces may require a subsequent polishing step, however this problem may be solved with more optimized techniques in the future. An example of a laser-machining station is shown in Figure 1-12.

Figure 1-12: Typical laser texturing machinery (from Control Micro Systems, Inc.)

.

1.6 Scope of present work

The purpose of this work was to investigate methods by which ring/liner friction can be reduced in the Waukesha VGF 18GL engine. The two fields considered were lubricant properties, with focus on the lubricant viscosity, and surface finish of the cylinder liner. For both studies, existing ring-pack friction and lubrication models were used, with minor modifications as were required to complete the study.

In the area of lubricant properties, viscosity and its dependence on temperature and shear rate were considered. The role of lubricant viscosity in controlling the balance between hydrodynamic and boundary friction was studied, as was the effect of variation of viscosity during the engine cycle. Effects of viscosity on both friction and wear were analyzed. Also, some consideration was given to boundary friction coefficient and its role in ring/liner friction.

In the area of surface texturing, a parametric study was performed to evaluate the effects of both grooved and dimpled textures on the cylinder liner. Simplified surfaces were used to calculate flow and stress factors for the cases considered, which were then used in the ring-pack model to predict ring/liner friction. While the model used did not allow a detailed analysis of the effects of these textures on asperity contact and oil flow, this type of parametric study can give an indication of which textures are effective and how changing the different parameters affects friction and wear.

The possibility of optimizing the lubricant and surface together was also investigated. With this combined approach, a greater friction reduction is possible than in the individual cases, and it is also possible to reduce negative side-effects such as increased wear and oil consumption.

2. Ring-pack lubrication and friction: fundamentals and modeling

The piston ring-pack is an integral component of engine operation, performing the essential task of sealing hot, high pressure gases in the combustion chamber. Without the rings, the internal combustion engine could not function. Beyond carrying out this fundamental task, the rings are put under many more demands, including controlling oil consumption and assisting in heat transfer, and they are required to perform with minimum friction and wear. In recent years demands on the ring-pack have increased, and so the need to understand ring operation and develop accurate analytical models has become more essential, for optimizing the ring-pack to meet more stringent requirements. Substantial progress in this direction has been made in recent decades, with work continuing on the development of increasingly detailed and comprehensive ring-pack models.

2.1 A history of piston-ring development and analysis

The problem of sealing the gap around a moving piston has existed for several thousand years, since the idea of the piston-cylinder arrangement was first conceived. Early seal designs were based on natural materials including leather and hemp, and lubricated with animal tallows. It was not until the introduction of metallic rings, and in particular the Ramsbottom ring in the 1800s, that seal performance was sufficient to support the pressures and temperatures of an internal combustion engine[16]. Half a century later, Osborne Reynolds would describe his theory of hydrodynamic lubrication, although it would be many years more before it was used for analysis of piston ring operation. More recently, the demands of increasingly high-performance engines and the opportunities offered by computer modeling have produced numerous ring-pack models, of varying levels of detail and sophistication.

Ancient Greek and Middle Eastern engineers found some success with their sealing mechanisms, as did Europeans in the 18th century, but these efforts were not sufficient to withstand the temperatures and pressures common in even early internal combustion engines. Indeed, it is thought that the absence of good sealing is what delayed the success of the I.C.E. in favor of the steam engine until the late 19th century. The moisture inherent in the steam engine was favorable to natural sealing materials such as leather, hemp and cloth, while cylinder pressures in early engines were relatively low. The first metallic rings, introduced at the end of the 1900s to cope with increasing steam engine demands, were pressed into the cylinder with springs or hemp, often with complicated pistons and systems of several rings to produce a good seal. In 1854 the Ramsbottom ring was proposed: a simple metallic ring that was made too large for the cylinder bore, and, when installed, would press itself outward and create a seal with its own elastic tension. This simple and robust design was used "almost exclusively" by 1910, and operated on the same principals as rings that are used today.[16]

Although the basic design of modern piston rings is very similar to that of the "Ramsbottom ring" of the early 20th century, much progress has been made in both material development and understanding of the principals behind the rings' functionality. Early studies determined that the rings experienced hydrodynamic lubrication for most of the stroke, paving

the way for many future ring studies based on Reynolds' theory of hydrodynamic lubrication. In the 1960s and '70s computers first enabled very detailed ring analyses to be performed, without many of the simplifying assumptions which had been required earlier. In addition, techniques allowing direct measurement of ring/liner friction and oil film thickness provided validation to the ring models.[16]

In recent years, progress in areas related to ring modeling, including contact mechanics, lubricant flow between non-smooth surfaces and piston secondary motion, has aided in the development of many analytical ring-pack models[17,12,18, etc.]. Also, progress continues in experimental investigations, which aid in further advancing understanding of ring-pack operation. Together, analytical and experimental results are helping to advance ring-pack design to cope with the very demanding conditions in the high-performance engines in operation today.

2.2 Ring-pack modeling

The ring-pack simulation used in this study was developed by Dr. Tian Tian [19] at MIT. In addition to modeling friction and lubrication between the ring and liner, the package contains an advanced ring dynamics module, allowing it to analyze details of ring movement such as flutter and collapse, and calculate parameters such as the ring dynamic twists and gas blow-by flows. In the study of surface finish a modified version of this model, developed by Jeffrey Jocsak [8] also at MIT, was used. This modified package includes sub-models that can account for a greater variety of surface textures than the original program, in both contact and fluid flow analysis. It is used concurrently with a numerical simulation created by Yong Li of MIT, which is used for the calculation of the flow and stress factors which are used in the analysis of rough surface fluid flow. A general diagram of the ring/liner system analyzed in these models is shown in Figure 2-1.

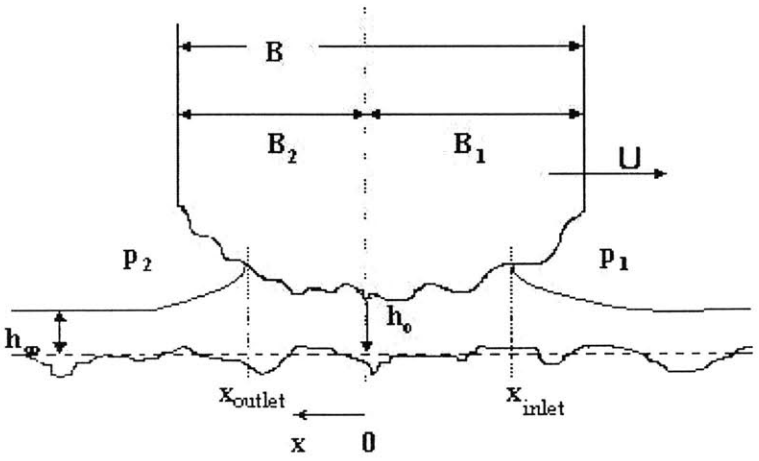

Figure 2-1: Schematic of ring/liner system. Surface roughness and ring curvature are exaggerated.

Calculation of ring/liner friction requires simultaneous solution of several relationships: a balance of radial forces on the ring must be satisfied, along with mass and momentum conservation for the lubricant flowing under the ring and a contact relationship for asperity contact. These relationships are interrelated by the oil film thickness and oil wetting locations on the ring. The hydrodynamic pressure, P_{hyd}, is strongly dependent on film thickness and wetting location, while the amount of asperity contact that occurs also depends on the film thickness. As the ratio between these two pressures changes, the radial force balance changes also. A solution is found at an oil film thickness and wetting condition at which the ring load is supported by asperity, oil and gas pressures, and all boundary conditions are satisfied.

2.2.1 Modes of ring/liner lubrication

The ring can experience three modes of lubrication - hydrodynamic, mixed, and boundary - illustrated in Figure 2-2. In pure hydrodynamic lubrication, there is no contact between the ring and liner, and the ring load is entirely support by hydrodynamic pressure in the oil film. In this regime, the ring/liner friction results entirely from shear stress within the oil. In pure boundary lubrication, the entire ring load is support by solid-solid contact between the ring and liner, with no hydrodynamic contribution. In this case, ring/liner friction consists entirely of rubbing friction losses. When the ring load is partially supported by the oil pressure, and partially by asperity contact, mixed lubrication occurs. In this situation, friction losses stem from both oil shear and metal-metal rubbing.

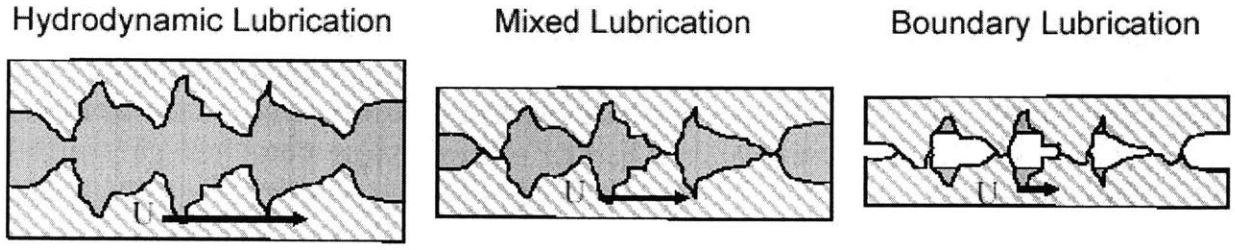

Figure 2-2: Modes of ring/liner lubrication

In the current model, the two surfaces are described stochastically, so it is not possible to ascertain whether any given asperity (local roughness peak) is contacting any other asperity. Instead a statistical limit is used, which determines the oil film thickness at which it is assumed negligible asperity contact occurs. This statistical limit is based on the combined roughness of the two surfaces, σ (where roughness is defined as the standard deviation of the surface height, measured from the mean):

$$\sigma = \sqrt{\sigma_{liner}^2 + \sigma_{ring}^2} \tag{2.1}$$

where σ is the combined surface roughness, σ_{liner} is the liner roughness, and σ_{ring} is the ring roughness. The amount of contact occurring is assumed to be negligible when the nominal separation between ring and liner and is greater than some factor, Ω, times this combined roughness. The model used in this study uses a value of $\Omega = 4$, where at the surface separation

of $h = \Omega * \sigma = 4\sigma$, statistically, the probability of contact is less than 2%. Then, it is assumed in the analysis that:

$$\begin{aligned} \frac{h}{\sigma} \le \Omega = 4 \quad & contact\ occurs \\ \frac{h}{\sigma} > \Omega = 4 \quad & no\ \ asperity\ contact \end{aligned} \tag{2.2}$$

where h is the mean oil film thickness.

2.2.2 Radial force balance

The ring load, including ring tension and gas pressure behind the ring, must be supported by some combination of asperity contact pressure, hydrodynamic pressure in the lubricant film, and gas pressures acting on the ring face. This balance is represented by the equation:

$$\begin{aligned} &\sum F_r = 0 \\ &= \int_{x_1}^{x_2} P_{hyd}\,dx + \int_{-b_1}^{b_2} P_c\,dx + P_1(B_1 + x_1) + P_2(B_2 - x_2) - P_b(B_1 + B_2) - T_r(B_1 + B_2) \end{aligned} \tag{2.3}$$

where P_{hyd} is the hydrodynamic pressure in the oil film, P_c is the asperity contact pressure between the ring and liner, P_1 is the gas pressure on the upper (combustion chamber) side of the ring, P_2 is the gas pressure on the lower (crank case) side of the ring, P_b is the gas pressure behind the ring, B_1 and B_2 are the upper and lower widths of the ring, x_1 and x_2 are the upper and lower wetting locations (x_1 is negative), and T_r is the ring tension, as shown in Figure 2-3. The ring inertia is not included in the radial force balance because it is much smaller than the other terms[19].

This relationship must be solved iteratively with asperity contact and hydrodynamic models, in order to determine oil film thickness, wetting locations, and pressure distribution in the lubricant.

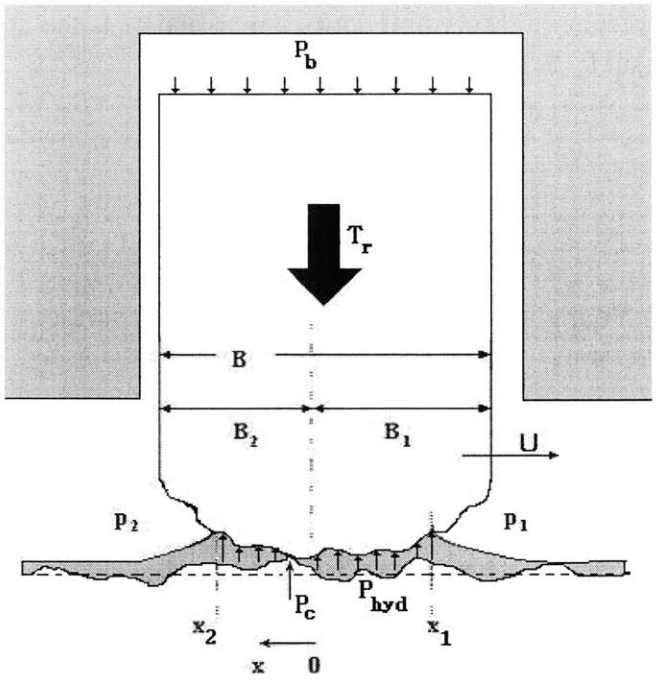

Figure 2-3: Schematic of ring/liner system

2.2.3 Asperity contact model

When solid to solid contact occurs between the ring and liner, an analysis that is based on the Greenwood and Tripp[20] asperity contact model, using a correlation developed by Hu[21], is used. Greenwood and Tripp's model describes the relationship of the elastic pressure of two contacting asperities with the distance between them:

$$P_c = \begin{cases} K' E' A\left(\Omega - \dfrac{h}{\sigma}\right)^z & \dfrac{h}{\sigma} \le \Omega \\ 0 & \dfrac{h}{\sigma} > \Omega \end{cases} \tag{2.4}$$

where P_c is the asperity contact pressure, K' is a constant related to the asperity geometry and distribution, E' is a constant related to the properties of the contact materials, A is a constant that can be used to calibrate predictions with measured data, σ is the combined roughness of the two surfaces, h is the nominal distance between the surfaces, Ω is the ratio of h/σ beyond which contact pressure is assumed to be negligible, and z is a constant. The coefficient K' is given by:

$$K' = \frac{8\sqrt{2}}{15}\pi (N\beta'\sigma)\sqrt{\frac{\sigma}{\beta'}} \tag{2.5}$$

where N is the number of asperities per unit contact area, and β' is the asperity radius of curvature. The coefficient E' is given by:

$$E' = \frac{2}{\left(\frac{1-\nu_1^2}{E_1}\right) + \left(\frac{1-\nu_2^2}{E_2}\right)} \tag{2.6}$$

where E_1 and E_2 are the Young's moduli for the two contacting surfaces, and ν_1 and ν_2 are their corresponding Poisson's ratios.

The relationship given in Eqn. 2.4 must be integrated over the apparent contact area to obtain a total contact force for the ring and liner. This can be done numerically, if deterministic surfaces are provided, or a stochastic model can be used. The analytical method used in this study uses a stochastic model, based on the Pearson system of frequency curves, which can describe surface characteristics based on RMS roughness, skewness, and kurtosis[22] (for definitions of Sk and Ku see Section 4.2). When reasonable assumptions are made for the values of asperity density and radius of curvature, this model can be used for predicting asperity contact pressure between ring and liner.

This asperity contact model assumes that deformation of the asperities is entirely elastic, and that plastic deformation does not occur. Although it is unrealistic to assume that this is the case in an engine, especially during the break-in period, it has been shown by Greenwood & Tripp that the asperity contact pressure calculated for pure elastic deformation is very similar to that calculated with plastic deformation taken into account. Certain assumptions about asperity shapes and distribution are also made in this model, which are described in greater detail in [20]. Also, it should be noted that surface coatings such as oxide films or chemical layers created by friction modifiers have not been considered.

2.2.4 Lubricant flow and stress conditions – averaged Reynolds analysis

When hydrodynamic or mixed lubrication occurs, an averaged flow-factor Reynolds analysis is used to model the lubricant pressure and flows, and the interaction between the lubricant and surface asperities. Hydrodynamic support of the ring load depends on a "wedge" effect in which relative motion between sliding surfaces and changing flow area combine to increase pressure in the lubricant. The fluid pressure is then able to support an external load. Because of this effect, a positive pressure increase will occur in the oil in the converging section of the ring/liner interface, and pressure will decrease in the diverging section, as shown in Figure 2-4. The figure also shows cavitation in the oil film, which may or may not occur, depending on engine parameters and running conditions. Cavitation and oil detachment conditions are discussed further below. If the net pressure in the lubricant is positive the ring load can, at least partially, be supported by this hydrodynamically generated oil pressure.

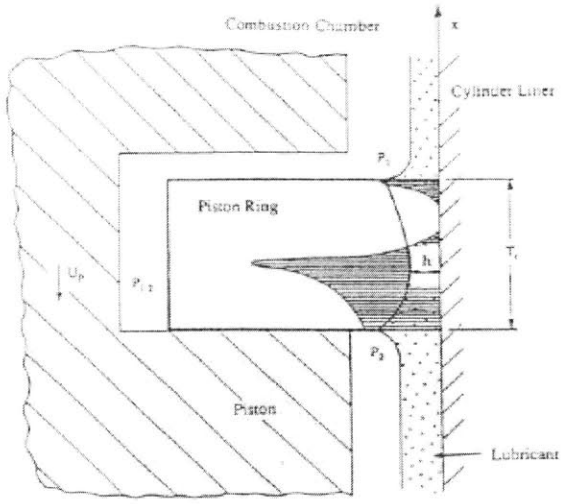

Figure 2-4: Schematic showing pressure distribution in the oil between ring and liner[23]

Analysis of the lubricant pressure and flow between ring and liner is based on Reynolds' equation (see Appendix A for derivation), which is applicable for thin film flows where viscous phenomena dominate fluid inertia. The Reynolds relationship is derived from conservation of momentum for the fluid (Navier-Stokes relations) and conservation of fluid mass (Continuity), and (for a one-dimensional system) is given by:

$$\frac{\partial}{\partial x}\left(\frac{h^3}{\mu}\frac{\partial p}{\partial x}\right) = -6U\frac{\partial h}{\partial x} + 12\frac{\partial h}{\partial t} \tag{2.7}$$

when both sliding surfaces are smooth, and h is the nominal separation between the surfaces, μ is the fluid viscosity, p is the pressure within the fluid, and U is the relative sliding speed.

In reality, the sliding surfaces are never perfectly smooth. When the oil film thickness is much larger than the roughness of both surfaces, this roughness has very little effect and can be neglected. However, when the oil film thickness and surface roughnesses are of the same order of magnitude, the effects of the surface texturing must be considered.

Both deterministic and stochastic methods are available for describing roughness effects. Deterministic techniques include more detail about actual surface features, and can account more accurately for fluid flows and asperity contact between the ring and liner. However, such techniques are complex and time-consuming to apply, and may not be necessary when a simpler understanding of trends and general effects of different surface parameters is desired. This study uses a stochastic approach, based on the averaged flow factor method of Patir and Cheng[24].

The averaged flow factor technique uses several factors to account for the differences between flow between two smooth surfaces, and flow between rough surfaces. The Reynolds

equation for smooth-walled flow is still used, together with three factors which account for the averaged effects of surface roughness:

$$\frac{\partial}{\partial x}\left(\phi_p \frac{h^3}{\mu}\frac{\partial p}{\partial x}\right) = -6U\frac{\partial}{\partial x}(h\cdot\phi_g + R_q\cdot\phi_s) + 12\frac{\partial h}{\partial t} \tag{2.8}$$

where ϕ_p is the pressure flow factor, ϕ_g is the geometric flow factor, ϕ_s is the shear flow factor, and R_q is the combined RMS roughness of the surfaces. Each factor is determined for a given surface, and accounts for the effect of the surface texturing on a given aspect of the fluid flow. The pressure flow factor represents the effect of the roughness on pressure-driven flow, while the shear flow factor represents the effects of surface roughness on shear-driven flow.

The geometric flow factor simply accounts for the fact that, as rough surfaces get closer together, they contact. The film thickness, h, used in the Reynolds equation is the nominal film thickness, taken as the mean distance between rough surfaces. However, the thickness required for shear flow calculation is the *mean* film thickness, which is equal to h in full hydrodynamic lubrication, but diverges from it when asperity contact occurs. When contact occurs, it is assumed that the overlapping asperities are simply sheared off, essentially changing the distribution of surface heights. Then, the location of the surface mean changes. The geometric flow factor takes this into account. When two surfaces are not contacting there is no change in surface mean heights and $\phi_g = 1$, nominal and mean surface separations are the same. When contact occurs, the mean film thickness becomes larger than the nominal, and $\phi_g > 1$.

Several methods for calculating flow factors are available. The technique used for factor calculation in this study is described in more detail in Section 2.2.5, below.

2.2.4.1 *Boundary conditions*

In addition to the flow factors, several boundary conditions are required to solve the Reynolds relationship given above. Continuity of pressures is required, so that the oil pressure at the top oil attachment point is equal to the gas pressure above the ring (P_1) and the oil pressure at the lower oil attachment point is equal to the gas pressure below the ring (P_2):

$$\begin{aligned} P(x_1) &= P_1 \\ P(x_2) &= P_2 \end{aligned} \tag{2.11}$$

Also, at the inlet, conservation of mass must be satisfied, so that the amount of oil flow under the ring at the inlet must be equal to the supply that was present on the liner prior to the arrival of the ring:

$$Q(x_{inlet}) = Uh_\infty \tag{2.12}$$

where $Q(x_{inlet})$ is the volumetric oil flow rate (per unit width) at the oil attachment point, and h_∞ is the oil film thickness before attachment occurs. This condition is not valid when the

ring inlet is fully-flooded - when there is more oil available than can be accommodated under the ring, and the excess is deposited on the leading ring face, as shown in Figure 2-5. In this case, the oil flow at the ring inlet is assumed to be equal to the amount flowing under the height of the ring surface at inlet:

$$Q(x_{inlet}) = U \cdot h(x_{inlet}) \tag{2.13}$$

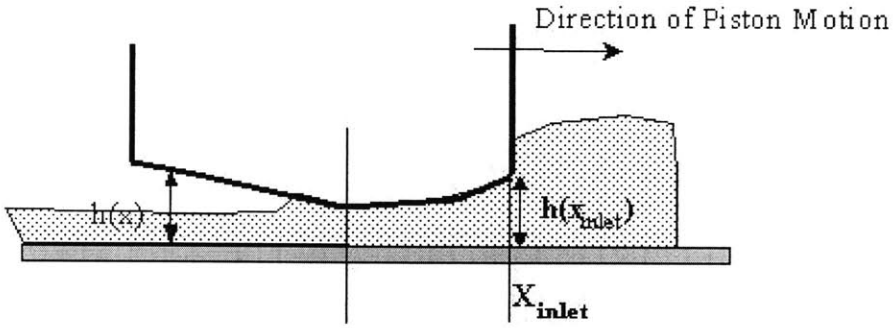

Figure 2-5: Illustration of fully-flooded inlet condition

An outlet condition must also be specified. A commonly used outlet condition is the Reynolds boundary condition:

$$\left.\frac{dp}{dx}\right|_{x=x_{outlet}} = 0 \tag{2.14}$$

which states that the pressure gradient in the oil must disappear at the ring outlet. This boundary condition can apply near the mid-stroke region of the cycle, where high relative speeds maintain hydrodynamic support of the ring, and at low enough gas pressures so that cavitation is not prevented. Near the end-strokes the Reynolds outlet condition is not applicable because, along with mass conservation, it requires oil to accumulate under the ring faster than it is being supplied at the inlet. In this region, then, a film-non separation boundary condition[25] is used, in which it is assumed that all of the oil exiting the ring/liner interface at the outlet stays attached to the ring, where it accumulates:

$$q_{x,outlet} = a \tag{2.15}$$

where $q_{x,outlet}$ is the flow rate of oil at the oil detachment point, and a is the accumulation rate of oil on the ring, defined as:

$$a \equiv h(x_{outlet}) \cdot \frac{dx_{outlet}}{dt} \tag{2.16}$$

2.2.5 Determination of flow and stress factors

The flow and stress factors that are used in the averaged Reynolds equation, and to determine shear stress are calculated deterministically, using the outputs from a numerical program developed by Yong Li at MIT. This model determines fluid flows and stresses between a smooth surface and the rough surface of interest, represented by a numerical matrix of surface height values. This matrix may be measured from an actual surface, (for example, using white-light interferometry) or generated analytically, as was done in this study. Comparing the deterministically calculated "actual" flows and stresses from this program to those calculated assuming smooth conditions and nominal surface separations provides the flow and stress factors.

Figure 2-6 outlines the program schematically. Conservation of mass and momentum are applied for the fluid, for each element in a grid. In the figure, q_x and q_y are the flows through a single control volume element in the x and y directions, respectively, and $\bar{\Delta}x$ and $\bar{\Delta}y$ are the distances between mesh points, which must be supplied as input. The cyclic boundary condition requires flows leaving the bottom of the flow region to re-enter at the top, thus conserving mass in the system. In the case of a piston ring, which can experience tangential oil flows, this is a more realistic boundary condition than the non-flow boundary condition applied by Patir and Cheng.

Pressure flow and stress factors are obtained by applying a pressure gradient across the system and calculating the resulting flow rate and shear stress. Shear factors are obtained by applying a relative motion to one surface, and calculating the resulting flows and stresses. All of these calculations must be made at a number of different mean film thicknesses, as the factors are functions of oil film thickness (or, more precisely, of the ratio of oil film thickness to surface roughness, h/σ.)

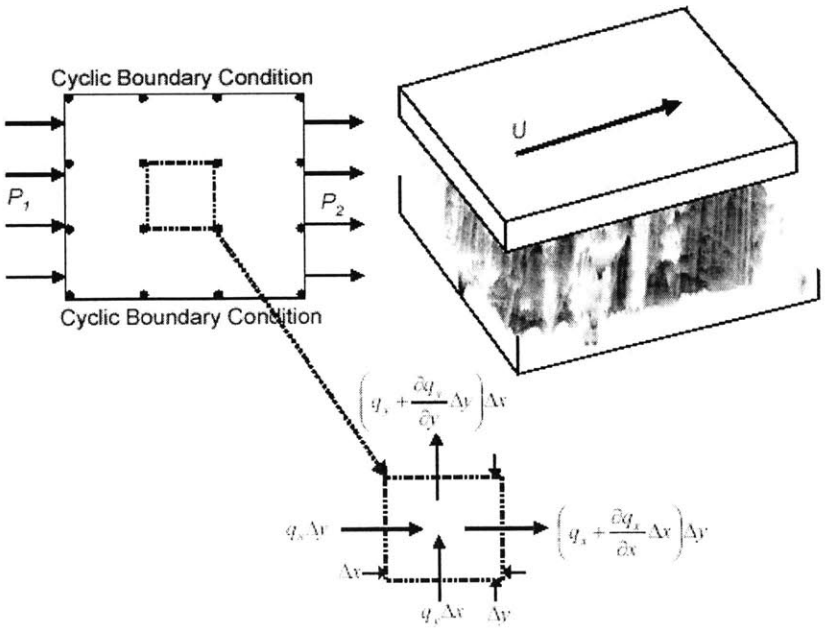

Figure 2-6: Schematic for Li's deterministic fluid flow and stress program

Once the flows and stresses are calculated numerically, the pressure and shear flow and stress factors are calculated by comparing these values to those calculated for smooth surfaces under the same flow conditions, and with the same nominal film thicknesses. The geometric flow and stress factors can be calculated from geometry only, and are defined by:

$$\phi_g = \frac{1}{h} \cdot \frac{1}{m(n-1)} \sum_{i=1}^{n-1} \sum_{j=1}^{m} H_s \tag{2.17}$$

$$\phi_{fg} = \frac{1}{h} \cdot \frac{1}{m(n-1)} \sum_{i=1}^{n-1} \sum_{j=1}^{m} \frac{1}{H_s} \tag{2.18}$$

where ϕ_g is the geometric flow factor, ϕ_{fg} is the geometric stress factor, m and n are the number of nodes in the x and y directions, h is the nominal surface separation, and H_s is the actual surface separation (when contact occurs $H_s = 0$). When there is no contact between the surfaces, both geometric factors are unity, the nominal and mean film thicknesses are equal. When contact occurs, the geometric stress factor, ϕ_{fg}, becomes unbounded and cannot be calculated. In these cases, H_s is set to a minimum height at which a limiting shear stress is assumed to occur. A detailed explanation for this substitution is given in [10]

The other flow and stress factors require input from the Li's numerical simulation for their calculation. With these values, calculation of flow factors proceeds from the definitions of the factors - each is defined as the ratio of actual flow to that which is predicted by a smooth-wall model:

$$\phi_p = \frac{q_p}{\left(\frac{h^3}{12\mu} \frac{\Delta P}{\Delta x} \right)} \tag{2.19}$$

where ϕ_p is the pressure flow factor, q_p is the deterministically calculated flow between the two surfaces due to a pressure gradient, h is the nominal surface separation, μ is the fluid viscosity and $\Delta P/\Delta x$ is the applied pressure gradient;

$$\phi_s = \frac{q_s}{\left(\frac{U \cdot R_q}{2} \right)} \tag{2.20}$$

where ϕ_s is the shear flow factor, q_s is the flow between the two surfaces due to a relative velocity, U is the relative velocity between the surfaces, and R_q is the combined surface roughness (R_q is present in the denominator because it also appears in the averaged Reynolds equation modifying ϕ_s, see. Eqn. 2.8);

$$\phi_{fp} = \frac{\tau_p}{\left(\frac{h}{2}\frac{\Delta P}{\Delta x}\right)} \tag{2.21}$$

where ϕ_{fp} is the pressure stress factor and τ_p is the shear stress in the fluid due to an applied pressure gradient and;

$$\phi_{fs} = \frac{\tau_s}{\left(\frac{\mu U}{h}\right)} \tag{2.22}$$

where ϕ_{fs} is the shear stress factor, and τ_s is the shear stress in the fluid due to a relative motion between the surfaces.

Each of the flow and stress factors are calculated for a number of film thicknesses. Once these values are obtained, a curve-fitted equation is derived for each, which is then used for flow factor calculation in the ring-pack simulation program.

Ā number of assumptions are made in the numerical calculation program, and some inherent limitations dictate the manner of program use and the situations to which it can be applied. The size of the rough surface "patch" analyzed must be chosen with care, in order to be both small compared to the actual expected sliding area of ring and liner, and large compared to the surface texturing of interest. This is because the method makes the assumption that the effects of surface texturing can be well-represented by the averaged effect of the combined features, without taking into account the effects of each feature alone. Then, the patch must contain a large enough sample of the pattern of interest to adequately represent all of the features and evaluate averaged effects. Also, since calculations are made based on sliding between nominally parallel surfaces, the patch must be small compared to the wetted area between ring and liner so that the curvature of the ring does not cause calculation inaccuracies. These requirements necessarily limit the size of surface features and patterns that can be studied using the averaged flow factor method, which must be small compared to the ring/liner wetted area.

Several assumptions are also made in the numerical calculations of fluid flows and stresses. Āsperity level cavitation is not taken into account, so that negative pressures do develop in diverging areas. In reality, cavitation is likely to occur when dissolved air leaves solution in the oil, at approximately ambient pressure. While the no-cavitation assumption was also made by Patir and Cheng[24], further investigation of micro-scale cavitation effects is required. Ālso, realistic deformation of surfaces, upon contact, is not considered. Instead it is assumed that contacting surfaces shear off cleanly, and the removed portions are then no longer part of the calculation. Because the simulation is numeric, and thus based on discrete data points, a method of interpolation is also required. Ā linear interpolation method is imposed between surface height data points, and a viscous wedge flow solution applied. Further information about this model and its limitations are given in [10].

2.2.6 Calculating ring/liner friction

The above equations must be solved simultaneously to find the film thickness and wetting locations of the lubricant. Once this has been done (an adjustable step-size iterative algorithm is used), the results can be used to calculate the ring/liner friction (as well as many other parameters). The total ring/liner friction force is the sum of friction due to asperity contact and that due to shear in the lubricant.

The contact friction is assumed to be proportional to the asperity contact pressure, where the proportionality constant used is the boundary friction coefficient, f_b:

$$F_{f,asp} = \int f_b P_{asp} dA \tag{2.23}$$

The hydrodynamic component of friction results from shear stress within the oil, and is derived from Newton's relationship:

$$\tau(x) = \mu \left. \frac{\partial u}{\partial y} \right|_{y=0} \tag{2.24}$$

where μ is the oil viscosity, u is the fluid velocity in the x direction, and the y direction is across the fluid film. Substituting in for u (see Appendix A for derivation):

$$F_{f,hyd} = \int_{wettedarea} \left(\frac{\mu U}{h} \left(\phi_{fg} + \phi_{fs} \right) - \phi_{fp} \frac{h}{2} \frac{dp}{dx} \right) dA \tag{2.25}$$

The total ring/liner friction force is then given by:

$$F_f = F_{f,asp} + F_{f,hyd} \tag{2.26}$$

This friction force is useful for assessing where, during the engine cycle, friction is generated, and what parameters contribute to friction. For reporting actual friction losses in an engine, however, another measurement is used. The work lost to friction, rather than the friction force, is the important parameter to consider when assessing a low-friction design. This is because this work determines the amount of extra fuel that will be required to overcome friction - the more fuel necessary, the lower the engine efficiency. Friction work is reported as the FMEP, friction mean effective pressure, which is the friction work normalized by engine displacement, and is given by:

$$FMEP = \frac{\int_{cycle} F_f dx}{V_d} \tag{2.27}$$

where V_d is the displaced volume of the cylinder (or of the entire engine, if the friction work evaluated is also for the entire engine).

2.2.7 Model applicability and limitations

Although it takes into account many of the complexities of the power cylinder system, the ring model used is nevertheless an approximation of reality, and is based on several assumptions that limit its applicability. Some of these are inherent in the averaged Reynolds method itself, while others stem from limitations in the current understanding of related phenomena.

Because it uses an averaged flow factor method, rather than a deterministic fluid analysis, the model used is limited in the surfaces to which it is applicable, as well as in the phenomena it can describe. It is inaccurate at very small film thicknesses (h/σ close to 1 or less) because, when it is continually interrupted by asperity peaks and flow blockages, the fluid flow is more strongly influenced by the actual, deterministic surface features than average effects. Also, textures to be analyzed cannot have features that are too large or "non-smooth." In the former case, the features and pattern under study must be small compared to the ring width, or the assumption that the cumulative effect of the texture features can be well-represented by average factors will be violated. (Details of patch size selection criteria are given in [10].) In the latter case, some textures may violate basic assumptions in development of the Reynolds equation, so that the Reynolds analysis itself may not be applicable for these surfaces.

One of the simplifications made in the development of the Reynolds equation (see Appendix A) is that, because the oil film is thin, there is no pressure gradient across the film thickness. However, for surface features that are very deep, have non-smooth edges, or otherwise cause too much disruption to a laminar flow, this will not apply. Figure 2-7 illustrates a case in which vortices appear in a deep feature, violating the stated assumption. In other cases sharp edges may cause turbulence, features may be too close together, or other phenomena may disrupt the assumed flow pattern [26]. When textures of this nature are to be analyzed, a more detailed analytical method should be employed.

Also, in the calculation of the flow and stress factors, it is assumed that the gap between the two surfaces is completely filled with oil. In an actual engine it is likely that the ring/liner clearance will not be entirely filled, especially when surface texturing is present. For example, lubricant may not entirely fill a honing groove, or may be pushed to one side of the groove by pressure from the gases and ring movement, leaving a non-lubricated region. The averaged flow factor analysis does not account for this type of situation.

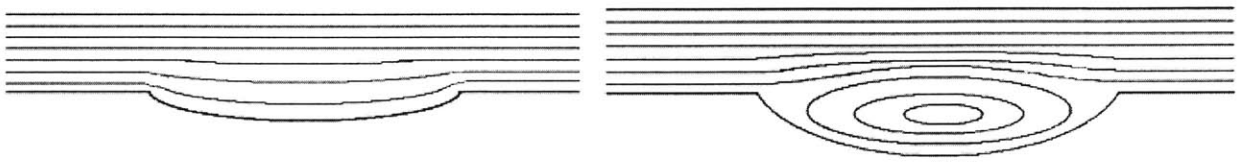

Figure 2-7: The averaged flow factor method is not applicable when surface features are too disruptive

Another limitation of the averaged method lies in its lack of ability to account for non-averaged phenomena. The averaged flow-factor analysis cannot describe many details of the flow and contact between ring and liner that may be of great importance in the actual ring/liner system. For example, flow of lubricant along honing grooves may play a major role in lubricant transport and friction, but this phenomenon cannot be modeled with the averaged method. Again, when phenomena of this nature is of interest, a more detailed, deterministic method is required.

In addition to some inherent limitations in the ring lubrication model itself, a limited understanding of related phenomena has lead to some simplifications. Oil transport is a very complicated phenomenon, and all of the mechanisms that affect it are currently not understood. Thus, the oil transport model used in the ring-pack analysis is necessarily simplified. In all of the analyses discussed, it is assumed that ample lubricant is available to the oil control ring, as well as to the second ring on down-strokes. Transport of oil into the "dry region" of the liner, studied briefly in section 3.8, is not well-understood and the results shown should be considered to be preliminary. Also, all results shown are calculated on the pin side of the piston, and effects of piston rotation and secondary motion are not considered. Although it is possible to consider piston secondary motion with the current ring-pack model, the added complication of including this effect may have impeded clear understanding of the parameters under study, and so it was not included.

(This page was intentionally left blank)

3. Effects of lubricant viscosity on ring/liner friction

The effects of lubricant viscosity on ring/liner friction were analyzed, with a focus on reducing friction by maintaining an optimal hydrodynamic/boundary regime balance throughout the cycle. A brief study of boundary friction coefficient is also included, as it can have a large effect on friction, and can be controlled to some extent by lubricant additives. The objective is to determine an optimized viscosity, including variations during the engine cycle, for the Waukesha engine design and operating conditions.

During the engine cycle, the piston rings experience hydrodynamic, mixed, and boundary lubrication, due to the wide ranges of sliding speed and mechanical loading. Oil viscosity affects friction directly in the hydrodynamic regime (Eqns.2.24, 2.25), and also indirectly affects boundary friction by influencing oil film thickness, and thus the amount of asperity contact that occurs. Reducing viscosity causes a decrease in oil film thickness, so that although hydrodynamic friction is reduced asperity contact is more likely. A thicker oil may reduce boundary friction but increases hydrodynamic losses. An optimized lubricant creates a balance between hydrodynamic and boundary modes, throughout the engine cycle.

Both idealized and more realistic cases are considered. First, ideal cases where the lubricant viscosity at each crank angle can be independently controlled are studied, to illustrate potential benefits in a well-controlled scenario. Then, a parametric study of more practical cases is presented, based on more realistic viscosity dependencies on temperature and shear rate. Also, the interaction between lubricant viscosity and other component parameters are studied to find any relationship between these factors. All results presented below are for the oil control ring only. Although the entire ring-pack is clearly affected by the lubricant viscosity, it is believed that the major impact of lubricant viscosity on friction will stem from the OCR (see Section 5.2.1).

While friction reduction is the focus of the current effort, other factors such as wear must also be addressed. A simple study of the effects of lubricant viscosity on wear is presented, with a slight benefit observed when viscosity variation during the engine cycle can be controlled. Also, the effect of boundary friction coefficient, which can be reduced via surface modifiers, is analyzed.

3.1 Summary of current lubricant trends

Recently, increasingly stringent controls on engine emissions have lead to major changes in lubricant formulation. Many of these changes have been in the additive packages, where important lubricant properties such as stability and the ability to keep potentially harmful substances in solution must be controlled with a minimal use of environmentally unfriendly chemical species.[27] Lubricant viscosity has also been used to improve fuel consumption, with "energy-efficient lubricants," which couple reduced viscosity with friction modifiers, becoming more widely available. Viscosity index improvers, which reduce the dependence of viscosity on temperature, are also used, so that lower-viscosity oils can be used while still maintaining good cold-start characteristics. Unfortunately, such advanced lubricants tend to come at a higher

price, so that a life-cycle cost analysis is required to determine if a given lubricant provides a financial advantage[28].

3.2 Ring/liner lubrication regimes, Waukesha engine

Many engine parameters influence the lubrication regime of a piston ring, including the ring load, piston speed and lubricant viscosity. In an internal combustion engine, these parameters are changing throughout the engine cycle. If viscosity is to be optimized for low friction at all times, it must be matched to these changing parameters, and thus it, also, must change throughout the cycle. Before this can be accomplished, an understanding of the lubrication conditions of the current Waukesha ring-pack is required.

The relative contribution of each lubrication mode to friction for a given ring depends on how well the ring load can be supported by the oil film. At high enough speed (and high enough viscosity), the oil pressure can fully support the ring load, resulting in pure hydrodynamic lubrication. For lower speeds and/or low viscosities, a thinner film is generated and may be thin enough to allow some asperity contact to occur, resulting in mixed lubrication. At very low speeds or viscosities (or very low oil availability, as in the case of the top dead-center region for the top ring) the oil film can break down, and the ring load is entirely supported by asperity contact. These three modes are illustrated in Figure 2-2.

For the Waukesha engine (as for virtually all internal combustion engines), hydrodynamic lubrication tends to dominate during mid-stroke, whereas near end-strokes boundary friction becomes important. This is largely due to the change in piston speed as the piston and rings reciprocate along the liner, and is illustrated in Figure 3-1. For the oil control ring, which is the focus of this study, there is very little change in ring load during the engine cycle. The top ring experiences a large spike in load near TDC of combustion, but lubricant viscosity is expected to have a relatively small effect here (see Section 3.8), so load is not considered in the discussion below.

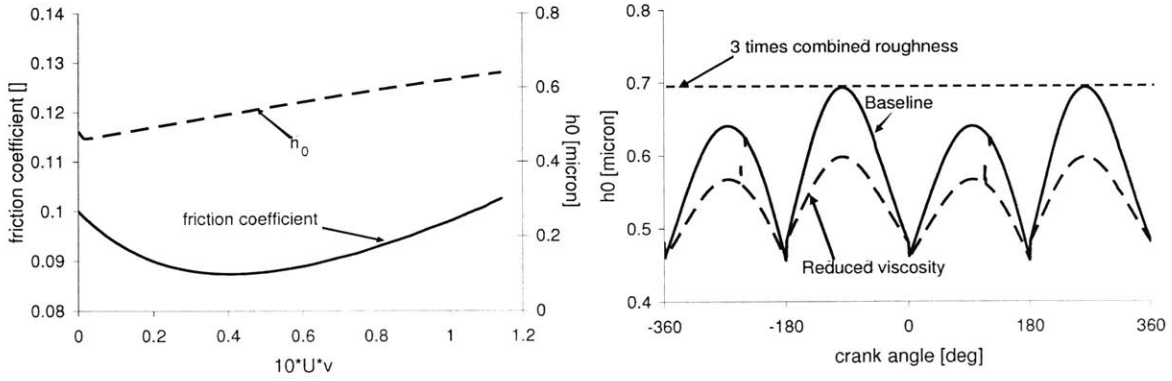

a)friction coefficient and h0 dependence on bearing # **b)minimum film thickness, for an engine cycle**

Figure 3-1: Effects of speed and viscosity on ring-liner separation (minimum film thickness) and friction, lower land OCR

Figure 3-1a shows how ring/liner friction coefficient and oil film thickness change with the ring speed, U, and lubricant viscosity, ν. (The factor 10 was chosen so that the bearing number N = 10Uν ranges between approximately 0 and 1). As the figure shows, as the bearing number approaches 0, film thickness decreases and the coefficient of friction increases to the boundary friction coefficient, $f_b = 0.1$ in this case. For high bearing number, friction increases as shear stress – proportional to U and ν - increases, and oil film thickness increases as well. In the mid-range, friction coefficient drops as the balance between boundary and hydrodynamic lubrication changes.

Figure 3-1b shows the ring/liner oil film thickness during the Waukesha engine cycle, for baseline running conditions (-360° is the beginning of the intake stroke) and for the baseline and a reduced viscosity lubricant. The h_0 shown is the oil film thickness between the lower land of the OCR and the liner - results for the upper land are the same, the lower land only is shown for illustrative purposes, for all figures. The line "3 times combined roughness" indicates the film thickness that is three times the combined roughness of the ring and liner, at which there is a 5% chance of metal to metal contact. In general, film thickness is small near dead-centers because ring speed approaches zero and hydrodynamic support is lost. H_0 does not disappear in this region because of the ring and liner roughness – there is still some oil trapped in the valleys when peaks are contacting – as well as the hydrodynamic "squeeze" effect on the oil. Still, there is very little hydrodynamic support. Near mid-strokes piston speed is high, and therefore film thickness is also large.

Comparing to Figure 3-1a, the film thicknesses shown in Figure 3-1b indicate that hydrodynamic lubrication dominates near mid-strokes for the baseline Waukesha engine (although there is a very small amount of asperity contact), while boundary contact supports most of the ring load near dead centers. In the reduced viscosity example, film thicknesses are lower and boundary contact becomes important both at mid-stroke and end-strokes, because the less viscous oil is less able to support the ring load.

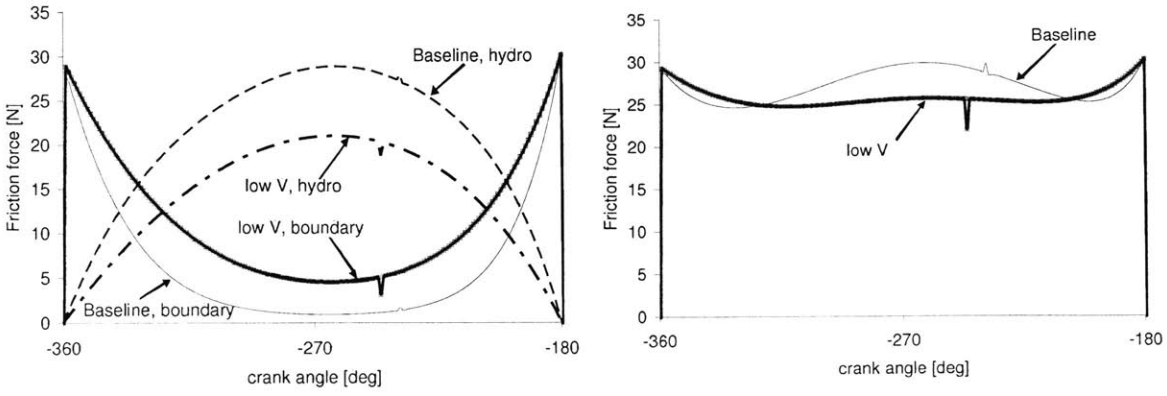

a)Ring/liner friction force, hydrodynamic and boundary

b)Ring/liner friction, total

Figure 3-2: Effect of viscosity on hydrodynamic and boundary friction, intake stroke, lower land OCR

This distribution of friction regimes is also shown in an analysis of ring/liner friction force. Figure 3-2a shows friction force between OCR and liner for a single (intake) stroke in the

Waukesha engine (lower land only). In the figure, boundary friction is high near dead-centers, where oil film thickness is small, while hydrodynamic friction is high near mid-stroke due to high piston speed, as expected. For the lower viscosity lubricant hydrodynamic friction is reduced, while boundary friction is increased corresponding to the reduction in oil film thickness shown in Figure 3-1b. Figure 3-2b shows the total ring/liner friction force. Overall, the lower viscosity oil provides a lower friction force near mid-stroke, because hydrodynamic lubrication dominates there, while it has a slightly higher end-stroke friction.

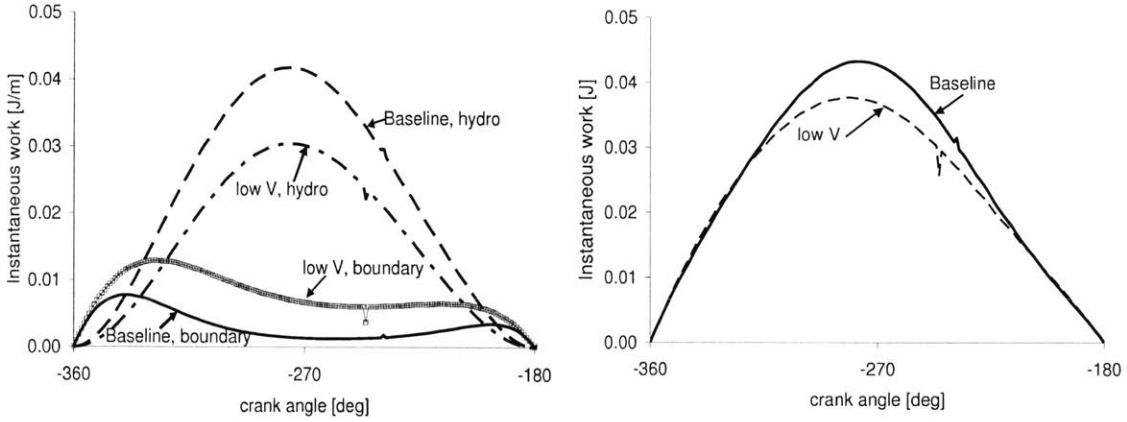

a)Ring/liner friction power loss, hydro and boundary b)Total ring/liner friction power loss, for 2 viscosity cases

Figure 3-3: Effect of viscosity on boundary and hydrodynamic friction work, per crank angle, intake stroke, lower land of OCR

While the friction force is useful for illustrating the lubrication modes between ring and liner, the work lost to friction is more important in the final analysis, as this is the loss that will have to be made up by burning more fuel. This loss is proportional to the ring/liner friction force and the piston speed at which that force is generated. Although the friction force near dead-centers is of a similar magnitude to that near mid-stroke, mid-stroke work losses are much higher because of the dependence on piston speed. This is illustrated in Figure 3-3.

Figure 3-3a shows the boundary and hydrodynamic work losses for ring/liner sliding. For the baseline case, most of the frictional energy losses stem from hydrodynamic lubrication near mid-stroke. For the reduced viscosity case, there is a decrease in hydrodynamic losses in the mid-stroke region, with a corresponding increase in boundary losses because of the increase in asperity contact there. The balance between these two changes determines the extent of the change in overall friction, which is shown in Figure 3-3b. In this figure, it is clear that the mid-stroke effects of changing viscosity almost entirely determine the change in overall friction, with almost no contribution from the end-stroke region. Also, the baseline viscosity appears to be higher than optimal – reducing viscosity reduces ring/liner losses.

While the goal of this study is to micro-manage lubricant viscosity by determining its optimal value at each crank angle, it is also useful to take a broader look at the effects of mean viscosity on ring-pack friction. Figure 3-4 shows the FMEP for the entire Waukesha engine

ring-pack. The figure shows the same trends presented above – friction tends to decrease with viscosity as long as the oil is thick enough to support hydrodynamic lubrication. When viscosity gets too low, friction begins to increase as boundary friction becomes large. An ideal viscosity is found at the balance of these trends, where a minimum friction loss is found.

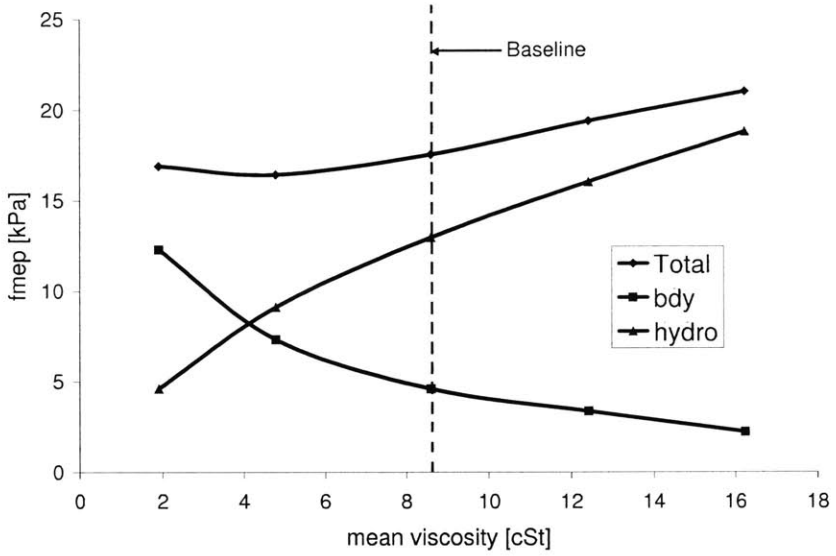

Figure 3-4: Ring-pack FMEP vs. mean cycle viscosity, for Waukesha VGF 18GL engine

3.3 Effects of baseline viscosity variation during the engine cycle

For the Waukesha engine, lubricant viscosity varies during the engine cycle because of its dependence on temperature. This case was compared to one in which viscosity is held constant for the entire cycle, in order to assess the effects of the variation in viscosity of the baseline oil. It was discovered that, although the variation in baseline viscosity affects lubrication modes within the engine cycle, its overall effect on FMEP is small.

Currently, the recommended lubricant for the Waukesha engine is an SAE 40 grade, a non-shear-thinning oil whose viscosity profile is shown in Figure 3-9 ("baseline"). The boundary and hydrodynamic friction forces between oil control ring and liner, with this baseline lubricant, are shown in Figure 3-5, for the intake stroke. The same forces are shown for s constant-viscosity lubricant, whose viscosity is held constant at the mid-stroke viscosity of the baseline oil.

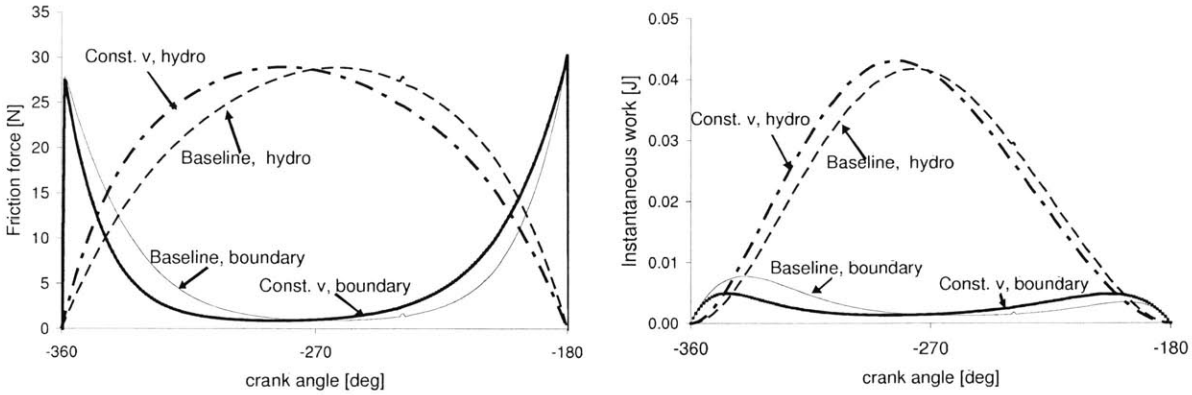

a) Friction force, per crank angle **b) Friction work loss, per crank angle**

Figure 3-5: Constant viscosity case compared to baseline viscosity case, lower land OCR, intake stroke

As the figure shows, the effect of the baseline viscosity variation is to skew the friction distributions to one side. However, the net change in FMEP for the cycle is very small (see Table 3-1). This is because the variation in viscosity is symmetric about mid-stroke for the baseline oil, so that viscosity effects that occur before mid-stroke tend to cancel out those that occur after. In the beginning of the intake stroke, the viscosity of the baseline lubricant is lower than that in the constant viscosity case, so that baseline hydrodynamic friction is lower, and boundary friction higher. The opposite occurs in the second part of the stroke, so that the effects tend to cancel and the overall change in friction is relatively small.

This is further illustrated in Figure 3-6, which shows the same friction work as a function of piston speed during the intake stroke (other strokes show the same trends), and where the arrows indicate the direction of increasing crank angle. This figure shows clearly the effects of the changing viscosity – plotting the friction force vs. piston speed for a stroke separates out the effect of the speed, so that viscosity effects are seen more clearly. Figure 3-6a shows that friction for the baseline case is lower than average in the first part of the stroke (where viscosity is lower) and higher in the second. Over the entire stroke, the friction in these two periods averages to a value that is close to that for the constant viscosity case. For the constant viscosity lubricant, there is almost no difference between friction in the first and second parts of the stroke.

Figure 3-6b shows the effect of reducing viscosity, (constant viscosity cases are shown). The lower viscosity case (ν = 5cSt) clearly has lower frictional losses, with the majority of the friction reduction occurring near mid-stroke due to decreased hydrodynamic friction. This figure shows that the effects of changing viscosity are greatest near mid-stroke, with relatively little effect on friction near dead-centers.

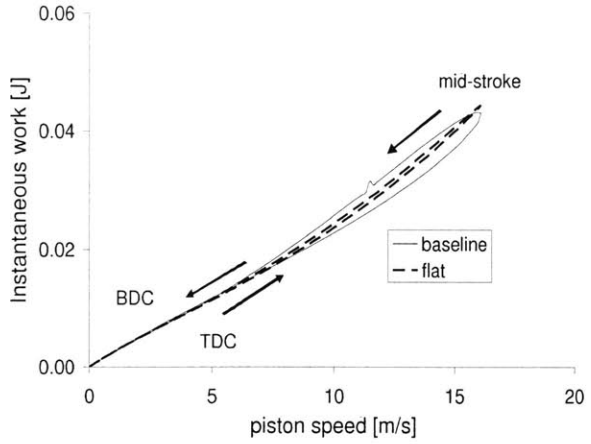

a) Instantaneous friction work, as a function of piston speed

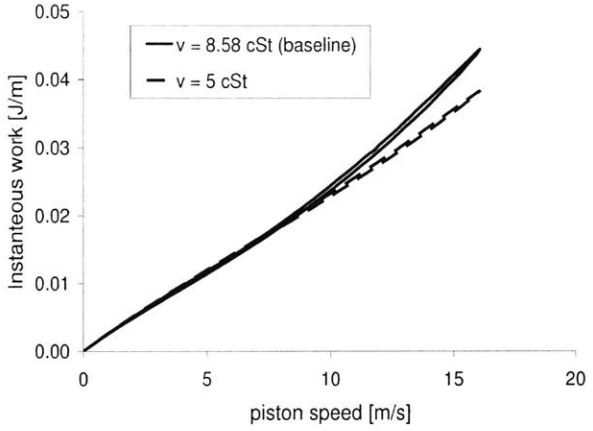

b) Effect of mean friction reduction, constant viscosity distributions

Figure 3-6: Effect of viscosity temperature dependence, comparing baseline and constant viscosity cases, intake stroke, lower land, OCR

3.4 Lubricant viscosity parameters

3.4.1 Temperature dependence

The viscosity of all lubricants depends on temperature. For the case of the piston rings, because the oil film is very thin, the temperature across it (in the radial direction) is assumed to be constant. Then, the viscosity of a lubricant with only temperature-dependence is assumed to be constant across the film thickness as well, with this dependence described by the Vogel equation:

$$\nu = z \cdot e^{\left(\frac{T_1}{T_2+T}\right)} \tag{3.1}$$

where ν is the kinematic viscosity of the lubricant, z is an oil "thickness" parameter, T_1 is an overall temperature-viscosity dependence parameter, T_2 is a lower bound parameter that is related to the glass transition temperature of the lubricant, and T is the lubricant temperature. Increasing T_1 increases the change in viscosity for a given temperature change, while increasing T_2 has the opposite effect. For a small T_1 or large T_2, the viscosity can become virtually independent of temperature.

To evaluate the effect of the strength of the viscosity-temperature relationship, lubricants with several values of T_1 were compared ,while z was changed accordingly to keep mid-stroke viscosity constant. The results of this study are presented in section 3.6. Figure 3-7 shows viscosity as a function of temperature for a few of the T_1 values studied. The liner temperatures at TDC for the top ring and BDC for the OCR are shown. A square-root distribution is assumed for the liner temperature, bounded between these two values.

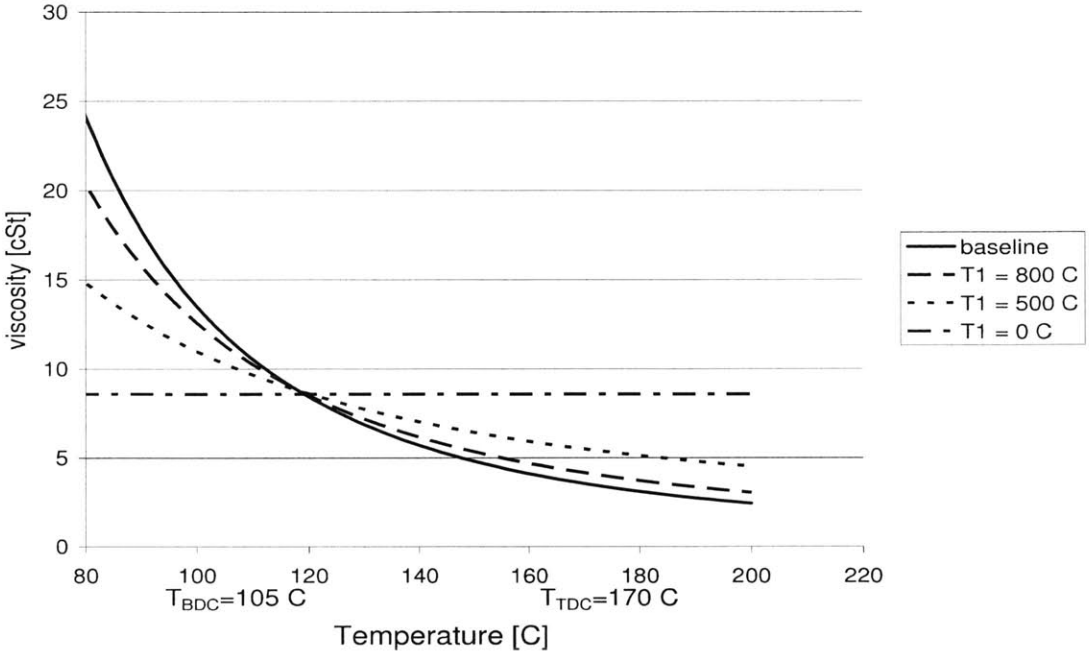

Figure 3-7: Examples of viscosity variation with temperature.

3.4.2 Shear-rate dependence

The large temperature variations in the internal combustion engine cause large variations in viscosity, as shown in Figure 3-7. Viscosity index improvers (VII's), are added to many engine lubricants to decrease this dependence of viscosity on temperature. A side effect of such additives is to cause shear thinning – the oil viscosity becomes dependent on its shear rate, where high shear rates cause the oil viscosity to be reduced.

The Cross relationship was used to model the dependence of viscosity on shear rate:

$$\nu = \nu_0 \frac{1 + \frac{\nu_\infty}{\nu_0}\left(\frac{\gamma}{\beta}\right)^m}{1 + \left(\frac{\gamma}{\beta}\right)^m} \tag{3.2}$$

where ν_0 is the low-shear viscosity (obtained from the Vogel equation, above), ν_∞/ν_0 is the ratio of high shear viscosity to low shear viscosity, γ is the lubricant shear rate, m is a parameter governing the width of the low shear-high shear transition region, and

$$\beta = 10^{c_1 + c_2 T} \tag{3.3}$$

is the critical shear rate, which controls the shear rate at which the low shear/high shear viscosity transition occurs. c_1 and c_2 are parameters controlling β.

For very low and very high shear rates, viscosity is approximately constant. A transition region, whose width is determined by the parameter m and whose location is determined by β, the critical shear rate, separates the high and low shear regions, as shown in Figure 3-8. The cases shown in this figure are those discussed in Section 3.7, below, with Cross equation parameters are given in Table 3-2. For most internal combustion engines, the lubricant between piston-ring and liner experiences a higher shear rate than the critical shear rate for almost the entire engine cycle, with the exception of a few crank angles near dead centers. Then, the lubricant is essentially dependent only on temperature. The value of the critical shear rate was adjusted in this study, to assess the effects of having the transition occur during the ring stroke.

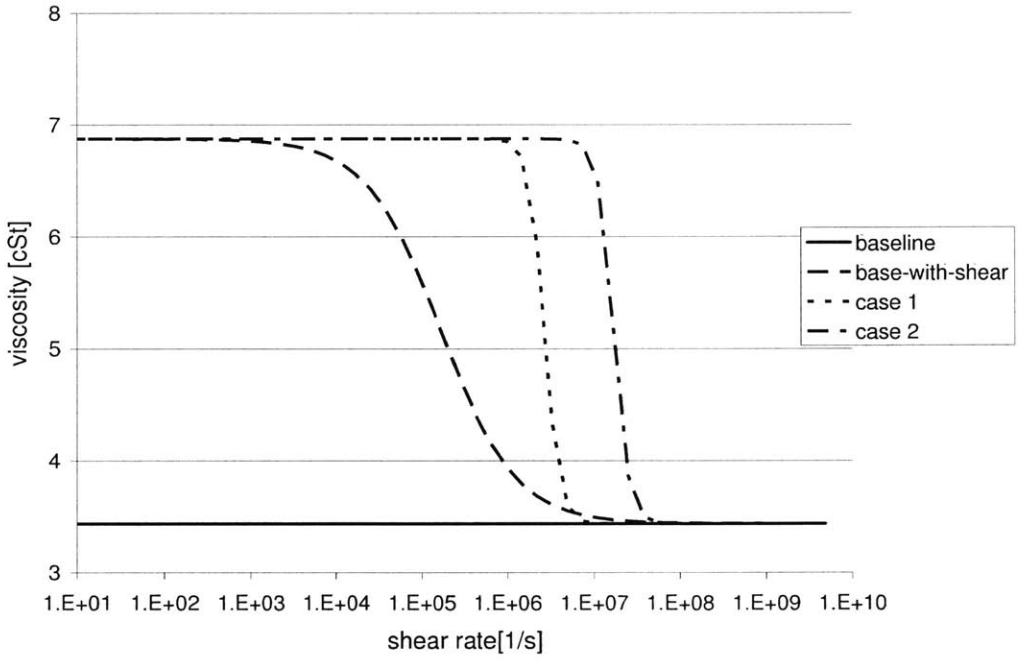

Figure 3-8: Viscosity variation with shear rate, for cases studied

3.5 Idealized cases: viscosity kept high near dead-centers

Ring/liner friction is closely related to lubricant viscosity - if viscosity variation during the engine cycle can be controlled, friction reduction may be possible. Several idealized cases were investigated analytically to assess this possibility. The main conclusion of these analyses is that viscosity in the mid-stroke region, where ring speed is high, is the most important parameter to control. Controlling viscosity near dead-centers was the focus of the initial investigation, and was shown to provide only a small possible friction reduction benefit. A greater advantage of controlling dead-center viscosity may lie in wear reduction, which is discussed in section 3.11.

As illustrated in Section 3.2, above, there is relatively little asperity contact between ring and liner near mid-stroke, but boundary friction becomes high near dead-centers. It was postulated that increasing end-stroke viscosity can reduce this dead-center friction, and thus reduce friction, as well as wear, overall. Several cases in which viscosity is increased or held high near dead-centers were studied. Initially, the mid-stroke viscosity in each of the cases is kept the same as the baseline case, so that the effect of the viscosity variation can be assessed independently of overall mean viscosity effects. The mid-stroke viscosity was chosen as a reasonable "mean" viscosity both because it is close to the actual mean for the baseline case, and because the mid-stroke region is the source of most of the ring frictional losses. The effect of reducing overall viscosity was subsequently evaluated. Examples of viscosity variation during the Waukesha engine cycle for the example cases discussed, as well as the baseline case, is shown in Figure 3-9.

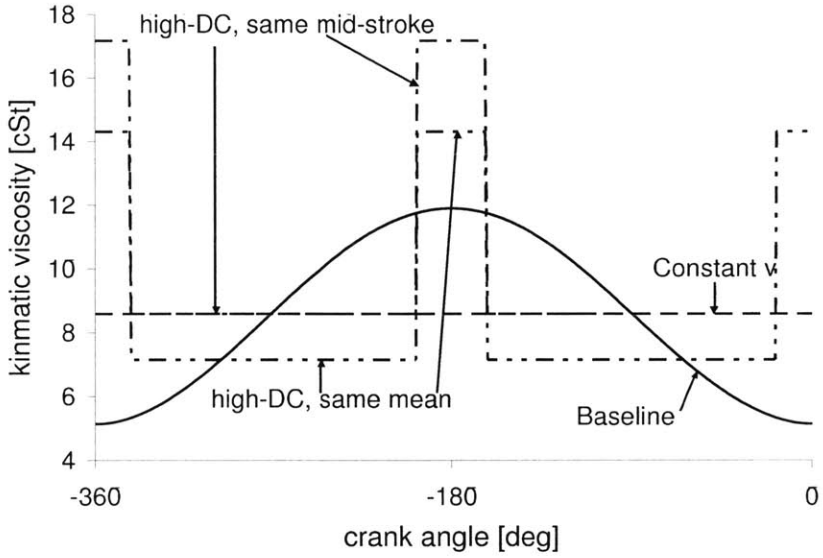

Figure 3-9: Viscosity variation during an engine cycle for three representative cases

Several different viscosity profiles were investigated in which viscosity near dead-centers was held high and viscosity near mid-stroke was held constant or reduced. In one group, a mean viscosity that was the same as the baseline case was maintained, and the width of the high-viscosity peak was varied (number of crank angles for which viscosity was held high). Because the mean was being held constant, the mid-stroke viscosity in this group varied. In a second group, the mid-stroke and dead-center viscosities were held constant, with the mid-stroke viscosity matching the baseline case, while the width of the high-viscosity peak was varied (so that here, the mean viscosity changed between cases). In both groups the end-stroke viscosity was maintained at twice the mid-stroke viscosity. These viscosity variation cases are referred to as "high-DC", for the high viscosity found near dead-centers. The group for which mid-stroke viscosity is kept constant is the focus of the results presented below.

When the mid-stroke viscosity is kept the same as the baseline case, there is only a small difference in friction between the baseline and high-DC cases. Two examples are shown, one in which the transition from high to low viscosity occurs near the crank angle at which boundary

and hydrodynamic friction are equal (about 18° ATDC), and one in which the transition occurs earlier (closer to dead-center) than this, at 12° ATDC (see Figure 3-11a). Figure 3-10 shows both high-DC cases compared to the constant viscosity case, which shows the effects of the viscosity variation more clearly than comparison with the baseline. Both high-DC viscosity strategies cause boundary friction to decrease near dead-centers, with a corresponding increase in hydrodynamic friction.

Figure 3-11b shows the net result of these changes. For the 18° case, there is a net reduction in friction close to dead-centers, but this is offset by a friction increase as the piston speed increases and hydrodynamic friction becomes important, (at around 12 ° ATDC, at the beginning of the stroke). The result is zero net change in FMEP compared to the constant-viscosity case – the reduction in boundary friction and increase in hydrodynamic cancel each other. For the12 ° case, there is the same net decrease in friction near the end-strokes, but the transition is timed well so that there is only a small subsequent increase in hydrodynamic friction. The result is a net decrease in FMEP, compared to the constant viscosity case. However, because the net reduction in friction is so small (note that the scale on the friction axis in Figure 3-11b is magnified) and the contribution to friction power loss near dead-centers is small, this reduction is negligible. Results for both cases are summarized in Table 3-1.

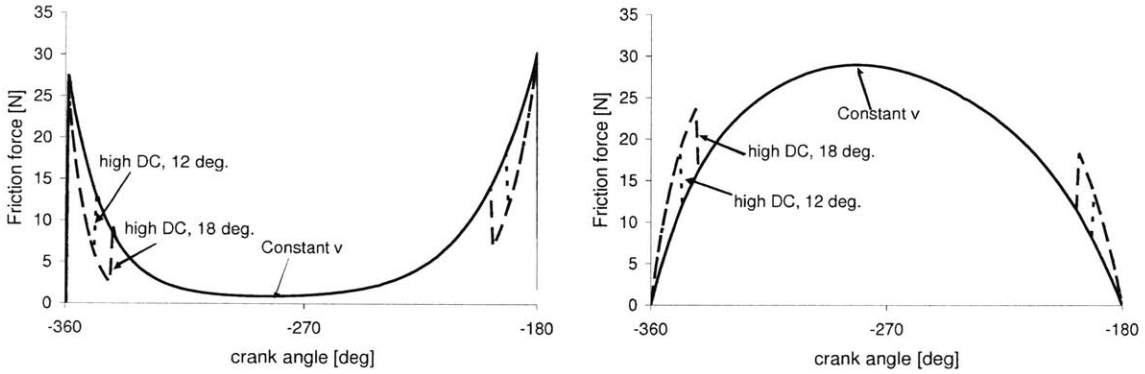

a) Boundary friction, constant viscosity and two high-DC cases, intake stroke

b) Hydrodynamic friction, constant viscosity and two high-DC cases, intake stroke

Figure 3-10: Effect of high-DC viscosity variation on hydrodynamic and boundary friction

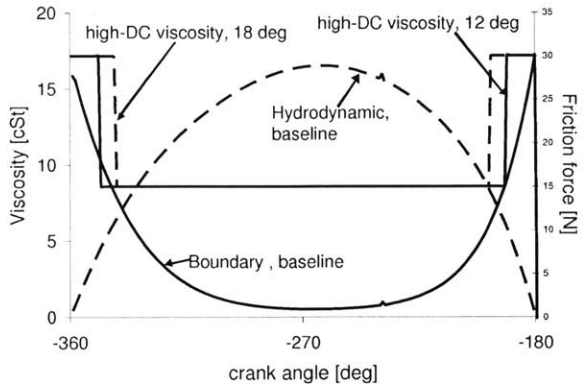

a)The transition crank angles for high-DC cases were based on the hydrodynamic/boundary transition

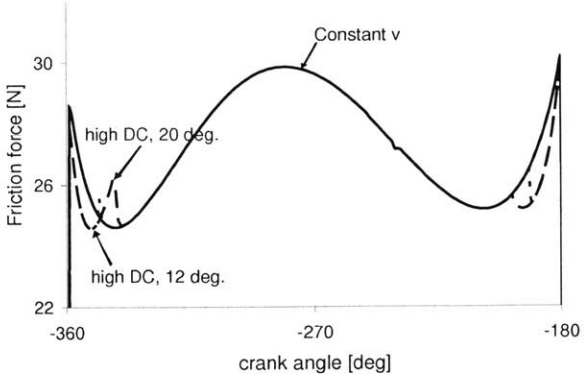

b) Total friction force for constant viscosity and two high-DC cases, intake stroke

Figure 3-11: Effect of high-DC viscosity on total ring/liner friction

A case in which mean, rather than dead center, viscosity was held the same as the baseline case was also considered. In the example shown in Figure 3-12, the high/low viscosity transition occurs at 18° ATDC. An overall reduction in friction of ~4% from the baseline was observed for this case, but the reduction was due entirely to a decrease in mid-stroke hydrodynamic friction, as shown in Figure 3-12 ,and did not stem from effects in the dead-center region. The same friction reduction could have been obtained by simply reducing mid-stroke viscosity.

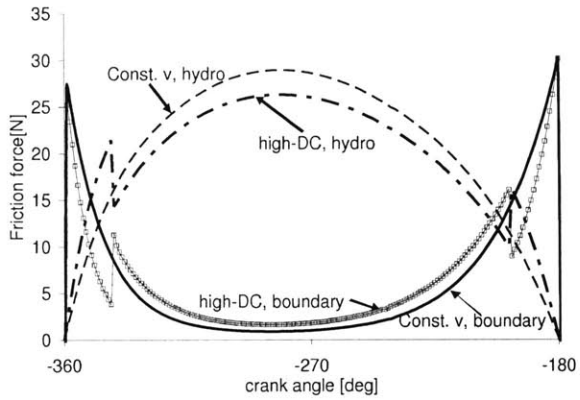

a) Hydrodynamic and boundary friction forces

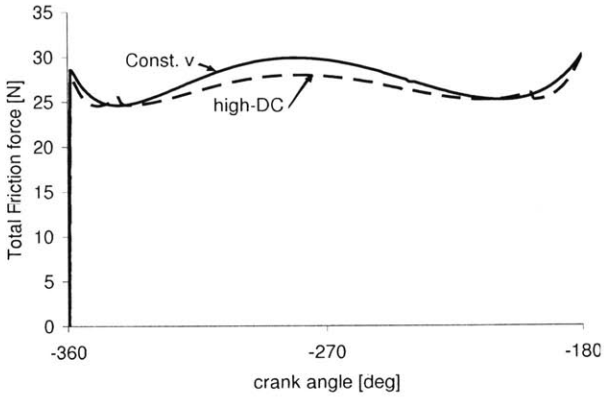

b) Total friction force

Figure 3-12: Comparison of friction force in high-DC and constant viscosity cases, lower land, OCR

These examples show that, for the cases studied, controlling viscosity near dead-centers has almost no effect on total cycle friction. One reason for this is that any reduction in boundary friction near dead-centers, if brought about by viscosity increase, is always at least partially offset by a corresponding increase in hydrodynamic friction. If the high/low transition is not well-placed, the increase in hydrodynamic friction may become large and result in a net increase in friction, rather than the desired decrease. If another method of reducing boundary friction – for example, with surface modifiers – can be used, and this increase in hydrodynamic friction can be avoided, a larger friction reduction benefit is possible, both at dead-centers and throughout the stroke

Another factor leading to the lack of benefit in controlling end-stroke viscosity is that the contribution to overall friction from dead-centers is only a small fraction of the total cycle losses. Although friction forces may be high, the slow piston speeds in this region keep friction power losses low. End-stroke boundary friction (where the "dead-center region" is taken as +/-18 crank-angle degrees around each ring-reversal) accounts for only a few percent of the total ring friction, as shown in **Error! Reference source not found.**. Then, any friction reduction associated with reducing boundary friction here is necessarily low.

Table 3-1: Friction affects of different viscosity variation cases, constant mid-stroke viscosity

	FMEP [kPa]	FMEP, boundary [kPa]	FMEP, hydrodynamic [kPa]	FMEP change, from baseline
Baseline	11.14	1.19	9.95	--
Constant viscosity	11.25	1.02	10.23	+1%
High–DC, same mid-stroke, 18 deg	11.25	0.88	10.34	+1%
High-DC, same mid-stroke, 12 deg	11.25	0.97	10.28	+1%
High-DC, same mean, 18 deg	10.72	1.32	9.4	-4%

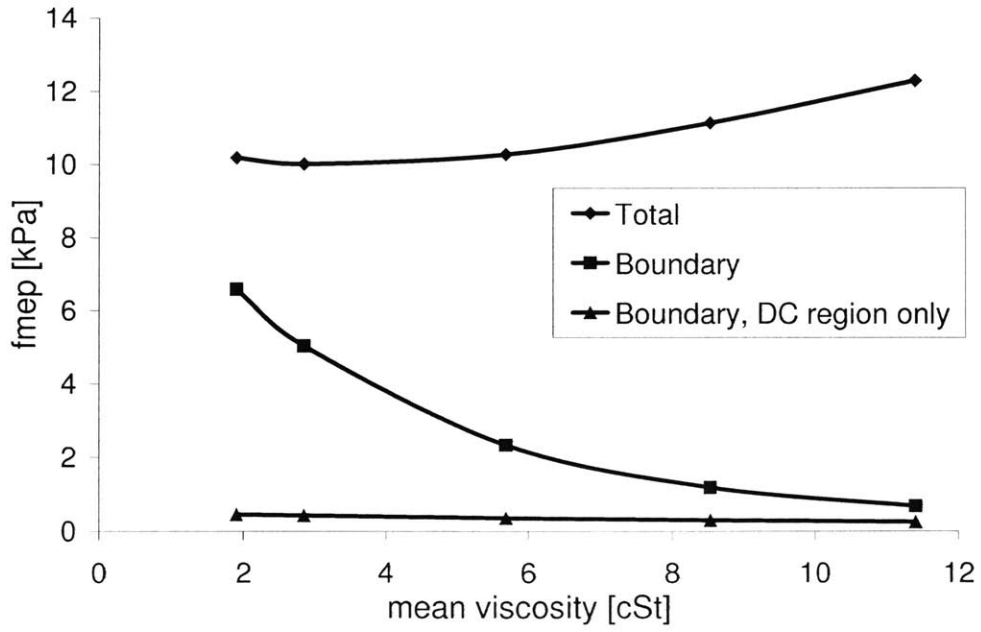

Figure 3-13: Friction forces and friction power loss, baseline viscosity

In poorly lubricated cases, surface dimples may also decrease friction by acting as "lubricant reservoirs" that help to maintain an adequate lubricant supply. Blatter, et. al.[39] demonstrated that the presence of small grooves (on a sapphire disk, sliding against steel) could cause a delay in the loss of lubrication in a case where a small amount of oil was introduced at the beginning of a sliding test, which was then allowed to run until failure (a sudden increase in friction coefficient). For some grooved cases, the number of cycles for which lubricated sliding was maintained was an order of magnitude greater than that for smooth surfaces. Lubricant reservoirs may be particularly useful where lubricant availability is intermittent. In these cases, dimples may act as "lubricant capacitors," storing oil when it is readily available and re-supplying it to the sliding interface when it is scarce.

4.1.2 Hydrodynamic effects

Like large scale converging surfaces, micro-scale asperities can create an asymmetric oil pressure distribution that results in hydrodynamic lift. In cases of mixed lubrication, this added lift can alter the balance between hydrodynamic and boundary lubrication, reducing the amount of asperity contact that takes place, and thus reducing both friction and wear. Also, even when contact does not occur, an increase in oil film thickness reduces shear within the oil, reducing hydrodynamic friction. Several studies, both analytical and experimental, have considered the effects of surface patterns in hydrodynamically lubricated cases.

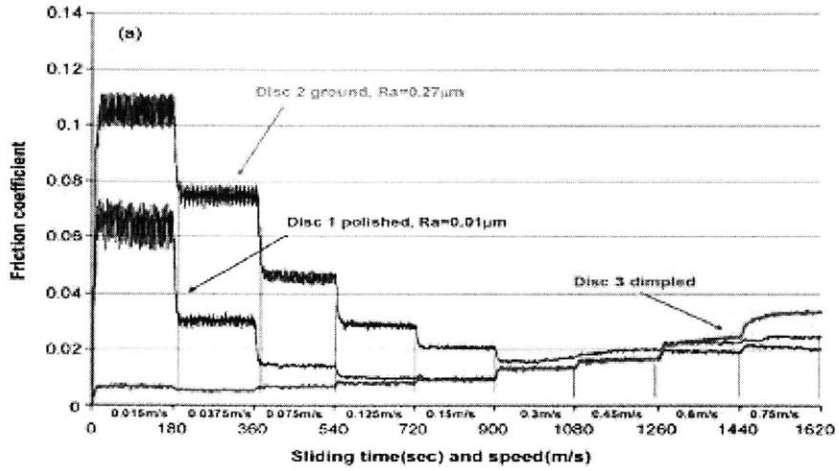

Figure 4-1: Adding dimples delayed the onset of asperity contact in this test, from Kovalchenko, et. al.[40]

Because they can assist in creating hydrodynamic pressure in the fluid film, textured surfaces have an effect on the lubrication regime of sliding surfaces. Kovalchenko et.al. looked closely at the lubrication regime effect in a series of experiments using a pin-on-disk test rig with unidirectional sliding, with a textured disk.[40] This study produced Stribeck-like curves for various lubricants and load conditions, and different dimpled area densities (the depth:diameter ratio for the dimples was maintained at an "ideal" value in all cases). In general, dimpling

3.5.1 Effects of mid-stroke viscosity, different viscosity variation cases

The three viscosity cases (baseline, constant viscosity, and high-DC) considered above were studied at different mid-stroke viscosities. For the high-DC case, the dead-center viscosity was held constant, and the mid-stroke viscosity reduced. As was indicated in Figure 3-4, total ring FMEP changes with viscosity, and a minimum FMEP is found at a balance between hydrodynamic and boundary friction. This study showed that this minimum friction loss is approximately the same for each viscosity condition studied.

In Figure 3-14, the results for the three cases are compared and plotted against mid-stroke viscosity. There is almost no difference between the three viscosity strategies for the range of viscosities studied, with the high-DC case showing a small (less than 1%) reduction in minimum FMEP. The high-DC case does provide a consistently lower boundary friction loss than the baseline case, but this is offset by a matching increase in hydrodynamic friction, as shown in Figure 3-15. Again, it is shown that the major effect of viscosity on friction is in the mid-stroke region, and controlling dead-center viscosity has a relatively small effect.

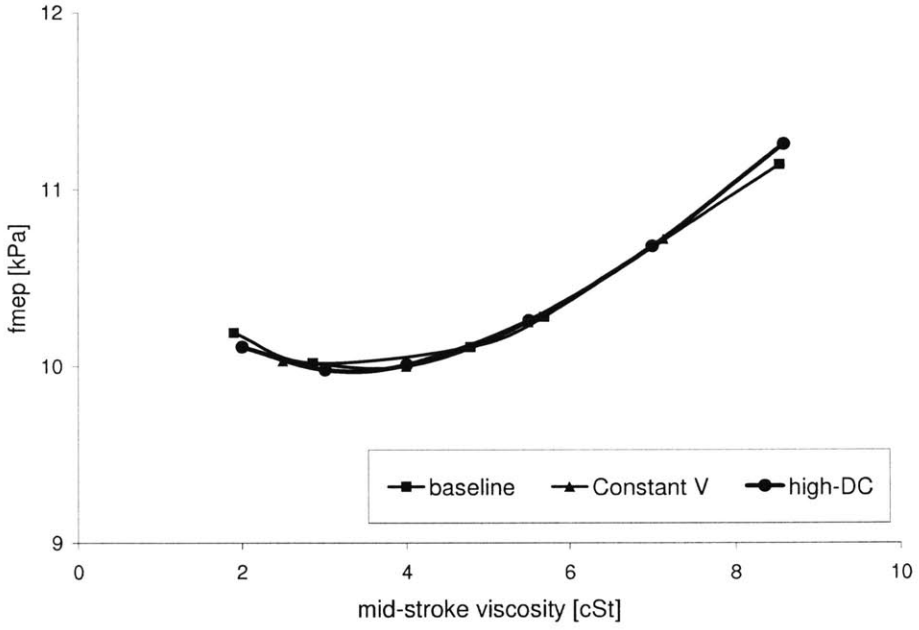

Figure 3-14: Reduction in total cycle friction with mean viscosity, three viscosity variation cases, OCR.

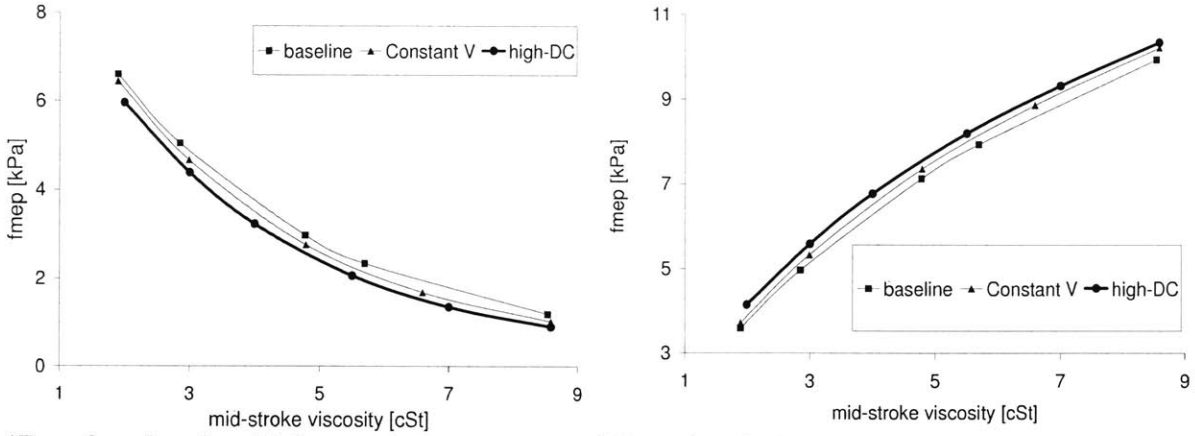

a)Fmep from boundary friction **b)Fmep from hydrodynamic friction**

Figure 3-15: Hydrodynamic and boundary contribution to total fmep, three viscosity cases

It should be noted that, although there is only a small friction benefit in controlling dead-center viscosity, there may be a wear benefit. High boundary friction is an indicator of wear, which indicates that a large amount of deterioration is expected near end-strokes. Although reducing asperity contact in this region may not substantially reduce frictional losses, it should cause a wear reduction. A simple analysis of this possibility was performed, and is discussed briefly in section 3.11.

3.6 Effects of viscosity temperature dependence

In addition to idealized cases, more realistic lubricants were also considered. Several temperature-dependence cases were considered, with the form of the dependence modeled using the Vogel relationship, given in Eqn. 3.1.The parameter T_1 was varied in order to vary the degree to which viscosity changes with changing temperature, while z was also changed proportionally, in order to maintain a constant average viscosity for the cycle. For all of the cases studied, the mean viscosity occurred near mid-stroke, so maintaining a constant mid-stroke viscosity was equivalent to maintaining a constant mean, with the amount of viscosity variation between TDC and BDC varying between cases. A range from a high temperature dependence to no dependence ($T_1 \sim 0$) was considered. Figure 3-16 shows the lubricant temperature change for an engine cycle, and the corresponding cycle lubricant viscosities for each case.

For each lubricant considered, the viscosity variation is close to symmetric about mid-stroke – that is, it is low on one side (either the beginning or end of the stroke), passes through mid-stroke at close to the mean viscosity, then is high on the other, as shown in Figure 3-16b. This is the same phenomenon that was described in Section 3.3, above. As in that case, the resulting change in friction is small, because the friction changes due to changing viscosity during each half of the stroke largely cancel each other out. Figure 3-17 shows that there is very little variation in FMEP for the oil control ring as the T_1 parameter is changed. Although there is a small decrease in hydrodynamic friction over the range of T_1 values, there is a corresponding increase in boundary friction that virtually cancels out this change.

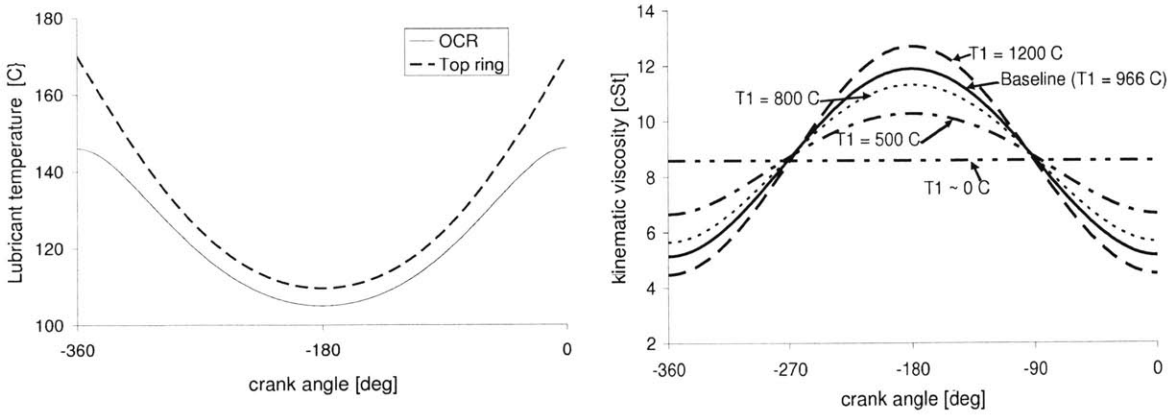

a) Temperature variation of oil film in the engine

b) Variation of viscosity for an engine cycle, 2 strokes

Figure 3-16: Variation of viscosity during an engine cycle for test cases considered

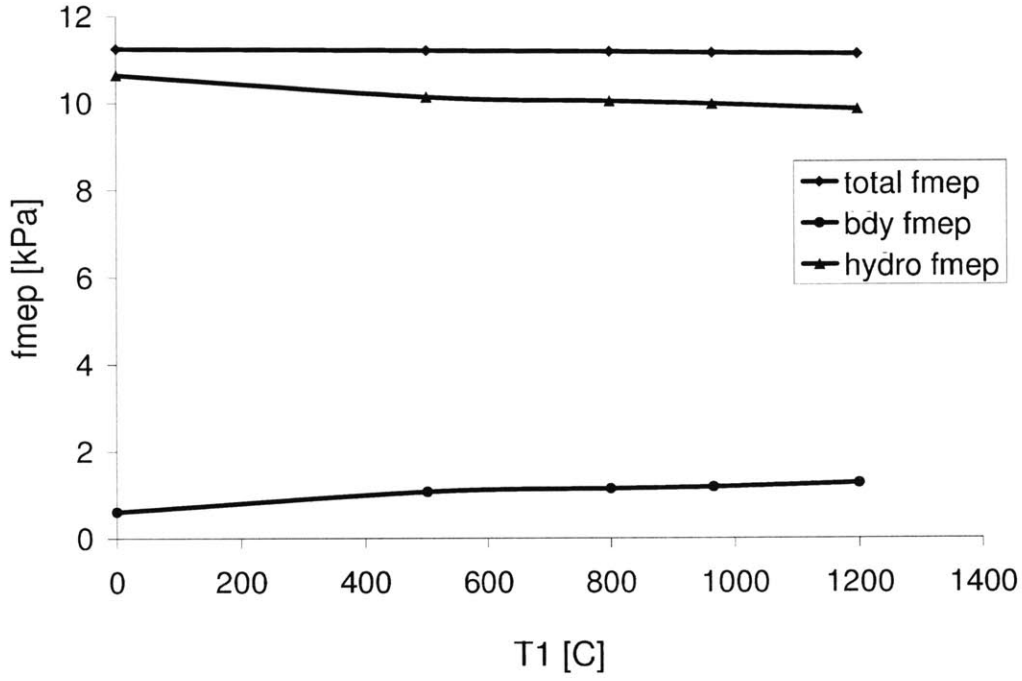

Figure 3-17: FMEP for the oil control ring is almost independent of viscosity temperature dependence

Simulations were also run considering the different temperature-dependence cases when the mid-stroke/mean viscosity was changed. An example of a group of profiles with different mean viscosities, with temperature dependency $T_1 = 800^{o}$ C, is shown in Figure 3-18. Figure 3-19 shows the results of the study – almost no change in friction losses is seen as the value of T_1 is varied, for any mid-stroke viscosity case. Cases with low T_1 (very little temperature dependence) showed slightly higher friction at high viscosities, due to a slight increase in hydrodynamic friction, but for the most part FMEP was unaffected by T_1, for the viscosity range

studied. Again, as described in Section 3.3, friction generation over a cycle remains approximately constant as long as the variation in viscosity is symmetric about mid-stroke.

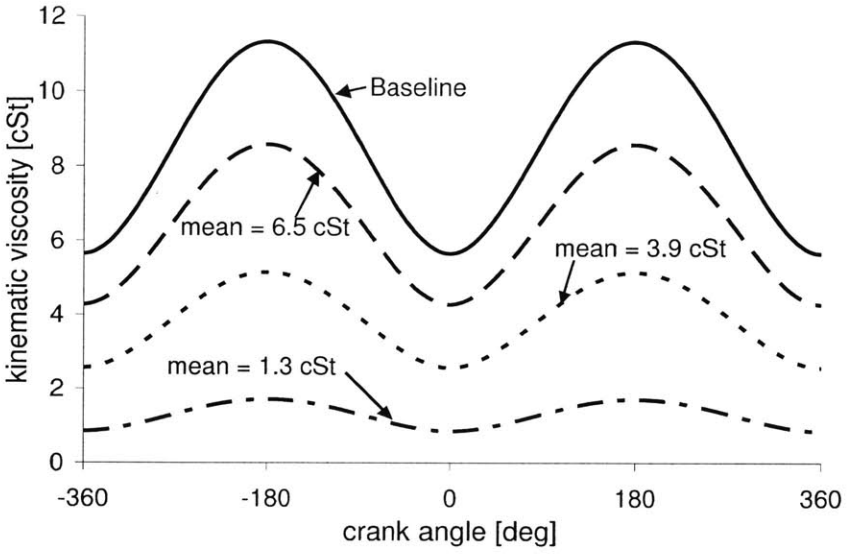

Figure 3-18: Viscosity variation during the engine cycle for changing mean viscosity, T_1 = 800C

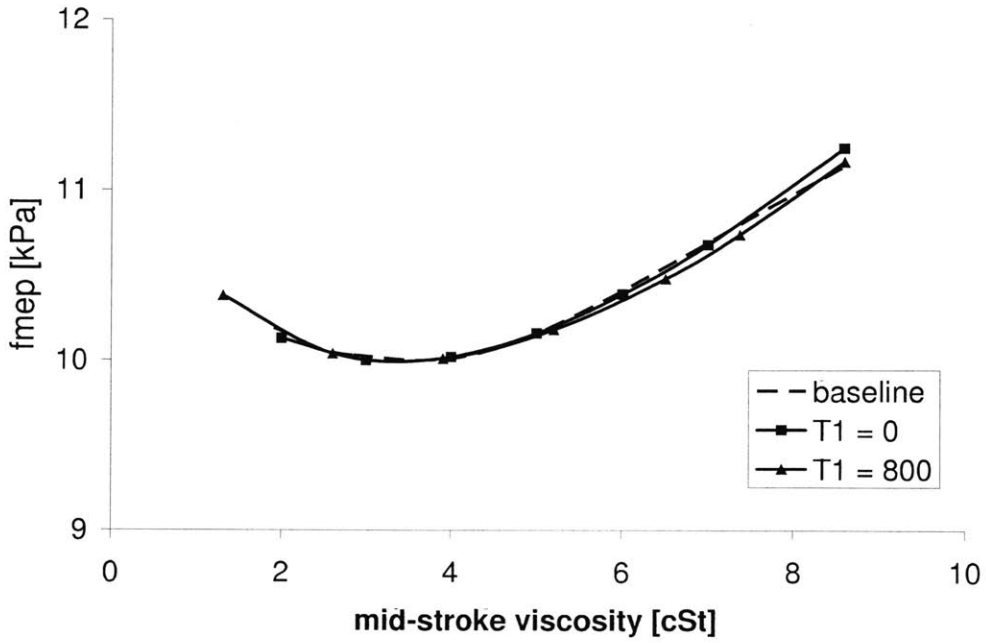

Figure 3-19: Dependence of fmep on mean/mid-stroke viscosity, different temperature dependence cases

3.7 Effects of viscosity shear-rate dependence

The effects of the shear-rate dependence of the lubricant viscosity were also studied. Evidence has shown that use of multigrade oils reduces engine friction compared to single grade, although the reason for this reduction is not well-understood, and the friction reductions measured may not have come from the ring-pack region[29]. The model used in this study indicates that, for most of the engine cycle, the piston rings experience a shear rate higher than the critical shear rate for most common engine oils. Because of this, the rings experience a lubricant that is virtually non-shear-thinning, except very close to dead-centers where very low piston speeds reduce the shear rate, and thus shear-dependency should have little effect.

In this study, shear-dependence properties were varied into ranges that are not currently found in typical engine oils. The effect of these unusual lubricants is to re-locate the critical shear rate so that the transition from high to low viscosity takes place during the stroke. The width of the transition region was also altered, between gradual and very sharp transitions. Using such unusual lubricants, the idealized cases described above, where viscosity can be held high near dead-centers and low near mid-strokes, are approximated (although the temperature dependence is still present). As is shown below, the results of this study are similar to those of the idealized case – friction benefits are relatively small – but the reduction in minimum friction that is achieved is slightly larger, ~1% below the baseline value.

Many sets of Cross equation parameters were studied, with the most successful (in terms of friction reduction) presented below. The parameters for these examples are given in Table 3-2, and variation in viscosity during the engine cycle corresponding to these cases is shown in Figure 3-20b, (the case "base-with-shear" is the baseline oil with shear rate dependence typical of common engine oils added, for use as a basis of comparison). As is shown in the figure, the effect of controlling the Cross equation parameters in this manner is to keep viscosity high near dead-centers and lower near mid-strokes, where the temperature dependency of the viscosity (which was kept at the baseline value) also contributes to the variation. The two cases 1 and 2 demonstrate the effects of changing the width of the high-viscosity region.

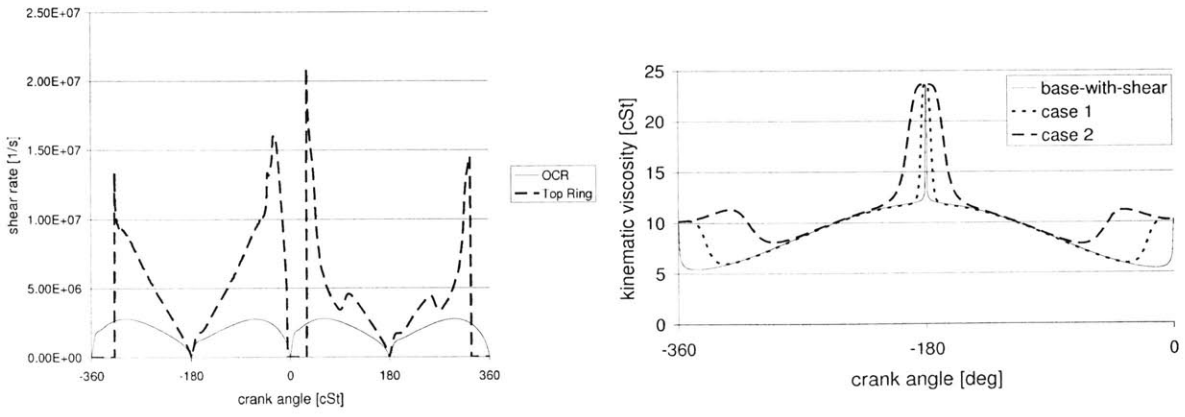

a) shear rate variation during an engine cycle **b) viscosity change during 2 strokes, studied cases**

Figure 3-20: Shear rate variation and viscosity (shear-rate dependent) variation during an engine cycle

Table 3-2: Cross equation parameters for three cases studied

Case	m	$\nu_{high\text{-}shear}/\nu_{low\text{-}shear}$	c_1	c_2	ν_∞/ν_0
baseline with shear*	1	.5	2.3	.0225	0.5
case 1	5	.5	3.8	.0225	0.5
case 2	5	.5	4.3	.0225	0.5

*** This case uses baseline parameters, except where ν_∞/ν_0=0.5, which adds shear dependence to the baseline case, which is a straight-weight oil. C_1 and C_2 are typical values for a shear-thinning engine oil.**

As in the idealized case, keeping viscosity high near dead centers causes a decrease in boundary friction there, with a corresponding increase in hydrodynamic friction, as is shown in Figure 3-21. When the mid-stroke viscosity is matched with the baseline case, the case 1 viscosity distribution shows a slight reduction in friction, vs. the baseline, while case 2 shows a slight increase. This is related to the hydrodynamic/boundary friction balance in the engine cycle. In baseline conditions, the high/low viscosity transition for case 2 occurs relatively late in the stroke, in a region where hydrodynamic lubrication accounts for a large fraction of the total ring/liner friction (see Figure 3-22.) Then, the effect of the high viscosity is to increase the already high hydrodynamic friction. For case 1, the high viscosity period remains within a zone where boundary friction is dominant, so that the reduction in boundary friction is slightly higher than the increase in hydrodynamic friction.

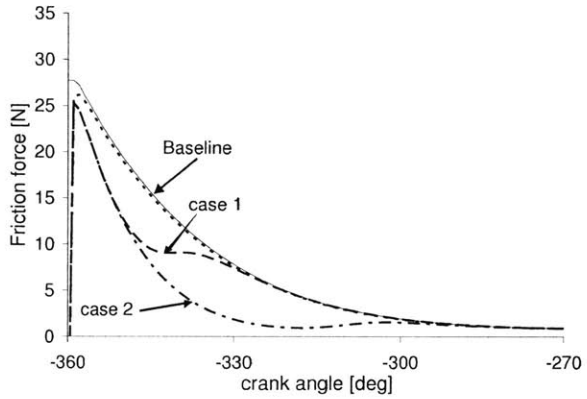

a)Boundary friction near TDC, intake, cases 1 and 2

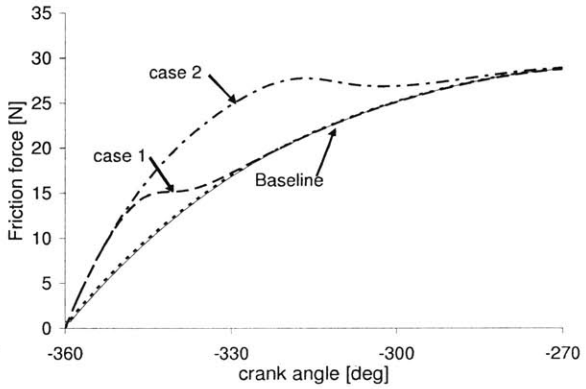

b)Hydrodynamic friction near TDC, intake, cases 1 and 2

Figure 3-21: Hydrodynamic and boundary friction effects in cases 1 and 2.

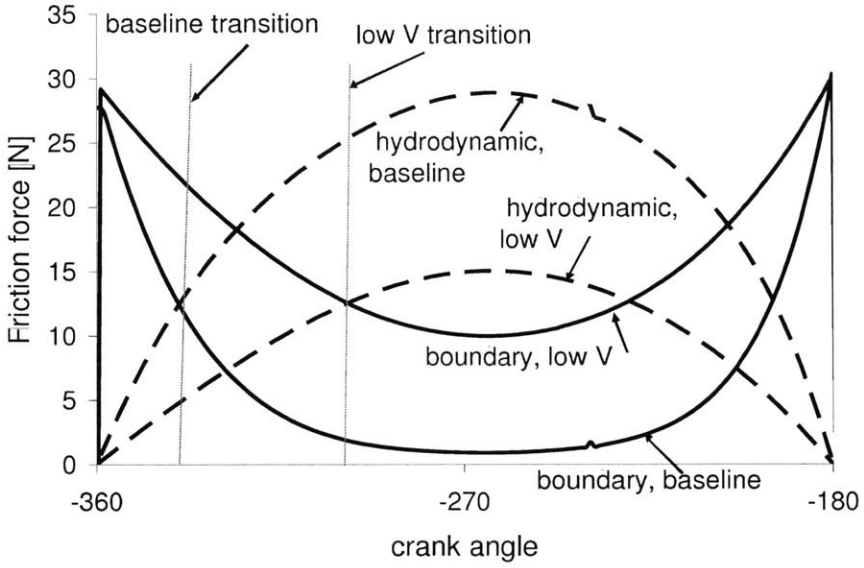

Figure 3-22: Transition from boundary-dominated to hydrodynamic-dominates regimes, baseline case.

As overall viscosity changes, the hydrodynamic/boundary friction balance in the engine cycle changes. In particular, as viscosity is decreased, hydrodynamic lubrication becomes less effective and boundary friction increases. The zone around dead-centers where boundary friction is dominant extends farther toward mid-stroke, and contributes more to total friction losses because it extends into a zone where piston speed is increased, as shown in Figure 3-22. Then, a larger high-viscosity zone, such as occurs in case 2, provides more benefit. This is shown in Figure 3-24, which shows the effect of changing mid-stroke viscosity on ring friction, for the cases considered. It also explains why no friction benefit is observed in the idealized case at low viscosity – the width of the high-viscosity region in the idealized case is not large enough to provide much friction reduction, because it remains within the low-speed, dead-center region.

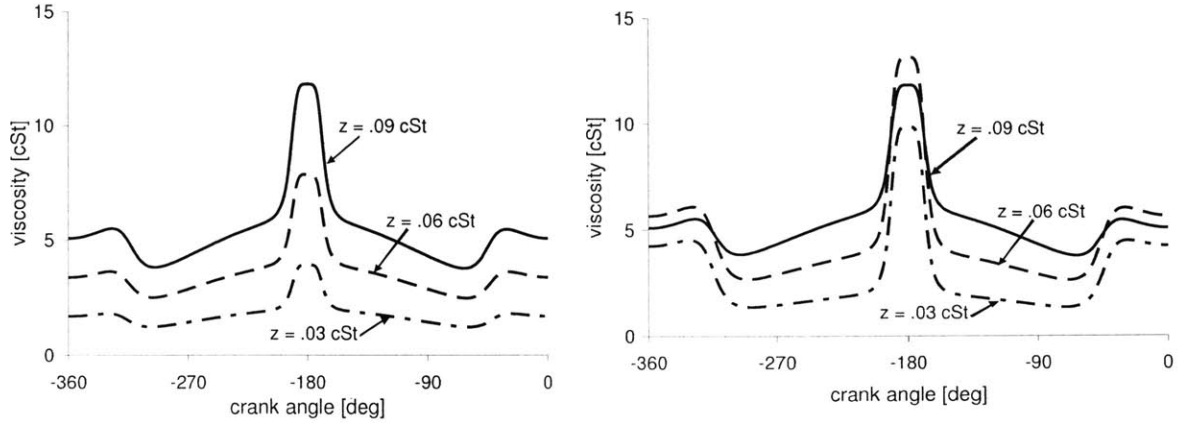

a) High/low shear viscosity ratio kept constant

b)High/low shear viscosity ratio set to maximize friction reduction for a given z value.

Figure 3-23: Viscosity variation during the engine cycle, case 2

It should be noted that, in Figure 3-24, the ratio of high-shear to low-shear viscosities is not kept constant as mean viscosity changes. This is because, as mean viscosity is reduced, the magnitude of the low-shear viscosity (the viscosity at dead-centers) decreases, as shown in Figure 3-23a. To counter this decrease and keep dead-center viscosity approximately constant, the high:low viscosity ratio was changed with mean viscosity - example of this are shown in Figure 3-23b.

Figure 3-24 shows the effects of changing mean viscosity for the cases considered, with the high/low shear viscosity ratio optimized for low friction, at a given mid-stroke viscosity. The figure shows that there is a small friction benefit of ~1% using case 2 parameters. Simply reducing mean viscosity can reduce cycle friction by about 10%. If viscosity variation is controlled in the manner described here, a total reduction in FMEP of ~11% may be possible, from the current baseline oil.

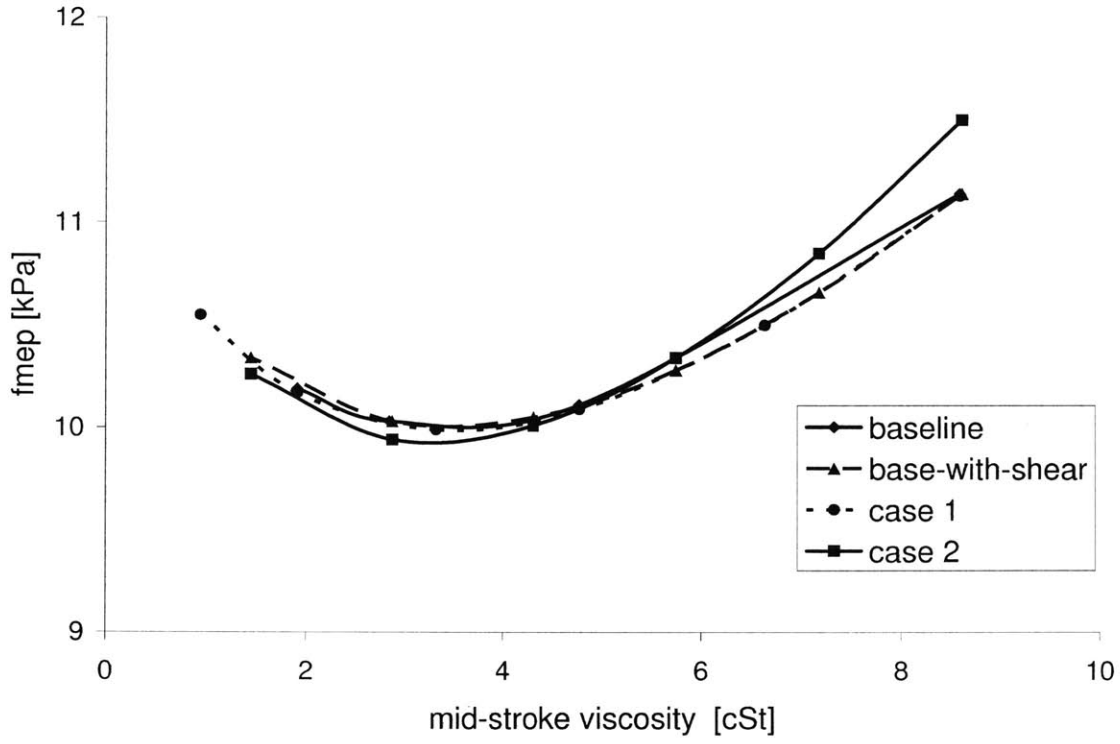

Figure 3-24: Dependence of OCR friction losses on mid-stroke viscosity, for different shear-rate dependence cases.

3.8 Top ring – dry region

Although changing the lubricant viscosity is expected to have its main influence on friction between the oil control ring and liner, the other rings may also be affected. Top ring friction may depend on oil viscosity via its effect on dry region lubrication, as described below. It should be noted, however, that the model used in this study includes only relatively simplified oil transport mechanisms and thus the results given here should be considered to be preliminary only.

The top ring experiences pure hydrodynamic lubrication during most of the stroke, but is subject to a large "spike" of boundary friction near TDC of combustion, as shown in Figure 3-25. This spike is caused by a combination of factors: very high post-combustion gas pressures and temperatures, slow piston speed and poor lubrication. Lubricant availability is very poor near TDC because the oil control ring does not reach this area, so the region is lubricated only by oil that is scraped up by the compression and scraper rings. Because of the very harsh conditions, this "dry region" is the site not only of high friction generation but also of high ring/liner wear and possible scuffing failure. It contributes the majority of top ring friction, and approximately 30% of total ring pack friction (see Figure 1-5).

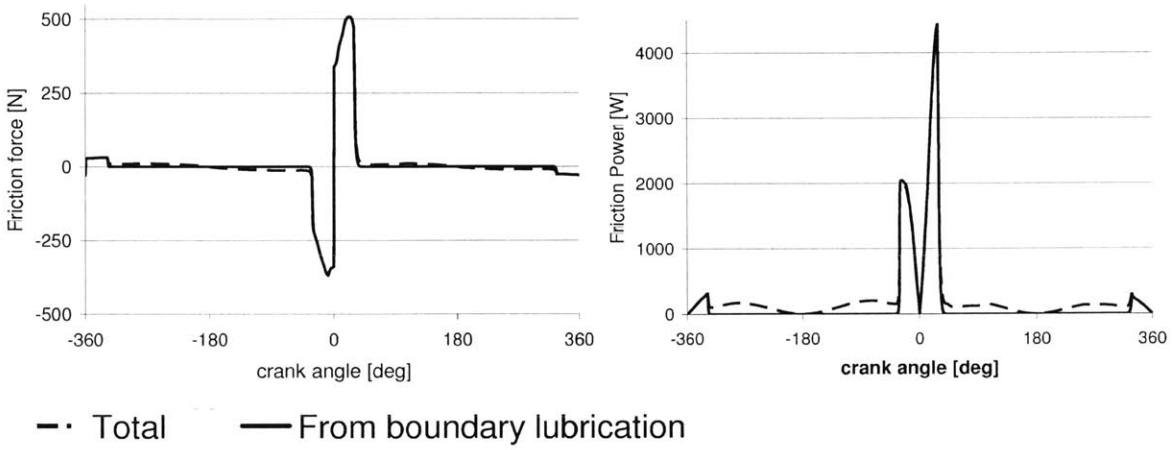

Figure 3-25: Top ring friction force (left) and friction power loss (right) for an engine cycle.

Lubricant viscosity does not have a direct affect on this major source of top ring/liner friction, because full boundary lubrication occurs there, and thus the frictional losses are affected only by the boundary friction coefficient. However, the lubricant viscosity may affect this region indirectly, by influencing the size of the poorly lubricated zone. As is shown in Figure 3-26a, simulations show that oil availability in the dry region is greater for thinner lubricants. The result is less asperity contact and a smaller "spike" of high ring/liner force, as shown in Figure 3-26b.

Figure 3-26a shows the change in dry-region width with oil viscosity, for an idealized case where viscosity is constant throughout the cycle. As the figure shows, the dry region (the relatively flat region, between the sharp drop and subsequent sharp rise in film thickness) increases in width as viscosity increases, approaching a maximum. For very low viscosity ($\nu = 1$ cSt) there is almost no dry width. For viscosities greater than $\nu \sim 5$ cSt, there is very little change in dry region width – a maximum dry width and maximum boundary friction have been reached. Between these values, the size of the un-wetted region increases with lubricant viscosity. This corresponds to the boundary friction force shown in Figure 3-26b. For the lowest viscosity case, the "spike" barely appears and is replaced by a region of gradually decreasing boundary friction. As viscosity increases, the width of the boundary friction "spike" increases with the viscosity until it reaches a maximum.

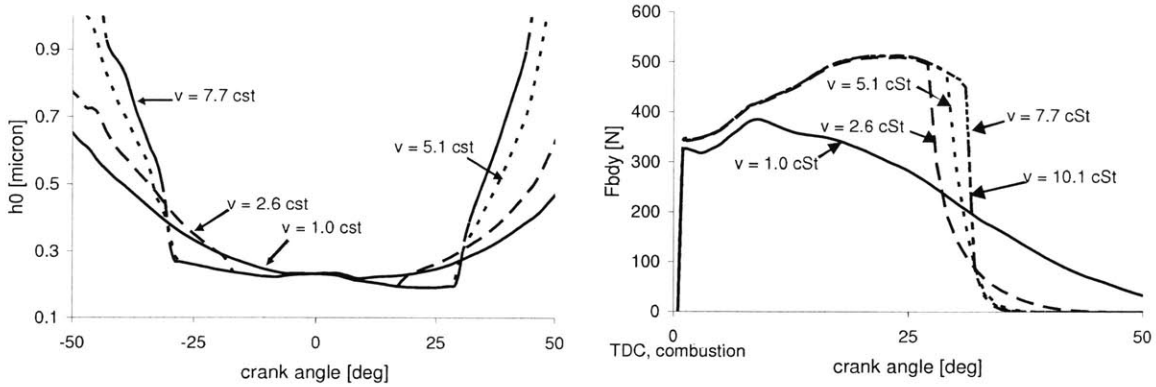

a)Minimum film thickness, h0, near TDC combustion **b)Boundary friction near TDC combustion (0 deg)**

Figure 3-26: Dry region width increases with lubricant viscosity, for the top ring

These results indicate that thinner oils are transported into the dry zone more easily than thicker oils. Figure 3-27 illustrates one mechanism related to this phenomenon. The extent of lubricant upscraping depends on oil availability on the liner before the dry region and the ring/liner clearance, as well as other factors such as the ring load. For thinner lubricants, the distance between ring and liner is smaller, because low viscosity oils create thinner hydrodynamic films in response to ring load. This is illustrated in Figure 3-27b, where h_0 can be used as an indicator of ring/liner clearance. This encourages up-scraping for thinner oils. However, there is also less available lubricant for thinner oils, for the same reason – the smaller clearance causes more oil to be scraped down the liner on down-strokes. The balance between these two factors plays a part in determining how much oil is scraped up the liner.

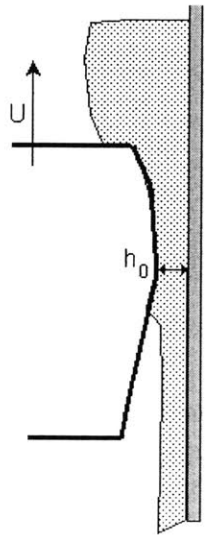

a) upscraping by top ring

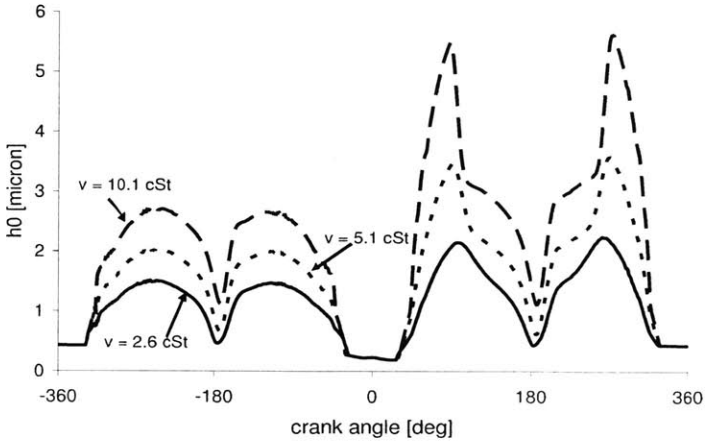

b) ring-liner separation increases with lubricant viscosity (units are cSt)

Figure 3-27: Lubricant upscraping mechanism

The total cycle friction losses for the top ring depend on both transport of oil into the dry region and the ability of the oil to support hydrodynamic lubrication in the rest of the stroke. This is illustrated in Figure 3-26b. For the lowest viscosity of 1cSt, the height of the dry region "spike" is decreased, but its width is increased. This very low viscosity oil was easily transported into the dry region, but then was too thin to support hydrodynamic lubrication for the remainder of the stroke. Higher viscosity oils may result in higher friction in the dry-region, but reduce boundary contact outside of it. In Figure 3-28, a minimum FMEP is found at a viscosity at which these factors are balanced. At higher viscosities, boundary friction remains approximately constant with viscosity, consistent with Figure 3-26, which shows that dry region width stays constant once a viscosity limit is passed. At lower viscosities, friction increases due to increased asperity contact outside of the dry region.

Comparing Figure 3-28 to **Error! Reference source not found.** for the oil control ring, the minimum frictional losses for the two rings occur at approximately the same viscosity. Then, an additional benefit in reduction of top ring friction may occur if viscosity is reduced to this value, without any negative effect on OCR operation. A reduction in top ring friction of ~ 30% is predicted, which corresponds to a ring-pack friction reduction of ~ 9%. However, increasing oil upscraping may increase oil consumption, which must also be considered in the total engine design. Also, it is not clear whether this is a real benefit, or only appears due to model assumptions or simplifications.

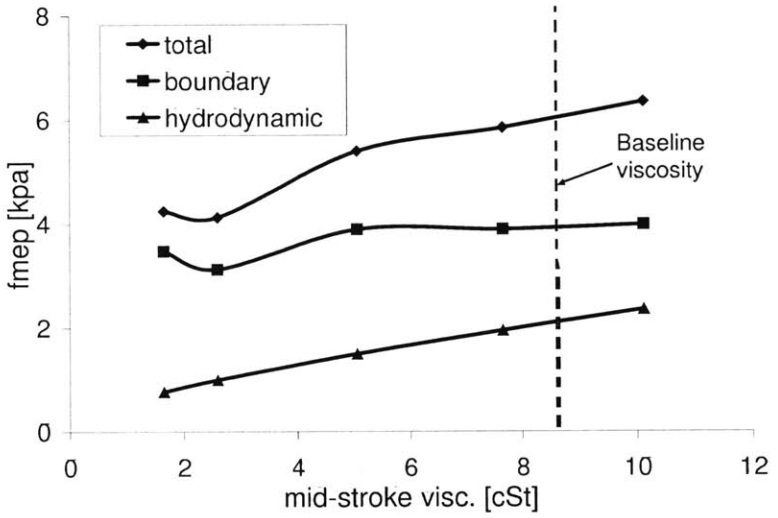

Figure 3-28: Dependence of top ring friction on lubricant viscosity, baseline viscosity case

The details of the oil transport mechanisms are not well-understood, and, thus, the results shown here should be considered to be preliminary. The ring-pack simulation used in this study uses a simplified oil transport model, which does not include several transport mechanisms that would affect dry-region lubrication. Also, other studies[30] have shown the opposite trend – an increase in dry-region wetting with higher viscosity. Further research is required to determine the extent of viscosity effects on dry region width and top ring friction.

3.9 Boundary friction coefficient

If ring/liner boundary friction coefficient can be reduced - for example, with surface-modifying lubricant additives - a large friction benefit is possible. Decreasing boundary friction coefficient, f_b, reduces ring/liner friction both directly, by reducing friction due to asperity contact, and indirectly, by allowing lubricant viscosity to be reduced and thus reducing hydrodynamic friction as well. The latter effect occurs because changing f_b alters the balance between hydrodynamic and boundary friction for the ring and liner - a low friction coefficient allows viscosity to be reduced without incurring a large friction penalty because of the increased asperity contact. The lower f_b becomes, the lower the viscosity can become before the corresponding increase in asperity contact - and thus boundary friction - out-balances the reduction in hydrodynamic friction that resulted from the viscosity reduction. This is illustrated in Figure 3-29, which shows the dependence of total ring-pack FMEP on boundary friction coefficient for changing lubricant viscosities (baseline temperature dependence assumed).

As is shown in the figure, at a given viscosity, reducing f_b causes a reduction in total friction - this results from the direct reduction of boundary friction with decreasing friction coefficient that is shown in Figure 3-29b. Also, the viscosity at which the minimum frictional loss occurs decreases with f_b, as does the minimum friction - this is a result of the effect of f_b on the hydrodynamic/boundary friction balance. Baseline values are $f_b = 0.1$, mean viscosity~8.6 cSt. Reducing boundary friction coefficient has a dual effect on ring/liner friction - it both reduces boundary friction and allows a lower viscosity lubricant to be used, thus reducing hydrodynamic friction – and thus can have a substantial, beneficial effect on overall ring-pack friction.

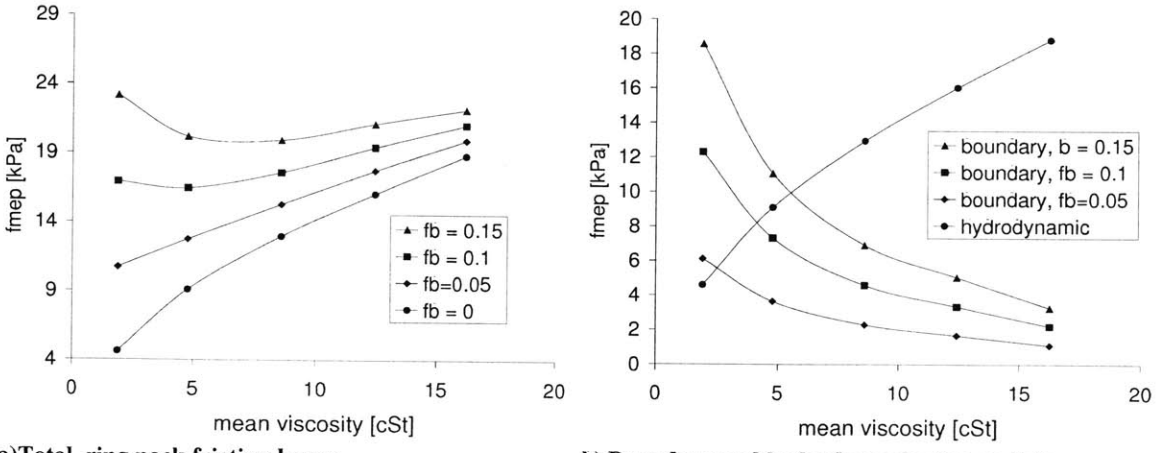

a)Total ring pack friction losses **b) Boundary and hydrodynamic ring-pack losses**

Figure 3-29: Effect of boundary friction coefficient on total ring-pack friction

3.10 Interaction of lubricant viscosity with other ring parameters

The effects of lubricant viscosity on ring/liner friction are dependent on the existing hydrodynamic/boundary lubrication balance. Depending on which lubrication mode dominates, an increase or a decrease in viscosity may be required to reduce friction. Several parameters affect this balance, including the ring tension and ring and liner roughnesses. The interaction between these parameters and lubricant viscosity were considered, and are presented below. Table 3-3 gives the ranges of ring parameters considered, as well as the ranges lubricant properties considered in the studies presented above.

Table 3-3: Ranges of ring and lubricant parameters considered

Parameter	Range	Baseline value	Unit
Ring tension	81-40	81	N
Ring surface roughness, R_q	0.05 – 0.2	0.1	micron
Boundary friction coefficient, ring/liner	0.05 – 0.15	0.1	-
T_1, Vogel equation (controls T dependence)	0 - 1200	965.76	°C
c_1, Cross equation (controls critical shear rate)	2.3 – 4.3	-	-
m, Cross equation (controls transition width)	1-5	-	-
μ/μ_0, Cross equation (controls high/low viscosity ratio)	1-.1	1	-

3.10.1 Ring tension

The ring tension is one factor that controls the hydrodynamic/boundary friction balance. With other parameters constant, as ring tension is reduced oil film thickness increases and asperity contact decreases. Regions of the ring stroke that experience mixed lubrication at high ring tension may experience pure hydrodynamic lubrication at lower tension (see Figure 3-30a). Also, the ring tension can affect the lubricant viscosity, if it is dependent on shear-rate, as shown in Figure 3-30b. A lubricant that is optimized to balance hydrodynamic and boundary contributions to ring friction must take these effects into account.

The interaction between ring tension and lubricant viscosity is illustrated using the example of the "case 2" viscosity distribution, which is described in section 3.7, above. For this case, the shear-dependence of the viscosity is controlled to produce high viscosity near dead-centers and low viscosity near mid-stroke. The high/low viscosity transition point is matched to the transition between the high boundary friction near dead-centers and high hydrodynamic friction near mid-stroke, for the baseline ring tension of T=81N. When the ring tension is reduced, the case 2 transition point is no longer well-matched to the lubrication regime of the ring.

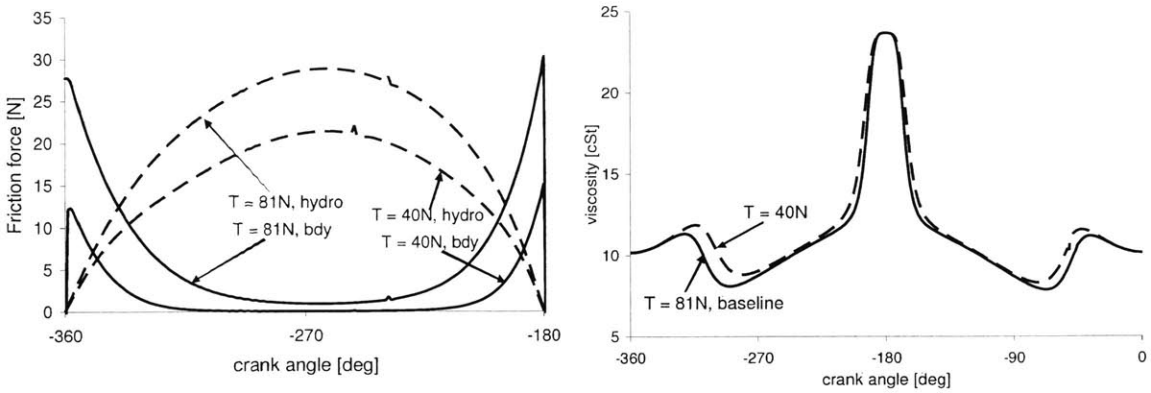

a) Lower ring tension leads to reduced asperity contact and a larger hydrodynamic region

b) Shear rate in the oil depends on ring tension, so lubricant viscosity does as well

Figure 3-30: The lubrication regime of the ring depends on ring tension

Figure 3-30a shows that for a ring tension of 40N only a small amount of asperity contact occurs, very close to dead-centers. For the case 2 viscosity distribution, viscosity is still held high outside of this region, because it was intended to apply to a higher tension ring that experienced more asperity contact. In addition to this, as is shown in Figure 3-30b, the high/low viscosity transition occurs even later for the reduced tension ring, because shear rates in the oil are lower. The result of these effects is a high friction loss, compared to the baseline viscosity, because of increased hydrodynamic friction. This is shown in Figure 3-31. For high mid-stroke viscosities (viscosities that are high enough to maintain hydrodynamic lubrication at mid-stroke), the case 2 viscosity distribution gives higher friction than the baseline. As ring tension is decreased, the increase in friction due to the case 2 distribution increases.

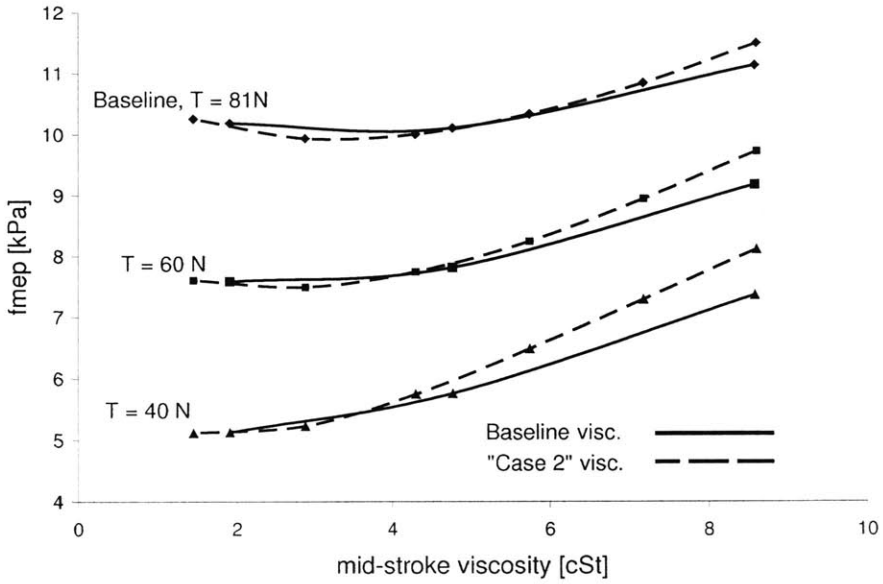

Figure 3-31: Interaction of ring tension and viscosity effects, comparing baseline and "case 2" viscosity distributions

Figure 3-31 also indicates that as ring tension is reduced the benefits of using the case 2 strategy at low viscosities are reduced. For T = 40N, the baseline and case 2 FMEP values are almost the same for mid-stroke viscosity less than 4cSt. This is because the friction benefit of the case 2 viscosity distribution lies in reducing boundary friction, and, as ring tension is reduced, boundary friction also decreases. For low ring tensions there is very little benefit to reducing dead-center asperity contact, because the high contact region is small and exists only where piston speeds are very low.

3.10.2 Ring surface roughness

Ring/liner friction has a more complicated dependence on surface roughness than on ring tension. Friction may increase or decrease with surface roughness, because this parameter (described here by the standard deviation of the surface mean height) affects both asperity contact and hydrodynamic lubrication. For a rougher surface asperities are larger, and so asperity contact occurs at a larger film thickness. Then boundary friction tends to increase with roughness, as shown in Figure 3-32a. However, hydrodynamic friction tends to decrease with roughness, as shown in Figure 3-32b, because of the effect of the surface texture on oil flow and hydrodynamic pressure generation. In general, friction tends to increase with ring roughness, but in the region near the baseline roughness of the Waukesha engine, R = 0.1μ, the opposing hydrodynamic and boundary effects make the influence of the surface texture less clear. In Figure 3-33 and Figure 3-34, it should be noted that ring friction is lowest for the mid-range roughness, R = 0.1μ, and both the smoother and the rougher cases exhibit higher friction.

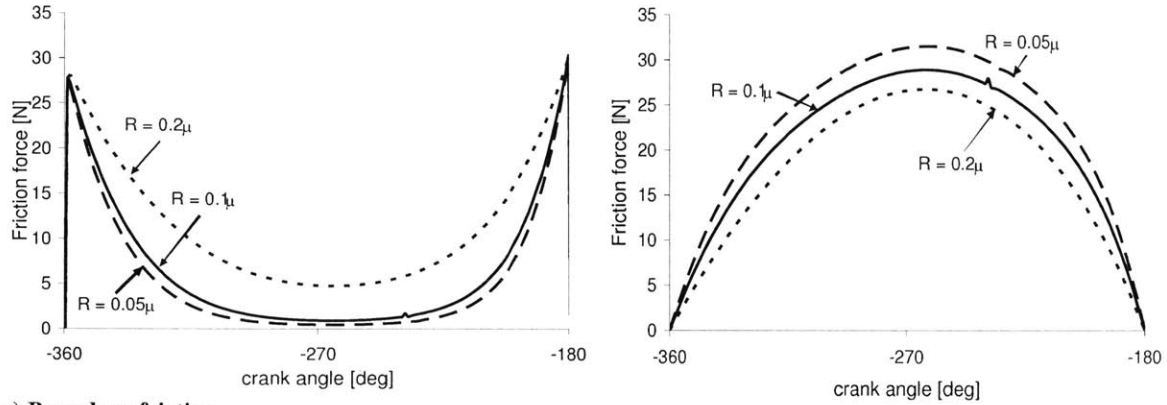

a) Boundary friction

b)Hydrodynamic friction

Figure 3-32: Effect of ring surface roughness on friction, intake stroke

The constant viscosity and "case 2" viscosity cases are compared to the baseline case, for different roughnesses, in Figure 3-33 and Figure 3-34. Both figures show that for the roughest case, R=0.2μ, viscosity effects are the weakest. This may be because the large asperities prevent a substantial reduction in boundary friction from occurring, negating any benefits from the constant viscosity and "case 2" cases. For the two lower roughness cases, the effects of viscosity are similar. A small reduction in minimum friction is observed for both the constant viscosity and case 2 distributions, while friction is slightly larger at higher viscosities. It appears that a

large roughness can negate the benefits of controlling viscosity variation during the cycle (for the cases considered), but for baseline and lower roughness, there is little lubricant/roughness interaction.

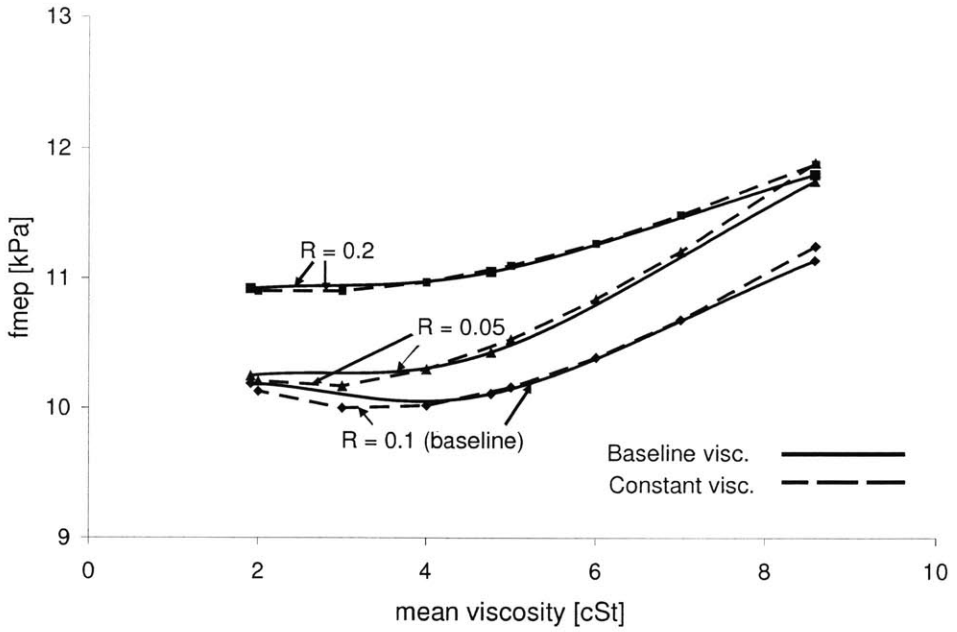

Figure 3-33: Interaction of ring roughness and viscosity effects, baseline and constant viscosity

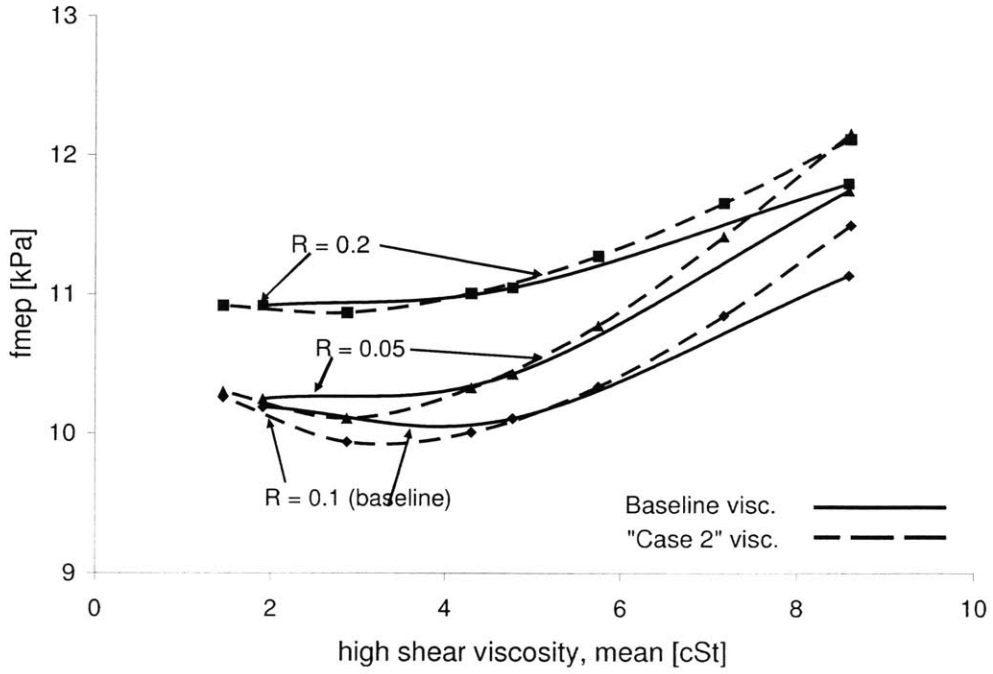

Figure 3-34: Interaction of ring roughness and viscosity effects, baseline and "case 2"

3.11 Wear

In addition to frictional losses, wear of the rings and liner must also be taken into account when designing an optimized lubricant. Ring/liner wear leads to leakage of combustion gases out of the engine cylinder ("blow-by") and a corresponding reduction in efficiency and increase in engine emissions. Limiting this degradation of engine performance, and avoiding the need to service and replace parts, requires that ring/liner wear be controlled.

The actual wear of the ring and liner is a complicated and not well-understood phenomenon, and real wear predictions have not been made in this study. Instead, a factor is calculated which takes into account the two main contributors to wear: asperity contact pressure and sliding distance. The wear factor presented is a mean factor for an engine stroke, and is calculated as the integral of the ring/liner contact pressure over the distance traveled by the ring.

The wear factor increases as mean lubricant viscosity is reduced, as is shown in Figure 3-35a, because the amount of asperity contact occurring increases for thinner oil films. Figure 3-35b shows that wear increases strongly even as frictional losses remain low – the minimum FMEP is found at a viscosity corresponding to a high wear rate. Then, choosing an ideal lubricant viscosity represents a balance between friction and wear considerations – the desire for low friction must be balanced against a need for low wear.

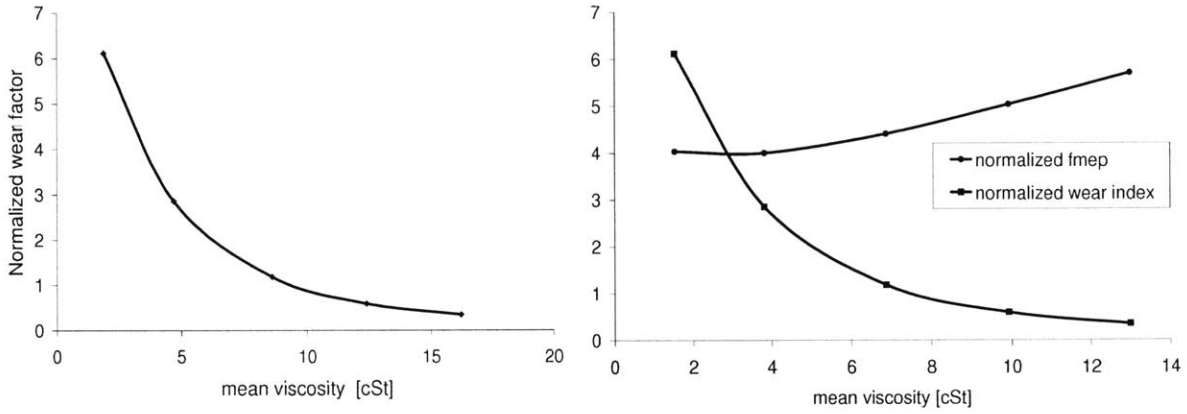

a) Wear increases as viscosity decreases

b) Minimum friction occurs at a large wear factor

Figure 3-35: Effect of lubricant viscosity on friction and wear parameter

It is possible to decrease wear somewhat by controlling the viscosity change during the engine cycle, as is shown in Figure 3-36, where the baseline lubricant is compared to the controlled shear-dependence "case 2" lubricant, described in section 3.7. Maintaining high viscosity near dead-centers can reduce asperity contact in the end-stroke regions, decreasing wear. Figure 3-36a shows that maintaining low viscosity near the end-stroke does cause a decrease in wear in that region (in the second half of the intake stroke baseline viscosity is also high near BDC because of low temperatures). Figure 3-36b shows the wear parameter integrated

over an engine cycle. As the figure shows, the "case 2" viscosity variation reduces wear parameter over a cycle by ~25%, by reducing end-stroke asperity contact.

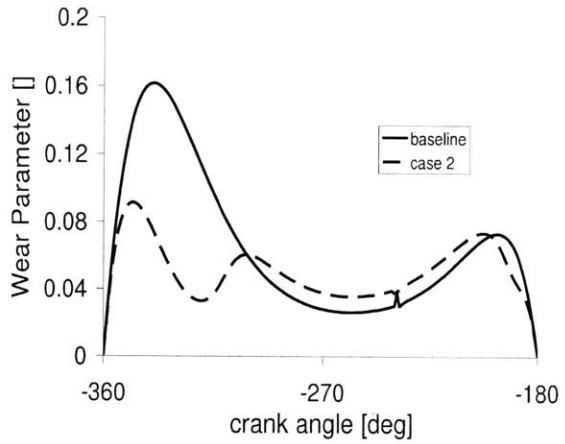

a) wear parameter is decreased when viscosity is increased

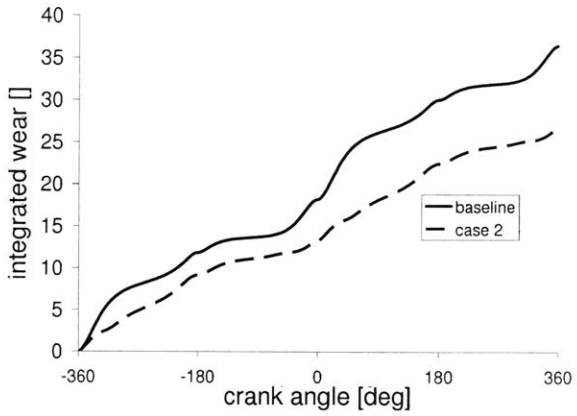

b) the "case 2" viscosity distribution shows lower net wear than the baseline case, for an engine cycle

Figure 3-36: Wear parameter is reduced when viscosity is kept high near end-strokes

3.12 Summary and conclusions of lubricant study

The piston rings experience hydrodynamic, boundary, and mixed lubrication modes during engine operation, where the amount of friction loss due to each mode depends on engine design and running parameters. For given parameters, the lubricant viscosity plays a main role in determining the lubrication mode, as well as the frictional losses during the engine cycle. In this study, the role of lubricant viscosity in controlling ring/liner lubrication, and thus ring/liner friction, was considered. The viscosity can be used to optimize the lubrication regime, leading to reductions in friction and wear.

Oil viscosity affects friction directly in the hydrodynamic regime, where hydrodynamic friction increases with viscosity. It also influences boundary friction indirectly by controlling oil film thickness, and thus the amount of asperity contact that occurs. Reducing viscosity can reduce hydrodynamic friction but also causes a decrease in oil film thickness that makes asperity contact more likely. A thicker oil may reduce boundary friction but increase hydrodynamic losses. At the optimum viscosity (the viscosity at which minimum friction losses are incurred) there is a balance between hydrodynamic and boundary lubrication.

As piston speed, ring loading, and other parameters change during the engine cycle, the optimum oil viscosity also changes. Near mid-stroke, high speeds support hydrodynamic lubrication, making a low viscosity lubricant desirable to reduce hydrodynamic losses. Near dead-centers, however, low speeds cause hydrodynamic support to decrease. Then, a high viscosity oil is desirable in these regions, to maintain thicker oil films and reduce asperity contact. It may be possible to control viscosity variation during the cycle so that the viscosity is optimum at all times. Several idealized and realistic cases were studied to quantify the friction

benefit obtainable with this method.

Idealized cases with low mid-stroke viscosity and high dead-center viscosity were considered, as were several more realistic cases based on typical temperature and shear-rate dependencies. It was found that friction reduction is possible when viscosity variation during the cycle is controlled, but it is small compared to the reduction that can be obtained simply by reducing mid-stroke viscosity from the baseline value. Two mechanisms lead to the small size of the friction benefit: the contribution to total cycle ring friction from the dead-center area is small, because of low piston speeds there; and any reduction in asperity contact is accompanied by an increase in hydrodynamic friction, which cancels out some of the benefit. Oil viscosity near mid-stroke, where most of the ring/liner friction is generated, is the dominant viscosity that controls the overall friction losses for the ring.

When this mid-stroke viscosity is reduced, the FMEP reduction for the Waukesha engine ring-pack, which is the focus of the current study, was found to be ~7% based on lubricant effects on the oil control ring alone. However, this reduction will come at the price of increased wear because of reduced oil film thicknesses. Although it does not contribute greatly to friction reduction, maintaining high lubricant viscosity near dead-centers can lead to a reduction in wear in that region. Then, although wear may increase in the mid-stroke, the end-stroke regions, where current engines experience the most wear, could actually see a reduction in asperity contact. If viscosity can be kept high near dead-centers, wear near end-strokes can be reduced by up to 25%, according to the current estimate.

Lubricants with the properties studied here – that is, with shear-dependencies that allow viscosity to remain high near end-strokes while being reduced near mid-stroke – do not currently exist. One of the applications of this study is to aid in evaluating whether the development of such lubricants will be worthwhile, given the possible benefits. Also, it is possible to create the viscosity variations studied here by controlling cylinder liner temperatures, using cooler temperatures near the end strokes and warmer ones near mid-stroke. Such liner temperature control systems are currently in use in some applications, such as large marine diesel engines[31]. The added complexity of such systems will certainly add to engine cost, which may outweigh the benefits. Further investigation of the costs of obtaining the desired lubricant viscosities are required to determine whether the apparent benefits are worth the investment.

This study has demonstrated that the main reduction in ring/liner friction that can be brought about by changing lubricant viscosity comes from reducing viscosity in the mid-stroke region. However, when viscosity is reduced in this region asperity contact increases, and an unacceptable level of wear may be reached. It may be possible to negate this increase in asperity contact by controlling surface texture as well as lubricant viscosity. Several studies have shown that controlling surface texture alone may reduce friction. It is further proposed that a combination of optimized surface texturing and lubricant viscosity may reduce losses even further, without an adverse effect on wear. Both possibilities were investigated with a parametric study, which is presented in Section 4 below, with an analysis of the combined effects presented in Section 5.

4. Surface modeling and analysis

Modification of the surface textures of the ring or cylinder liner may reduce ring/liner friction. Such modification may also increase friction, however, or cause other adverse effects, so care must be taken to match the texturing to the system and conditions under study. Several mechanisms are proposed for the effect of surface finish on friction, including the removal of wear particles from the sliding interface by negative textures, use of negative textures as "lubricant reservoirs" to supply otherwise poorly-lubricated areas, and increase in hydrodynamic support due to "micro-hydrodynamic" action of surface features. In addition, several types of surface modification are considered. These can be separated into the two broad categories of stochastic modifications, including the control of statistical surface parameters such as the roughness and skewness, and deterministic modifications, which consist of placing specific features, such as dimples, at specific locations on the surface.

This study focuses on adding deterministic textures to the cylinder liner, and the effects of such texturing on the hydrodynamic support of the ring load. An averaged Reynolds analysis, using deterministically calculated flow factors, was used to perform a parametric study on both grooved and dimpled textures. The main friction-reducing effect of such textures is to increase flow resistance, thereby increasing oil film thickness. When film thickness is increased, asperity contact is reduced and hydrodynamic friction also decreases, because of the corresponding decrease in oil shear rate. While limitations of the model must be taken into account, results of this study indicate that both grooved and dimpled surface features can cause a reduction in ring/liner friction, where the optimum texture is determined by engine parameters and running conditions.

4.1 Background and review of current surface texture research

Surface texturing has been recognized as a method for enhancing the tribological properties of surfaces for many years. Adding a controlled texture to faces in relative motion can have many positive effects, such as reduction of friction and wear and increase in load capacity. Early studies recognized the potential of microasperities to provide hydrodynamic lift during film lubrication[32][33][34], while later research indicated that small-scale texturing could also trap wear particles[35] in boundary and dry lubrication. A further use of microtextured surfaces may be found in the use of partial texturing – a textured region can take the place of macro-geometry such as steps or inclined planes meant to provide hydrodynamic lift[36]. All of these effects may decrease friction and wear between two sliding surfaces, but some experimental results also show a negative effect from surface texturing. In some cases texturing is not optimized for a given case, in others there is no optimal case – any kind of texturing may be worse than a smooth surface. Research and analysis presented to date demonstrates both the potential to improve tribological properties via surface texturing, and the need to understand materials, lubricants, and running conditions before a surface texture is applied.

Micro-topography consists of micron-scale surface features, either negative (cut into the "flat" surface) or positive (protruding). Early textures were limited to grooves and troughs,

expanded the range of parameters under which hydrodynamic lubrication took place, extending the non-contact regime to low speeds and viscosities. An example of Kovalchenko's results is shown in Figure 4-1.

Sadeghi, et al. has also demonstrated that texturing can reduce asperity contact, analytically showing that adding dimples in the end-stroke region of a reciprocating slider can reduce overall friction by reducing contact in this area[41]. A deterministic model of mixed lubrication was used in this study, which showed that friction reduction for a reciprocating cycle is possible when round dimples are added to one surface. (The metric for "friction" used here was the cycle average friction coefficient. This over-represents the importance of end-stroke friction compared to friction power loss, which represents the actual energy required to overcome friction.) An example of Sadeghi's predictions are shown in Figure 4-2, which shows an almost complete removal of asperity contact in the textured region.

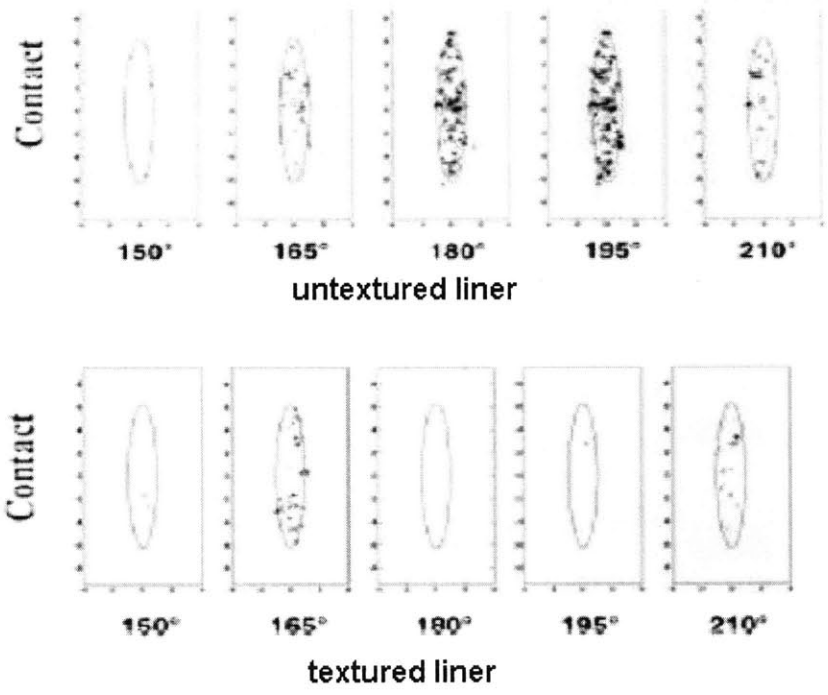

Figure 4-2: Modeling shows a reduction in asperity contact when liner texturing is added[41]

Studies have also shown that friction can be reduced when surface dimples are added even when no contact occurs. Etsion, et. al. have completed several analytical and experimental studies considering the effects of round dimples on sliding friction and load support. Early studies, based on a CFD model in which contact was not considered, predicted increased load support in face seals with the addition of dimples, where the ratio of depth:diameter was the main factor in optimizing the texturing. A depth:diameter ratio of approximately 0.1 was predicted to be optimal for almost all cases.[42] (As in the case of Sadeghi, the measurement of friction used in Etsion's study is mean cycle friction coefficient.) In-place testing in working

while new techniques have allowed complex patterns of different shapes, including circular, triangular, and other geometric shapes, to be used. Asperity shape, geometry, depth, area ratio (the ratio of asperity to flat area) and orientation can all impact the effectiveness of a given texture.

Several methods are now available for creating this surface micro-topography. Mechanical techniques such as viborolling and abrasive machining can be used to create grooves, while other methods including reactive ion etching (RIE), other forms of etching, and lithography can produce a variety of shapes in both metals and ceramics. In recent years laser surface texturing (LST) has emerged as a versatile and high-speed texturing method that can provide well controlled surface characteristics for a variety of materials. This method has been used in the magnetic storage industry for several years, and is currently the focus of several studies.[14]

Recent and past studies have explored the effects of these various methods and of different microasperity parameters on friction, wear, and other issues. A limited number of analytical models have been proposed, mostly considering hydrodynamic effects of microtexturing, while the majority of studies have been experimental. The outcome of research to date indicates that optimal surface texturing parameters depend on the running conditions studied and on the dominant mode of lubrication considered. Surface texturing can provide a benefit in several ways: decreasing friction during well-lubricated sliding by providing hydrodynamic lift, acting as reservoirs for lubricant, and removing wear particles from the sliding interface. Each of these modes is discussed in further detail below.

4.1.1 Boundary and non-lubricated sliding

When lubrication is poor (or non-existent) or hydrodynamic lubrication is made difficult for other reasons, the main effect of micro-texturing is likely to be its ability to remove wear particles from the sliding interface. In general, it is expected that this particle-removal action will reduce friction and wear, as in many engineering situations most friction is due to plowing. Suh, et. al.[35,37] performed much of the pioneering research in this field, demonstrating that the addition of grooves to a surface caused wear particles to be removed from the interface, and measuring reduced sliding friction for many cases.

Other research, however, has shown that friction can increase when grooves and other textures are added to sliding surfaces. In cases where plowing is not the main friction mechanism, removing particles from between sliding surfaces can cause an increase in friction due to adhesion, because the surfaces can come into closer contact when wear particles are not present to keep them apart. In other cases, a beneficial chemical reaction may generally occur between sliding surfaces and wear particles, and when the particles are removed the reaction no longer occurs. Petersson and Jacobson[38] conducted an experimental study in which adding dimples greatly increased the sliding friction of silicon coated with diamond-like carbon (DLC), because a beneficial tribo-film did not form in the textured case. In other tests, adding texturing can increase friction but the mechanism is not clear. While many studies have shown that texturing removes wear particles from a sliding interface, a good understanding of the chemical interaction of the two sliding materials is required to predict what effects on friction will be.

pumps showed increased life and reduced wear as predicted[14]. Subsequent analysis of "piston-ring like" cases showed that optimized dimpling could also decrease friction in reciprocating sliding, again, due purely to hydrodynamic friction reduction as asperity contact was not considered. Reciprocating-slider testing showed reduced friction, as well as a dependence on oil supply, suggesting that the dimples were effective only in a well-lubricated regime, and may actually be harmful in poorly-lubricated situations [43][44].

Many other studies, both analytical and experimental, have studied the effects of surface texturing. Stephens and Siripuram[45] as well as Hsu[46] considered the effects of different dimple shapes. Stephens and Siripuram considered circular, square, diamond, hexagonal and triangular cross-sections, and concluded that friction reduction was generally independent of shape. Hsu, however, concluded that dimple shape could have some effect, and that, in particular, shapes with an orientation more perpendicular to the sliding direction could delay the onset of asperity contact. (Results also indicated, however, that round dimples had almost no effect, in disagreement with several others). Other researchers have also predicted that texture orientation has an effect on friction and oil film thickness. Michail and Barber[18] predicted increased oil film thickness for textures more perpendicular to the sliding direction, while Jocsak[10] also predicted increased film thickness and reduced friction for lower honing groove cross-hatch angles (grooves more perpendicular to the sliding direction).

Many experimental and analytical studies have predicted friction reduction with the addition of appropriate texturing to sliding surfaces. As can be seen from this brief literature review, however, there is no general agreement on what types of textures should be added, what texture parameters are the controlling factors in friction reduction, and even what the effects of various texture parameters are. Much work still remains in this field before a good understanding of the effects of surface texturing is achieved.

4.2 Describing surface textures and finishes

Several different systems have been created for stochastically describing surface textures, while in deterministic studies patterns must generally be represented by actual measured or simulated data sets. Both stochastic parameters and deterministic descriptions are used in this analysis of surface texture effects, with deterministic surfaces used to calculate flow and stress factors and stochastic parameters used to define asperity contact mechanics. The deterministic surfaces are generated using a method described in Section 4.4.1, while the system of stochastic parameters used is described below.

Several methods and standards exist for measuring and characterizing surface finish. Techniques such as white-light interferometry (WLI) can give three-dimensional measurements of surface textures, while profilometers and similar instruments provide two-dimensional measurements of surface height along a linear path. Both types of measurement can be used directly when a deterministic description of a given surface is desired. However, in many cases the use of a deterministic measurement in an analysis or as a description of a given surface is too complicated or time-consuming, and stochastic parameters are used. These parameters statistically describe the variation in height of a surface, and can provide a general understanding of surface characteristics.

There are several different standards which are used to define stochastic parameters for surface measurement, most of which describe only variations in the surface height, and not spatial variations along the length and width. In this study, three parameters are used to describe surface height distribution: the roughness, skewness, and kurtosis. These three parameters are all derived from a statistical analysis of the distribution of surface heights, where the roughness, σ, is defined as the standard deviation of the surface heights, the skewness, Sk, is the third standardized moment about the mean, and the kurtosis, Ku, is the fourth:

$$\sigma = \sqrt{\frac{1}{N}\sum_{i=1}^{N}(x_i - \bar{x})^2} \tag{4.1}$$

$$Sk = \frac{\frac{1}{N}\sum_{i=1}^{N}(x_i - \bar{x})^3}{\sigma^3} \tag{4.2}$$

$$Ku = \frac{\frac{1}{N}\sum_{i=1}^{N}(x_i - \bar{x})^4}{\sigma^4} \tag{4.3}$$

where N is the number of data points included in the distribution, x_i is the surface height at a given point, and $\bar{x}$ is the mean surface height. These parameters can also be defined using the probability distribution function of the surface height distribution, if this function is known.

The surface roughness, σ, is simply the standard deviation of surface heights, and is an approximate representation of the height of the surface asperities above the mean. Skewness can be thought of as the asymmetry of the distribution. A negatively skewed surface has a plateau surface and many low valleys, while a positively skewed one has wide, flat valleys along with high peaks, as illustrated in Figure 4-3a. Kurtosis is often described as the "peakedness" of the distribution, and represents the number of surface height measurements that are very far from the mean. A surface with high kurtosis has a very wide distribution ("thick tails") of surface heights, with many high peaks and low valleys, while a low kurtosis surface is relatively flat, with most of the surface heights close to the mean, as shown in Figure 4-3b. For a Gaussian surface, skewness = 0, and the kurtosis = 3. The effect of these parameters on friction was not considered in this study, as the focus was on larger scale patterns, but they have been considered extensively by others.[10, 47]

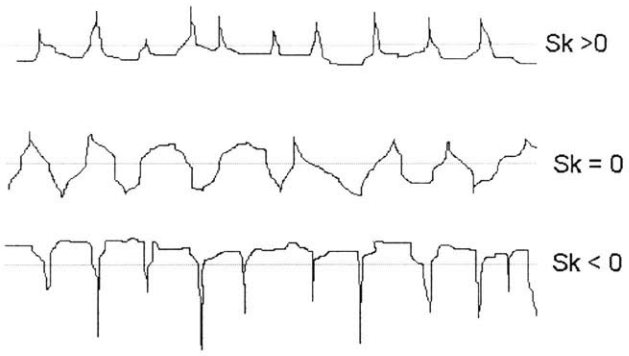

a) Illustration of surface skewness. Sk=0 is Gaussian.

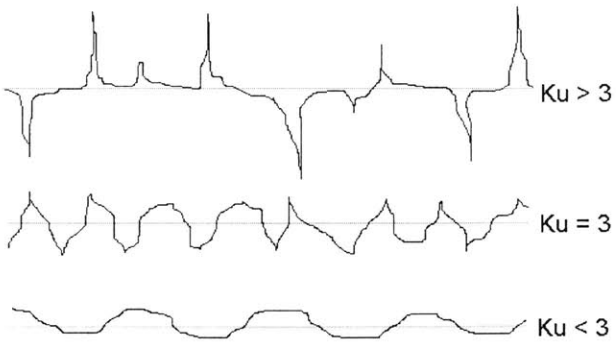

b)Illustration of surface kurtosis. Ku=3 is Gaussian.

Figure 4-3: Illustrations of surface skewness and kurtosis

These parameters can be used, along with the Pearson system of frequency curves, to represent a rough surface in the calculation of contact pressure. The Pearson system is a curve-fitting method that derives the probability distribution function of a surface from its roughness, skewness and kurtosis. This distribution is then used to determine the amount of contact expected to occur, statistically, at a given separation between surfaces, and to then determine the contact force.

4.3 Averaged flow-factor Reynolds analysis

An averaged flow-factor Reynolds analysis was used in this study to evaluate the effects of grooved and dimpled surfaces. This method, and its limitations, are described in detail in Section 2. Because this method was used, the surface features studied were limited to a relatively small size, compared to many that have been studied in the literature. Also, the method does not allow the detailed analysis of flows and stresses that would be possible using a deterministic method. Still, the averaged method can provide information about the effects of various surface finishes, and reveal the trends in film thickness and ring/liner friction whose discovery was the object of this parametric study.

The averaged flow factor method can also shed some light on the physical effects of rough surfaces, in the interpretation of the flow and stress factors themselves. While a physical explanation of the factors' meanings is not agreed upon, understanding the various interpretations can give some intuition into the effects of rough surfaces. Also, looking at the relative importance of each factor in affecting fluid flow and stresses can aid in understanding the relative importance of the various physical parameters in the ring/liner system.

4.3.1 Physical interpretation of factors

The flow and stress factors represent the difference between the sliding of two smooth surfaces and the sliding of rough, textured surfaces. The physical effect of surface roughness on fluid flow is complex and depends on the nature of the actual surfaces under study. However, it is possible to give a general physical interpretation of what the factors represent, to partly describe what occurs in the lubricant between rough surfaces.

Figure 4-4 illustrates one possible interpretation. For two smooth surfaces, there is a clear definition of the distance between them, which is also the thickness of the oil film if it is entirely filling the gap. For rough surfaces, the definition of gap height becomes complicated – its actual value depends on the surface features – and so an average value is used. Generally, this average value is taken as the difference between the mean surface heights of the rough surfaces, h_{mean} as shown in Figure 4-4b. In determining flow and stress factors, a comparison is made of smooth surface conditions vs. rough surface conditions at the same film thickness, where for the rough surface h_{mean} is used, and for the smooth surfaces h is used.

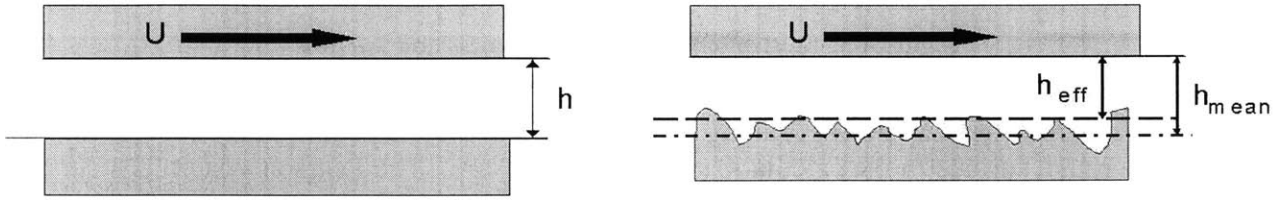

a) sliding of two smooth surfaces **b) sliding of one smooth and one rough surface**

Figure 4-4: Flow and stress factors can be interpreted in relation to an effective film thickness

The effect of the roughness, however, is to make the effective region in which flow occurs even smaller than h_{mean}. If fluid remains trapped and stagnant in the roughness valleys, an effective flow thickness will be smaller than h_{mean}, and be closer to h_{eff}, in Figure 4-4b. In this interpretation, the roughness impedes flow simply by making the effective flow area smaller. For a pressure-driven case, the roughness will impede flow and increase pressure in the fluid for any rough surface. For shear-driven flow, fluid transport will be impeded if the stationary surface has a higher roughness, while it will be increased (due to transport of the stagnant fluid trapped in the valleys) if the moving surface is rougher.

The reduced effective film thickness also has an effect on shear stress. For a thinner oil film the shear rate within the fluid is higher, so shear stress is also higher. These effects can be observed in Section 4.3.2, below, which shows the effects of the different flow and stress factors on oil film thickness and ring/liner friction.

A second interpretation of the flow factors is based on their locations in the equation for oil flow rate:

$$Q = -\phi_p \frac{h^3}{12\mu} \frac{dP}{dx} + \frac{U}{2}\left(h\phi_g + R_q\phi_s\right) \tag{4.4}$$

In this equation, the pressure flow factor appears with the viscosity, μ, while the shear flow factor is coupled with the film thickness. Then, the effect of the pressure flow factor can be considered to modify the viscosity, and an "equivalent viscosity" can be defined:

$$\mu_{eq} \equiv \frac{\mu}{\phi_p} \tag{4.5}$$

An increase in ϕ_p can be thought of as a decrease in equivalent viscosity, and vice versa. Then, a low pressure flow factor indicates increased flow resistance, (high equivalent viscosity) as expected. Similarly, an equivalent film thickness:

$$h_{eq} \equiv h \cdot \phi_g + R_q \phi_s \tag{4.6}$$

is defined, with the shear and geometric flow factors. A decreased shear flow factor reduces the equivalent film thickness, decreasing shear-driven flow. The shear flow factor is related to the relative velocities of the sliding surfaces, so that when the rougher surface is stationary the shear flow factor will be negative, thus causing a decrease in equivalent film thickness.

4.3.2 Relative contributions of flow and stress factors

Each of the flow and stress factors has some effect on predictions of flow and stress within the lubricant. The pressure flow factor, however, has by far the dominant effect on flow, stress, and overall friction losses for the ring and liner. This suggests that the main effect of adding roughness to a sliding surface is on pressure-driven flow, and specifically in increasing the resistance to pressure-driven flow, and thus increasing hydrodynamic pressure within the fluid. Thus, the main effect of adding roughness appears to be increasing load support, or, for a given load, increasing film thickness. This has the simultaneous friction-reducing effects of reducing asperity contact, if there was any to begin with, and decreasing shear rate, and thus shear stress, in the fluid.

Figure 4-5 and Figure 4-6 show the effects of changing each of the flow and stress factors. A "smooth" case, in which flow factors were kept at their smooth surface values, is compared to cases in which a single factor is changed to its value for a surface with horizontal grooves, a surface with very different flow and stress factors than the smooth case. Then, each curve shows the effect of changing a single factor. As the figures show, changing the pressure flow factor has the dominant effect, with a smaller contribution from the shear stress factor. The shear flow and pressure stress factors have negligible effects, and cannot be distinguished from the "smooth" baseline in the figures.

Figure 4-6, which shows the total friction force between the ring and liner, also illustrates that the effects of the different factors are approximately additive. The change in pressure flow factor causes a large decrease in friction force, while changing shear stress factor causes a small increase. When all factors are changed to their rough surface values, the resulting friction force is the summation of those resulting the individual factor changes.

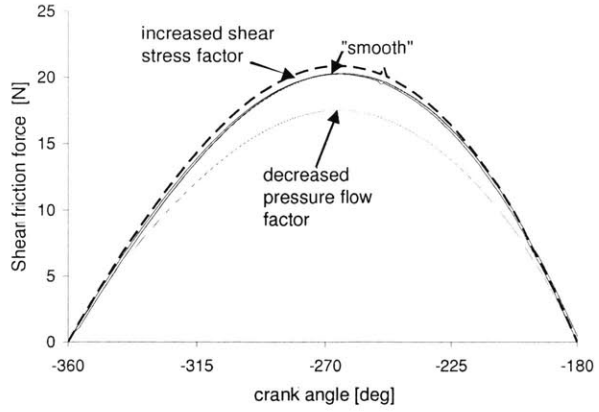

a) Factor effects on shear stress

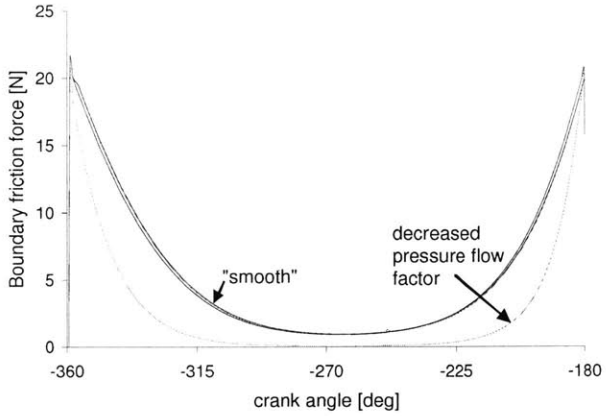

b) Factor effects boundary friction

Figure 4-5: Flow and stress factor effects on hydrodynamic and boundary friction

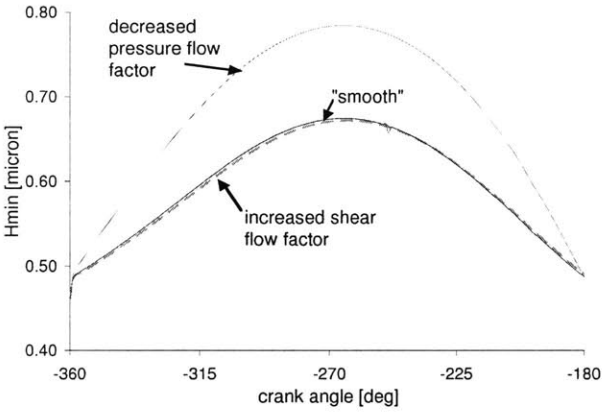

a) Factor effects on oil film thickness

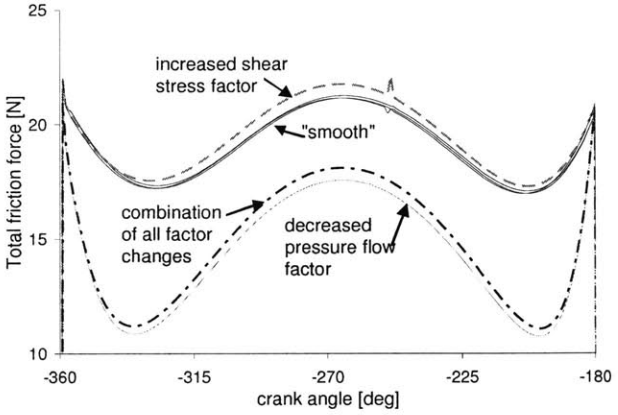

b) Factor effects on total ring friction

Figure 4-6: Flow and stress factor effects on oil film thickness and total ring/liner friction

4.4 Parametric study: grooves and round dimples

The averaged Reynolds equation method, summarized above and in Section 2, was used to study the effects of dimpled and grooved surface features on ring/liner friction. Surfaces with dimpled and grooved surface textures were first generated using a MATLAB program written for this purpose. Several programs written to facilitate the calculation and curve-fitting of flow factor relationships were used to obtain flow and stress factors. These factors were then used in the MIT ring-pack simulation program to predict ring/liner friction for different cylinder liner surface textures. Although not able to predict complexities of lubricant flow and surface contact that require a deterministic approach, this study was able to demonstrate trends in frictional losses with changing surface parameters.

This study did not consider the effects of stochastic surface properties such as roughness and skewness. Rather, the effects of patterns of discrete features, specifically dimples and grooves, were studied. Parameters considered include: for the dimples, diameter, depth, area ratio, and arrangement (hexagonal or rectangular); and for the grooves, width, depth, area ratio, angle, and arrangement (cross-hatch or parallel grooves). Area ratio is the percentage of the surface occupied by the surface features. The range of parameter values studied is given in Table 4-1.

As for the lubricant study, this study of surface texturing focused on the oil control ring, and all friction results presented below are for the oil control ring/liner interface only. This is because, as noted previously, the oil control ring contributes the majority of ring-pack friction, and most of the remaining losses stem from the top ring in the "dry region" where hydrodynamic effects are not expected to make any impact on friction (since there is little to no oil present). Thus, all predicted FMEP trends are for the oil control ring only, although they can be expected to also be representative of trends for the entire ring-pack, as surface texturing of the type studied should have little effect on the other major sources of ring-pack friction.

Table 4-1: Range of surface texture parameters studied

Parameter	**Range**
Dimples:	
Diameter	5-25 μ
Depth	3-8 μ
Area Ratio	10-22%
Arrangement	hexagonal or rectangular pattern
Grooves:	
Width	11-30 μ
Depth	3-8 μ
Area Ratio	15-35%
Angle	0-90°
Arrangement	parallel or cross-hatch pattern

4.4.1 Method of surface construction

The textured surfaces used in this parametric study were simplified so that the effects of the surface features under consideration could be considered alone, rather than being coupled with the effects of a realistic surface roughness. Instead of using a rough texture, then, the "flat" part of the surface was assumed to be smooth, with either grooves or round dimples the only features present. Two examples of these surfaces are shown in Figure 4-7. In both Figure 4-7a and Figure 4-7b the vertical scale is exaggerated, so that the feature depth seems very large and the profile very sharp. In fact, the grooves and dimples studied were quite shallow.

The surfaces were generated using a two-stage process. In the first stage, the desired feature parameters were used as inputs to generate a matrix that indicated where the given features were to be placed on the surface. Then, this matrix was convolved with a second matrix

that was built based on the desired feature profile. In all of the cases presented below, the features were given a Gaussian profile, because of its ease of construction and smooth shape. Because of the modular structure of the surface-generating program, however, it is easy to accommodate different profiles as well as different patterns and shapes.

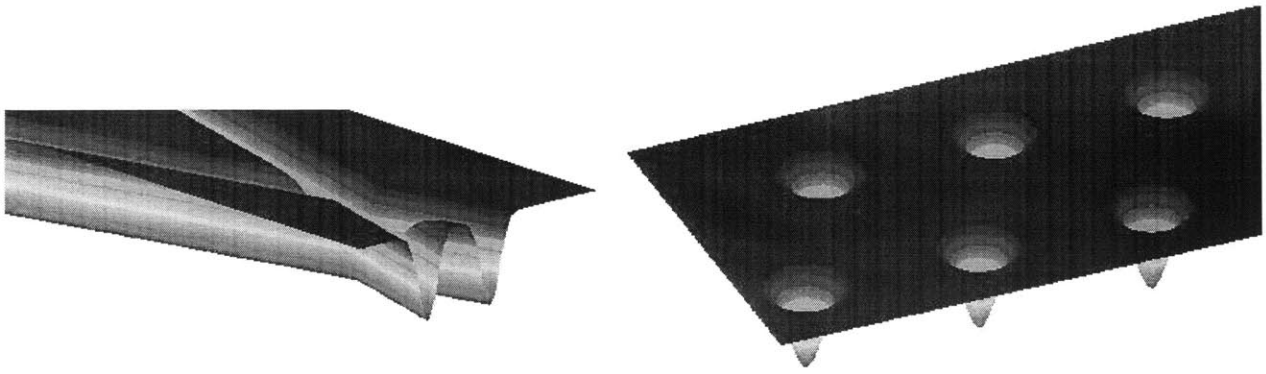

a) cross-hatch grooves b) dimples

Figure 4-7: Examples of generated surfaces

It should be noted that the definition of groove angle was based on a cross-hatch groove pattern, as shown in Figure 4-8. The stated groove angle, in all results presented below, is twice the angle between the groove and a line perpendicular to the flow direction. This standard was adopted because optimization of a cross-hatch pattern, which is commonly found on honed cylinder liners, was thought to be the most likely application of the groove analysis. The same definition of angle was used for both cross-hatch and parallel groove patterns.

a) cross-hatch b) parallel

Figure 4-8: Definition of groove angle for cross-hatch and parallel patterns

4.4.2 Grooves: effect of linear surface features on sliding friction

Surfaces with various grooved patterns were studied, to find the effects of the groove parameters on ring/liner friction. Groove angle had the largest effect. Within the range studied, very small angles (grooves more perpendicular to flow direction) caused a reduction in friction, while grooves more parallel to the flow caused a friction increase. Depth also had a large effect, with deeper textures generally showing reduced friction. In some cases, an ideal depth at which friction was minimized was found. Friction also decreased with increasing area ratio, and with groove width to a point, after which increasing width had no effect.

Both flow factor and FMEP results are presented below. Pressure flow factor, which has the largest effect on ring/liner friction, is shown, as are friction results. It should be noted that, for very deep textures in particular, the surfaces studied may be on the edge of the range of applicability for the averaged-flow-factor model. Also, this model is known to have inaccuracies at very small film thicknesses.

4.4.2.1 *Flow factor results*

Only pressure flow factor results are presented below, because this factor has the main effect on ring/liner friction, as demonstrated in Section 4.3.2. All flow and stress factor results are given in Appendix B. In general, a lower pressure flow factor indicates a decrease in ring/liner friction, because of the implied increase in hydrodynamic pressure generation.

Groove pattern had almost no effect on flow factor or ring/liner friction calculations. Figure 4-9 shows an example comparison of pressure flow factor calculations for cross-hatch and parallel ("single") groove patterns. In general, very little difference was found between cross-hatch and parallel groove results, as is indicated in the figure. Because of this, only parallel-groove results are presented in the remainder of this report.

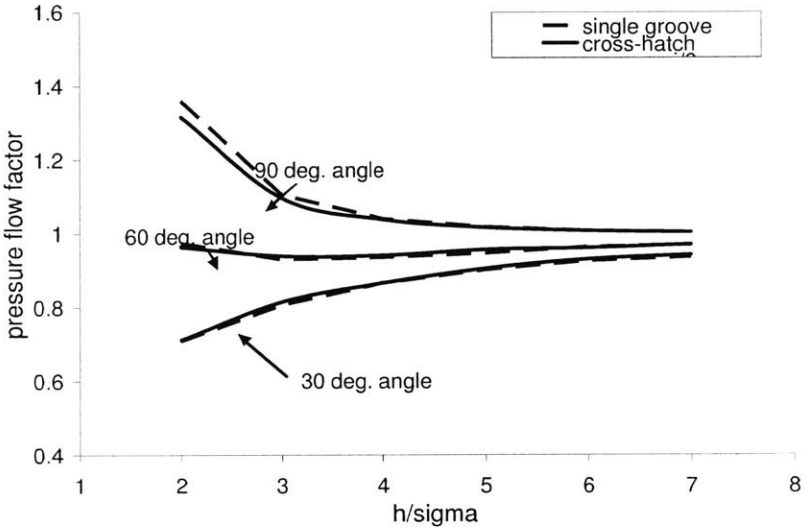

Figure 4-9: Flow factor results for parallel and cross-hatch groove patterns are very similar

Figure 4-10 shows the effects of groove angle on pressure flow factor. As Figure 4-10a shows, pressure flow factor decreases with decreasing groove angle – as the grooves become more perpendicular to the flow direction. For large angles, $\theta > 60^{\circ}$, pressure flow factor increases beyond 1, the smooth surface value, and increases for larger angles. This means that for large groove angles, the presence of the grooves causes fluid to flow more easily, reducing load support and, as is shown in Section 4.4.2.2, also increasing friction.

For more perpendicular grooves, the diverging/converging nature of the texturing creates a "micro-hydrodynamic" pressure peak in the fluid, where oil that enters the groove is pushed against the opposite wall, which creates flow resistance and a pressure increase. This flow impedance causes a reduction in flow and thus pressure flow factor. For grooves with larger groove angles, which run more parallel to the flow direction (the largest angle considered is 90°, in which the grooves run at 45° to the flow direction) oil that enters the groove is partially pressed against the opposite wall, but is also able to flow along the groove relatively easily. For high groove angles, then, the effect of the addition of the grooves is to increase the effective flow area for the fluid, by adding the area within the grooves. This increases fluid flow, thus increasing the pressure flow factor.

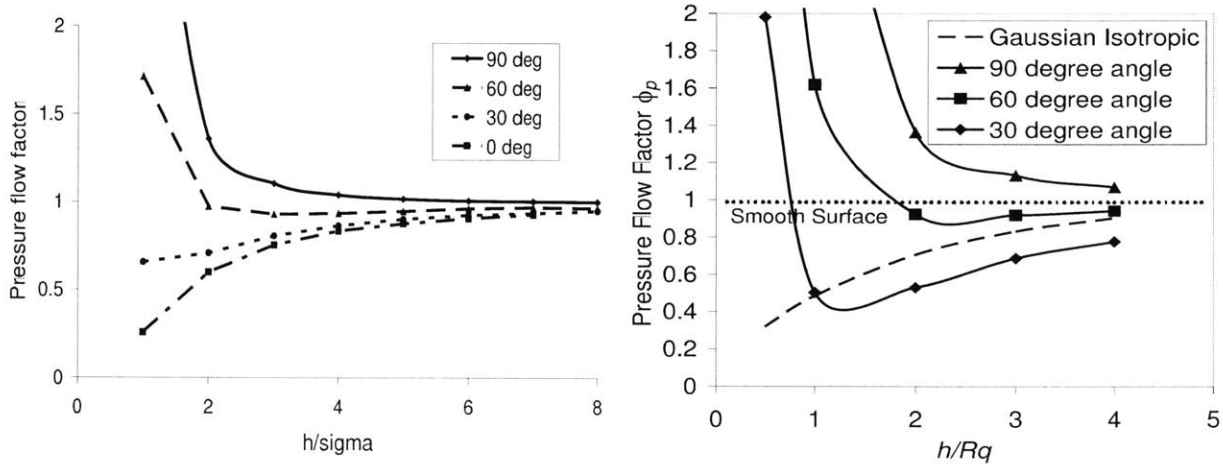

a) Pressure flow factor for varying groove angle, this study

b) Pressure flow factor for varying groove angle, from Jocsak

Figure 4-10: Groove angle effects, with comparison to previous calculations by Jocsak[10]

Figure 4-10b shows results from Jocsak [10], looking at the same groove angles as were considered in the present study. The same flow factor calculation methods were used in both studies, however Jocsak's results consider more realistic surfaces, with realistic roughness and groove profiles. Because the surface roughness is included, Jocsak's pressure flow factors are lower than those obtained in the current study. Also, groove spacing, rather than area ratio, is kept constant in Jocsak's study. Despite these discrepancies, the two sets of results show a good match in trends.

Figure 4-11 shows the effects of varying groove depth on pressure flow factor. As Figure 4-11a shows, there is no change in the pressure flow factor with groove depth, when ϕ_p is presented as a function of h/σ (σ is the RMS surface roughness). This is because the effects of groove depth on pressure flow factor are the same as the effects of groove depth on surface roughness, so that the flow factor as a function of h/σ does not change. This suggests that there is a fundamental relationship between ϕ_p and groove depth, that mirrors the relationship between depth and the standard deviation of the surface heights, σ.

When studying a specific case in which the approximate value of the oil film thickness is known, it is useful to consider changes in ϕ_p at film thicknesses close to the expected values.

Figure 4-11b shows the pressure flow factor as a function of h alone, for different groove depths. As the figure shows, at a given film thickness, ϕ_p decreases with groove depth. The depth of the grooves influences the micro-hydrodynamic effect, just as, in the macro-hydrodynamic case, the size of a step in surface height influences the amount of hydrodynamic pressure generated. (In the case of a macro-sized step bearing, the pressure generation is expected to be related to film thickness, depth, groove width and the distance between grooves[48]). For the surfaces studied, the flow impedance increases with groove depth, suggesting that hydrodynamic action and thus oil pressure also increases with depth.

It should be noted that Figure 4-11 shows flow factor results for grooves at an angle of 30^o, so that the effect of increasing depth is to decrease ϕ_p. For larger groove angles, ($\theta > 60^o$) the effect of increasing depth is actually to increase the pressure flow factor, because in this case the effect of the grooves is to reduce flow impedance and thus increase ϕ_p. The effect of increasing groove depth is to amplify the effect of the grooves, whether that be to block flow, for low groove angles, or increase it, for high groove angles. Because the purpose of this study was to identify surface textures that may be used to reduce friction, the flow factor results shown below are for a low groove angle ($\theta = 30^o$).

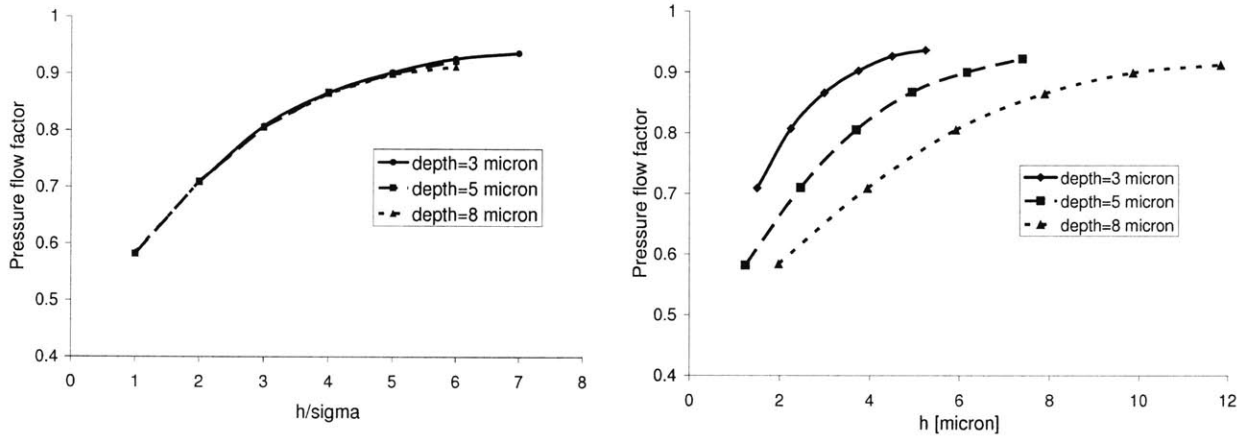

a) Pressure flow factor vs. h/sigma

b)Pressure flow factor vs. film thickness, h

Figure 4-11: Effect of groove depth on pressure flow factor, 30^o angle, width=20μ, area ratio=0.24

Plotting the pressure flow factor as a function of h/σ can show fundamental effects of surface texturing on pressure-driven fluid flow, including its relationship to surface roughness. It is also useful to show the relationship of ϕ_p to film thickness itself, however, when the effects of a given surface texture in a specific case are of interest. Thus, flow factor results in both this section and section 4.4.3.1, which presents the flow factor analysis for dimpled surfaces, are plotted vs. both h/σ and h, in order to illustrate both general and specific effects.

Figure 4-12 shows the effects of area ratio on the pressure flow factor. On the physical surface, the effect of increasing area ratio is to decrease the distance between grooves, so that the effect of increasing area ratio can be also interpreted as the effect of a reduced groove spacing. The decrease in ϕ_p with increasing are ratio may then be due to the effect of groove spacing on

hydrodynamic action within the grooves. When grooves are very far apart, they can be considered to be independent in their effects on the lubricant flow and pressure. When they are closer together, there may be a cross-influence between grooves, where the presence of each groove affects the flow within the others. For the textures studied, the spacing between the grooves is relatively small (on the order of a few groove widths) so that some cross-influence is expected. More closely spaced grooves (higher area ratio) will have more influence on each other, and may work together to increase flow resistance.

The effect of area ratio may also be due to the simple fact that, when more of the surface is occupied by converging and diverging regions, there is a larger hydrodynamic effect. More "microhydrodynamic" bearings are present, so their net effect is greater. A combination of this and the cross-influence of more closely spaced grooves is likely the main contributor to the effect of area ratio on ϕ_p.

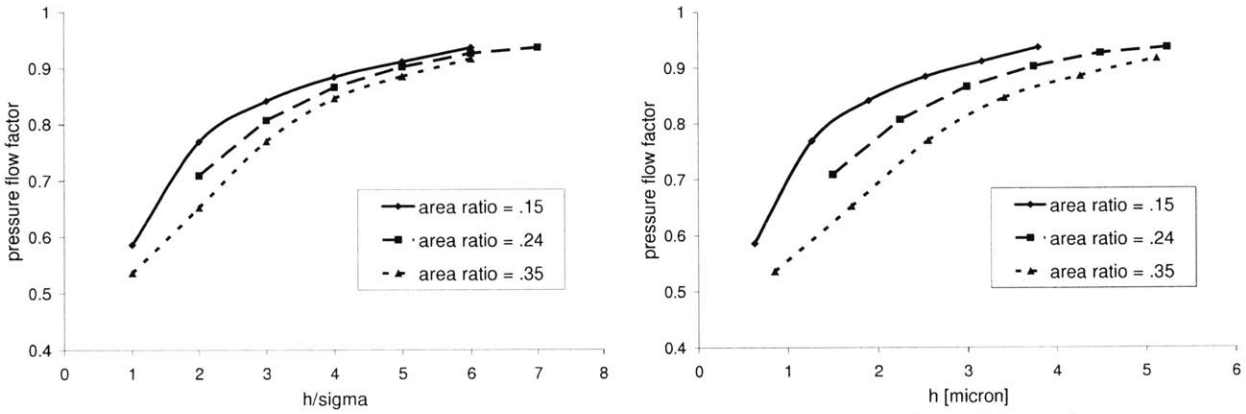

a)Pressure flow factor vs. h/sigma

b) Pressure flow factor vs. film thickness, h

Figure 4-12: Effect of groove Area ratio on pressure flow factor, 30° angle, width=20μ, depth=3μ

Figure 4-13 presents the changes in pressure flow factor with changing groove width. As the figure shows, the groove width has almost no effect on the pressure flow factor except at very small film thicknesses. This may indicate that the width has only a small effect on micro-hydrodynamic action within the groove – the pressure build-up due to the converging geometry of the groove exit is not strongly influenced by the width. There is no clear explanation for the change in trend at small film thickness, where groove width suddenly becomes important. It should be noted, however, that flow factor analysis becomes inaccurate at very small h/σ values, where the film thickness is close to the surface roughness, because the roughness asperities and flow blockages make the flow situation too far removed from a smooth, Reynolds case. Then, these thin-film effects may not be realistic, and should be studied further with a deterministic analysis.

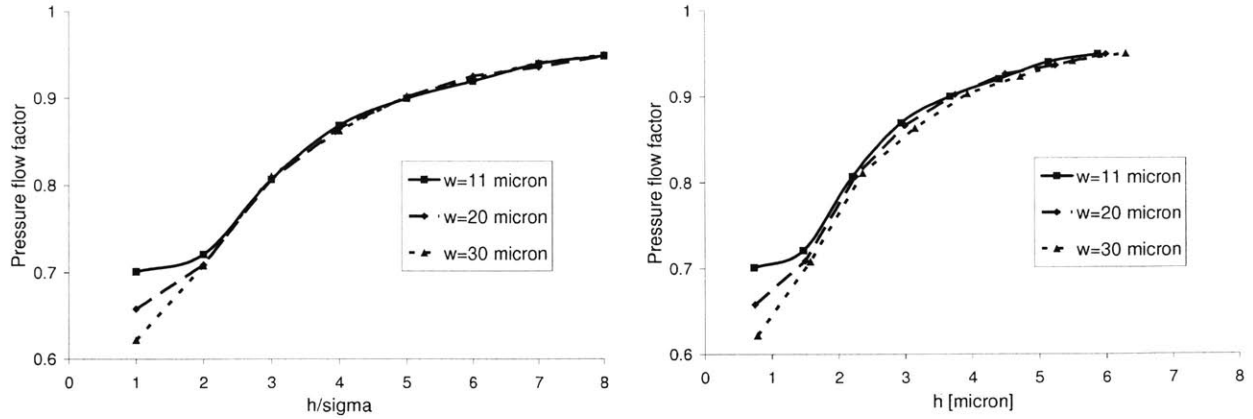

a) Pressure flow factor vs. h/sigma

b) Pressure flow factor vs. film thickness, h

Figure 4-13: Effect of groove width on pressure flow factor, 30° angle, Area ratio = 0.24, depth=3μ

4.4.2.2 *Ring/liner friction results*

Friction results were consistent with expectation given the flow factor results presented above. Friction tends to decrease with increasing depth and decreasing groove angle, and also shows some reduction with increasing area ratio and width. The change in FMEP between best and worse cases is relatively large, up to ~30% between the highest and lowest friction examples (not including large groove angles, which cause friction to increase). While this result cannot be used to predict actual friction reductions in realistic situations, it indicates that liner surface texturing may have a major effect on ring/liner friction, and is worth studying further.

Ring/liner friction depends on the surface texture in two ways: oil film thickness, which influences both hydrodynamic friction and asperity contact, depends on the influence of the texturing on the oil flow (represented by flow and stress factors in this study); and asperity contact friction depends on the surface roughness and other features of the surface texture. For this parametric study, as described in Section 4.4.1, the surfaces are smooth except for the added grooved or dimpled patterns. This allows the hydrodynamic effects of the patterns to be studied more easily, but makes the asperity contact mechanics very unrealistic.

To account for this issue, the ring-pack friction program was modified slightly so that the surface properties related to contact mechanics were separated from those related to oil flows. Then, for each friction case studied the contact mechanics were be kept the same, even as flow parameters were allowed to vary. For the sake of simplicity, the surface used to calculate contact pressures was kept constant as a Gaussian surface with a roughness of $\sigma = 0.21\mu$. This roughness is typical of the "truncated" roughness of a cylinder liner, where the surface is negatively skewed and the effects of the deep valleys are ignored. The presence of the surface features should have little to no effect on the contact mechanics, since the features are negative – that is, they are formed by the removal of material, rather than the addition – and so no extra asperities are added when the texturing is added. Changing area ratio of the texturing will affect the amount of surface area available for contact, but this should have only a small effect as the

contact force should be proportional to the material properties (hardness) and the load, and not to the apparent area of contact[37].

While contact surface features were kept constant, the surface properties controlling oil flows and stresses were varied. These surface properties were defined by the curve-fitted flow factor equations, which are functions of h/σ and derived from the values calculated deterministically using Li's program, and the surface roughness, σ, which together determine the value of a given flow or stress factor at a given film thickness, h. The value input as σ effectively defines the depth of the texture under study, since the flow and stress factor equations contain no information relating to the surface roughness itself, but only to its effects relative to h/σ. Then, friction results are presented as FMEP (friction mean effective pressure) vs. σ, as this roughness was used as the input in this study. As the value of σ approximately corresponds with the depth of the surface features, the trends of FMEP with σ shown should be considered to correspond to the same trend of FMEP with respect to depth. A value of $\sigma = 0.7\ \mu$ is roughly equivalent to a groove depth of 3μ, indicating that the feature depths studied were relatively shallow. This is in agreement with the literature, which predicts maximum friction reductions for shallow features [42].

Figure 4-14 shows the change in ring/liner FMEP with groove angle as well as depth. As expected from the flow factor results, FMEP decreases with groove angle. Friction also decreases with groove depth for low groove angles, while increasing with depth for a large angle (the $\theta = 90^\circ$ case, not shown in the figure, demonstrated even higher friction than $\theta = 60^\circ$), as expected – the effects of the texture increases as depth is increased. As shown in Figure 4-15, these reductions in total FMEP are the result of decreases in both the hydrodynamic and boundary contributions to friction, as the presence of the texturing causes the oil film thickness to increase.

For the $\theta = 0^\circ$ grooves, the surface texturing is able to almost entirely eliminate boundary contact, as well as cause a large decrease in hydrodynamic friction. At the maximum groove depth studied FMEP is continuing to decrease, indicating that the maximum effect of these grooves may occur at a greater depth. For the $\theta = 30^\circ$ grooves however, a minimum FMEP is found at a roughness of $\sigma \sim 0.55\ \mu$, or a depth of slightly more than 2μ. It is expected that the hydrodynamic effect of the grooves will not increase indefinitely with depth – as the grooves become too deep, fluid at the bottom will become stagnant and no longer contribute to the hydrodynamic system. At this point, the averaged flow-factor method also becomes inadequate to describe the fluid flow, and more detailed model must be used. For grooves that are not entirely perpendicular to the flow ($\theta > 0^\circ$), there may also be a trade-off between the hydrodynamic effect and the increased flow area. As groove depth increases hydrodynamic effects will increase (to a point), but the extra area available for fluid transport also grows. The minimum FMEP point predicted for the $\theta = 30^\circ$ groove case may also reflect this trade-off.

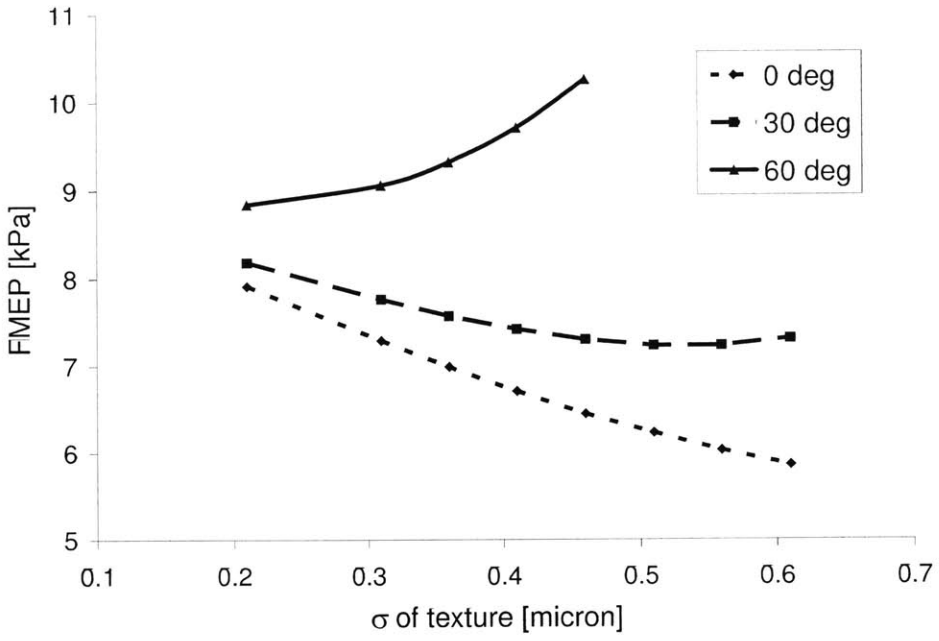

Figure 4-14: Effect of groove angle on ring/liner friction, width = 20μ, area ratio = 0.24

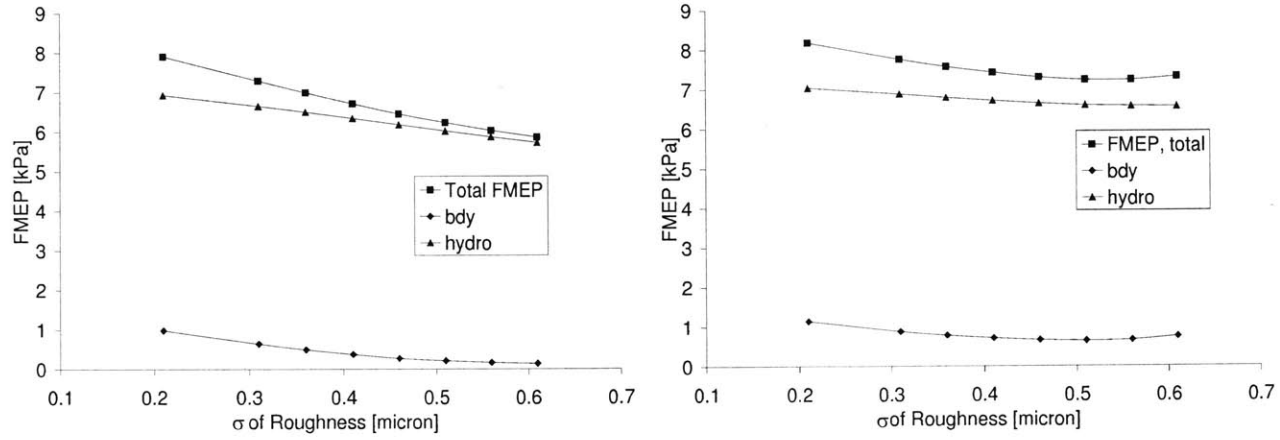

a) 0° groove angle **b) 30° groove angle**

Figure 4-15: Hydrodynamic and boundary contributions to frictional losses, 0° and 30° groove angles

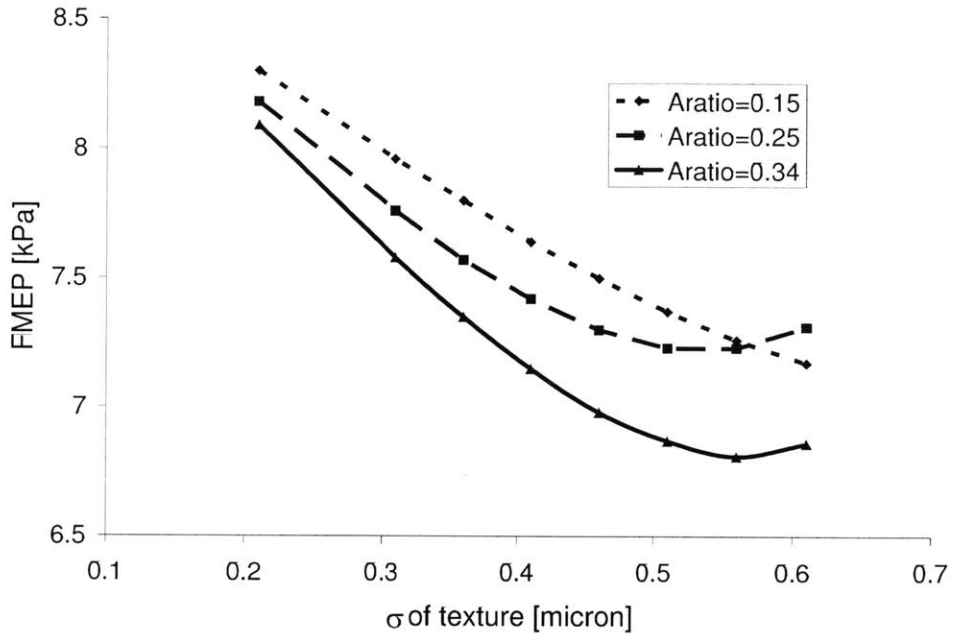

Figure 4-16: Effect of groove area ratio on ring/liner friction, angle = 30°, width = 20μ

Figure 4-16 and Figure 4-17 illustrate the effects of the area ratio and width, respectively, of the grooves on ring/liner FMEP. Again, friction decreases as depth increases, until an optimum point is reached at $\sigma \sim 0.55$ μ for most of the cases. This may reflect the trade-off between hydrodynamic effect and flow area discussed above (the results shown are for $\theta = 30^{\circ}$). FMEP also decreases as area ratio increases, as expected from the flow factor results, and also increases with groove width but only to a point. As Figure 4-17 shows, friction decreases as the groove width increases from 11μ to 20μ, but the further increase to w=30μ has no effect.

This results from the relation of the flow factors to oil film thickness, shown in Figure 4-13. For large film thicknesses, groove width does not affect the pressure flow factor - a width effect is only shown for thin films. Because the presence of the grooves increases oil film thickness, there is a feedback effect that removes the dependence of friction on groove width as width grows. When the grooves are narrow, the hydrodynamic effect is small as is the oil film thickness, which is small enough to be in the range where groove width matters. The increase in width from 11μ to 20μ increases the hydrodynamic pressure in the oil and also the value of h, into the regime in which groove width becomes unimportant. Then, for any further increase in width the oil film thickness is in a regime where the width has no effect on the pressure flow factor, and there is thus no effect on friction.

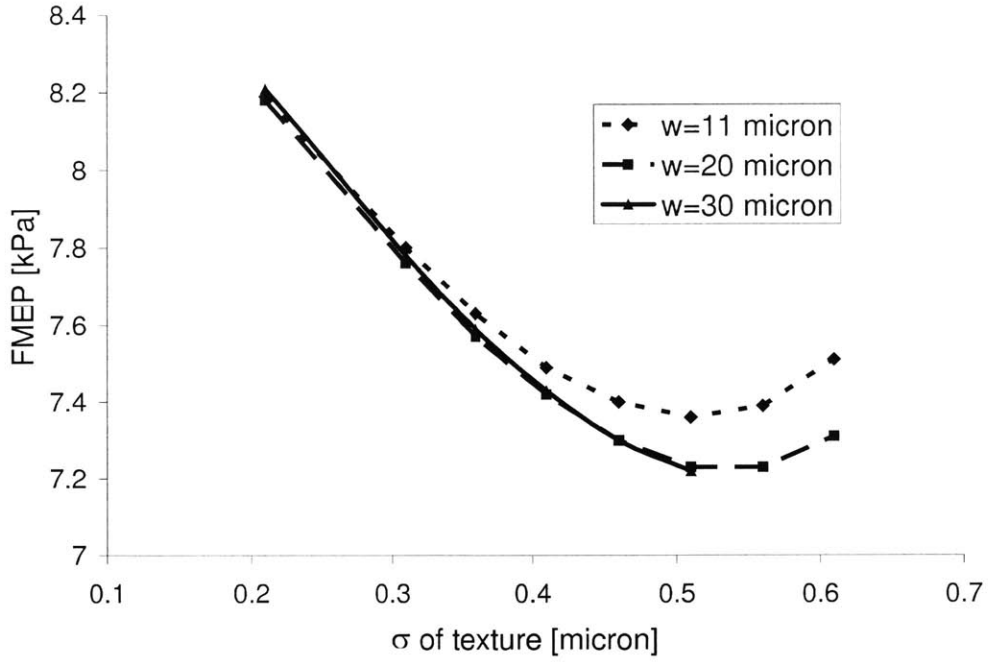

Figure 4-17: Effect of groove width on ring/liner friction, angle = 30°, area ratio = 0.24

4.4.3 Round dimples: effect of discrete surface features on sliding friction

In addition to the grooved patterns, surfaces with patterns of round dimples were also studied, as such discrete surface features are also thought to hold promise for the reduction of ring/liner friction. FMEP was found to decrease as dimple area ratio and depth were increased, as was the case with the grooves, and to be minimized at an optimum dimple diameter. In general, the effects of the various dimple parameters on friction was smaller than the effects of comparable parameters for the grooved surfaces. This suggests that dimpled surfaces may allow more freedom in selecting feature parameters, and may be useful over a larger range of running conditions than grooved patterns.

Both pressure flow factor and FMEP results are presented. As for the groove analysis, it should be noted that the averaged flow factor model is limited in its applicability, and results at very small film thicknesses and for very deep textures may be pushing this limit. The results presented below are intended to illustrate the friction-reduction possibilities of dimpled surface textures, and the effects of some dimple parameters. Further analysis is required before recommendations can be made for friction-reducing surface textures in specific applications.

4.4.3.1 *Flow factor results*

Only pressure flow factor results are presented below, because this factor has the main effect on ring/liner friction, as demonstrated in Section 4.3.2. All flow and stress factor results

are given in Appendix B. In general, a lower pressure flow factor indicates a decrease in ring/liner friction, because of the implied increase in hydrodynamic pressure generation.

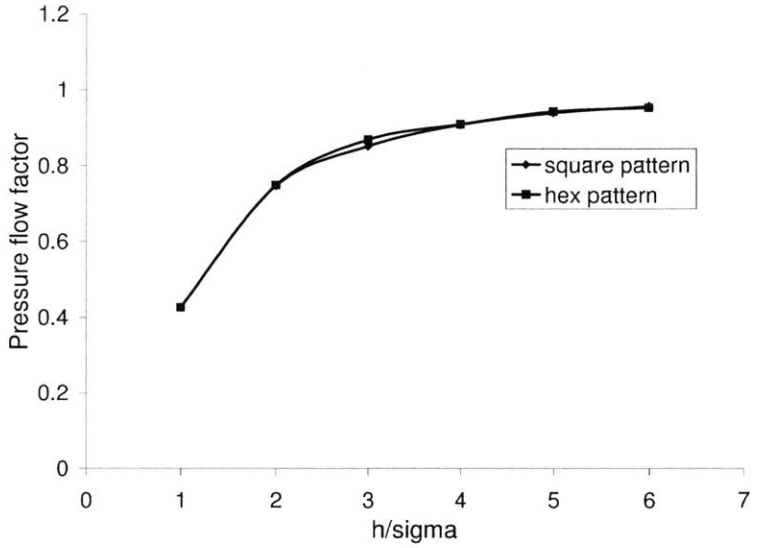

Figure 4-18: Flow factor results for square and hexagonal dimple patterns are very similar

Flow factor results for the dimpled cases showed several of the same trends that were observed for the grooved surfaces. For example, the dimple pattern had almost no effect on flow factor or ring/liner friction calculations, similar to the lack of influence of a cross-hatch vs. parallel groove arrangement on friction. Figure 4-18 shows an example comparison of pressure flow factor calculations for square and hexagonal dimple arrangements. Because the pattern appears to have no effect, all results presented below are for the hexagonal pattern only.

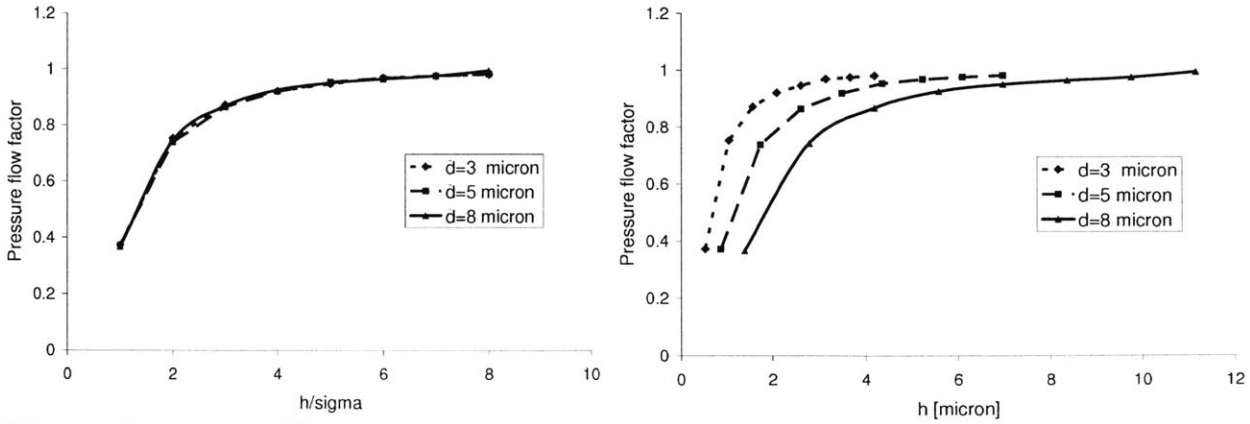

a) Pressure flow factor vs. h/sigma

b) Pressure flow factor vs. film thickness, h

Figure 4-19: Effect of dimple depth on pressure flow factor, diameter = 19μ, area ratio = 0.25

The dimpled patterns were also similar to the grooved cases in that the change in pressure flow factor with the depth of the features mirrored the changing surface roughness, so that

plotting pressure flow factor as a function of h/σ shows no effect from depth changes. Figure 4-19 shows this, along with the pressure flow factor plotted vs. h only, which illustrates the effect of dimple depth at a given film thickness. Further discussion of this phenomenon is given in Section 4.4.2.1. Because it is useful to observe both the non-dimensionalized effects of various parameters and to evaluate the pressure flow factor at an expected film thickness for a specific case, ϕ_p is shown as a function of both h/σ and h alone in the examples below.

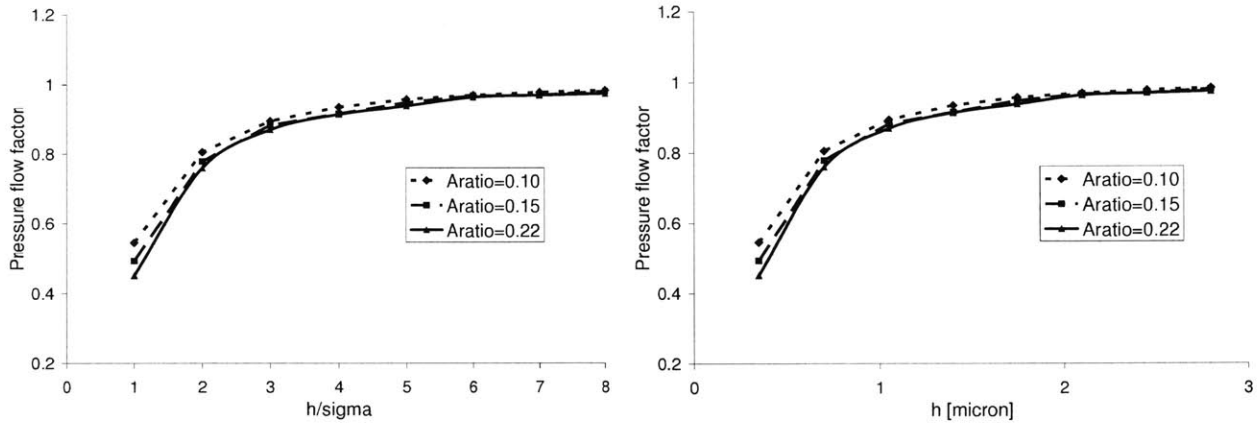

a) Pressure flow factor vs. h/sigma **b) Pressure flow factor vs. film thickness, h**

Figure 4-20: Effect of dimple area ratio on pressure flow factor, diameter = 19μ, depth = 3μ

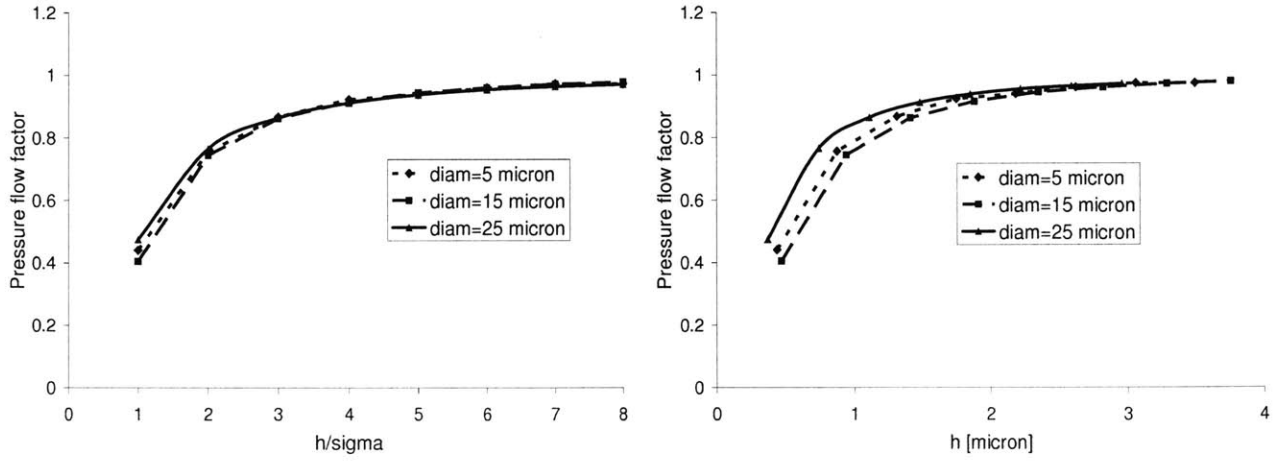

a) Pressure flow factor vs. h/sigma **b) Pressure flow factor vs. film thickness, h**

Figure 4-21: Effect of dimple diameter on pressure flow factor, depth = 3μ, area ratio = 0.25

Figure 4-20 shows the effect of dimple area ratio on the pressure flow factor. As the figure shows, pressure flow factor decreases slightly with area ratio, but the effect is weak. As for the grooves, it is expected that the effect of increasing area ratio will be to increase both the amount of interaction that occurs between dimples and the number of "micro-hydrodynamic" bearings

that are present on the surface, and is expected to cause a decrease in pressure flow factor. It is unclear why this effect is so weak for the dimpled cases, although several studies have also shown this for dimpled surfaces, including Etsion et. al.[49] and Ronen, et. al.[50].

Figure 4-21 also shows a relatively weak effect, of the dimple diameter on pressure flow factor. In this case, there is an optimum diameter at which pressure flow factor is minimized – the mid-range diameter, d = 15μ, shows the lowest ϕ_p. The optimal dimple diameter occurs at a value where the diameter and depth combine to define a dimple shape that provides the maximum hydrodynamic pressure generation, and is also similar to an effect observed by Etsion[49] in which an optimal ratio of dimple depth:diameter was found.

4.4.3.2 *Friction results*

Ring/liner friction predictions for the dimpled surfaces were consistent with those expected given the flow factor results presented above. Ās the effects of the surface parameters on the pressure flow factor were small, changes in FMEP for different surfaces considered were also small relative to those predicted for different grooved patterns. It appears that dimpled surfaces are less sensitive to changes in feature geometry – except for dimple depth – than grooved surfaces, and may thus be easier to design for given slider geometry and running conditions. Ās for the friction analysis for the grooved surfaces presented above, the following results are based on an approximate analytical method and cannot be used to predict actual friction reductions in realistic situations, but they do indicate that liner surface texturing can reduce ring/liner friction, and should be studied further.

Some modifications were made to the ring-pack simulation program in order to obtain the results presented below. Details of these modifications are given in Section 4.4.2.2. In the model, the depth of the dimples was represented by the overall textured surface roughness, σ, which has therefore been used to represent dimple depth in the figures shown below. In both figures, FMEP is plotted as a function of σ, which is the RMS roughness of the surface under study. This should be understood to correspond to dimple depth, where a roughness of σ=0.5μ corresponds approximately to a depth of d=3μ.

Figure 4-22 shows the effects of both dimple depth and area ratio on ring/liner FMEP. Ās the figure shows, the effects of depth are much greater than those of area ratio, which has only a small influence on friction. FMEP decreases strongly with depth, and shows no sign of leveling off at large depths, as the grooved cases did. It is expected that the effect of dimples on FMEP with increasing depth will eventually disappear, as for very deep dimples the fluid in the bottom will simply be stagnant and not contribute to the hydrodynamic action of the texturing. However, this limit appears to be beyond the level of dimple depth that has been investigated here. The effect of area ratio is much smaller than that of dimple depth, so that it may not be necessary to optimize for this parameter in designing a friction-reduction surface.

Figure 4-23 shows the effects of dimple diameter on ring/liner friction. The effect of diameter is also small, with the minimum FMEP found at a mid-range value. This optimal diameter phenomenon has also been observed in the literature (see Section 4.4.2.1) and is the

result of the effect of the dimple geometry on the amount of hydrodynamic pressure generation that occurs as lubricant flows through the dimple. The effect of diameter on both the converging/diverging length and the dimple profile contribute to this effect.

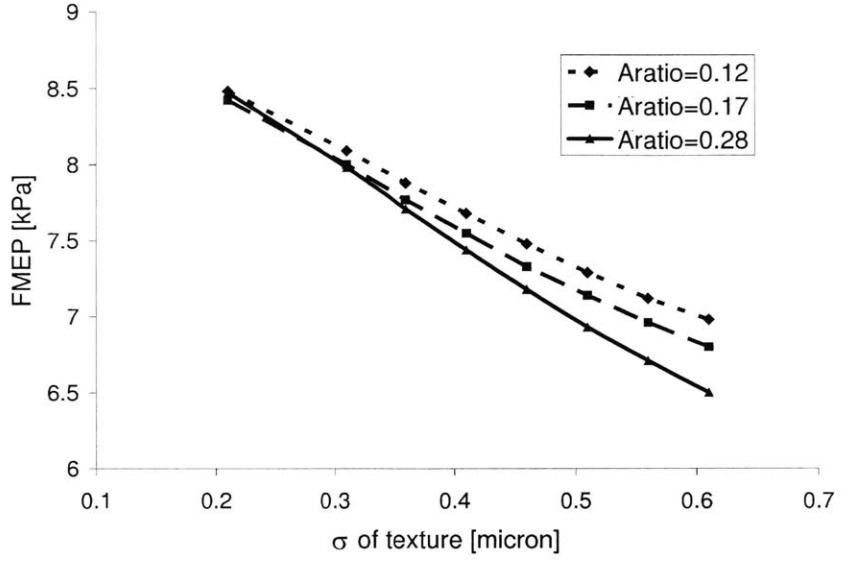

Figure 4-22: Effect of dimple area ratio on ring/liner friction, diameter = 19μ

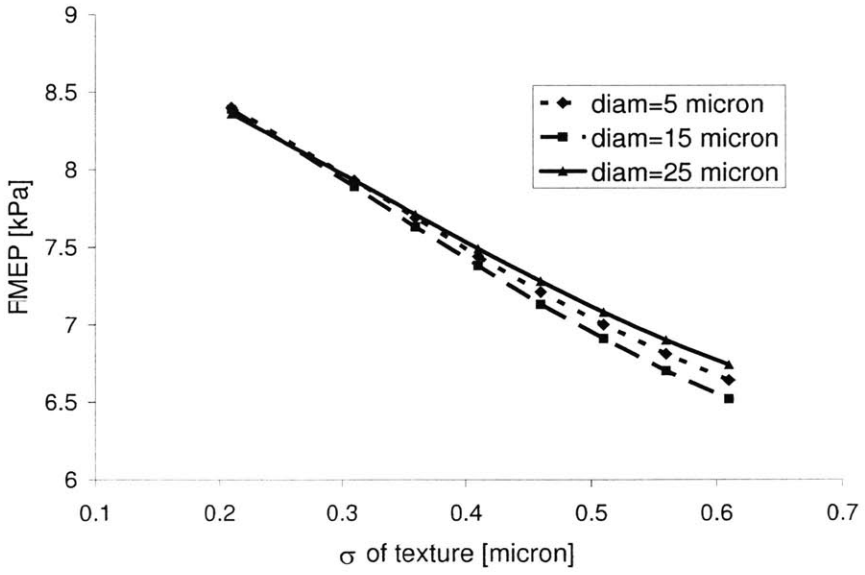

Figure 4-23: Effect of dimple diameter on ring/liner friction, area ratio = 0.25

4.5 Summary and conclusions of surface texturing parametric study

Surface features can affect sliding friction in many ways, including removing wear particles from the sliding interface and acting as fluid reservoirs to provide adequate lubrication where it is needed. This study considered the role played by surface texturing in the hydrodynamic regime, and its potential to reduce piston-ring/liner friction under this condition. An averaged flow-factor Reynolds analysis was used to evaluate the effects of patterns of either grooves or dimples on the cylinder liner. Because this averaged technique was used, a detailed study of the lubricant pressures and flows could not be made. Still, the results of this parametric study can be used to estimate the potential of surface texturing for, and the effects of various texture parameters on, friction reduction.

In a well-lubricated regime, surface texturing affects both hydrodynamic and boundary friction between the ring and liner by influencing the hydrodynamic pressure generation within the lubricant, and thus the oil film thickness. Textures that impede lubricant flow increase oil pressure and thus increase film thickness, at a given load. This increase in h can cause a reduction in asperity contact, if any was present in the baseline case, and also reduces shear stress by reducing the shear rate in the oil. Thus, an appropriate surface texture can decrease both hydrodynamic and boundary friction between ring and liner. An inappropriate texture, however, can cause an increase in friction by allowing oil to flow more easily and thus reducing oil film thickness. It is necessary to understand the effects of different textures, and their relation to slider parameters and running conditions, in order to design surfaces for friction reduction in actual applications.

Both stochastic parameters, such as roughness and skewness, and deterministically defined features such as dimples influence the way in which a surface affects sliding lubrication and friction. This study focused on two texture categories: patterns of round dimples and patterns of grooves. For the dimpled cases, the effects of dimple diameter, depth and area ratio were studied, while for the grooved surfaces groove angle, depth, width, and area ratio effects were assessed. The results of a parametric study of both the flow factors, which give an indication of the physical effects of the surface texturing, and predicted friction losses, for Waukesha engine geometry and running conditions, were presented.

The effects of many of the surface parameters studied were similar for the dimpled and grooved surfaces. Friction was found to decrease as the depths of both dimples and grooves were increased, as well as with increasing area ratio for both pattern types. The effects of groove width and dimple diameter were both relatively small. In the case of the dimples, an optimum effect was observed in which the minimum friction was found at a mid-range diameter, because of the dependence of hydrodynamic pressure generation on the shape and size of the dimples. There may also be an optimum effect in relation to groove depth, stemming from a trade-off between hydrodynamic effects and lubricant flow area. Friction was also found to decrease strongly with groove angle, (where a groove with a lower angle is more perpendicular to the lubricant flow direction) in agreement with previous studies[10].

The analytical method used in this study is subject to several limitations and approximations, and therefore the results are not intended to be used directly in the design of

friction-reducing surface textures. Rather, the trends presented here are used to illustrate the potential of appropriately designed surface textures to reduce friction both in the engine and other sliding friction applications, and to indicate the relative importance of the various texture parameters that define two common surface patterns. The study has showed that even relatively small-scale textures (compared to others that have been studied in the literature) can have a large effect on ring/liner friction, in some cases reducing FMEP by as much as 30% from a smooth surface case. Also, it may be possible to combine the effects of lubricant viscosity and surface texturing to reduce friction even further, while mitigating unwanted side-effects such as wear and oil consumption. This possibility is discussed in Section 5.2.3.

(This page was intentionally left blank)

5. Application of lubricant and surface texture studies to Waukesha engine

The lubricant and surface texture studies presented in Sections 3 and 4 were applied to an analysis of the piston ring-pack in the Waukesha VGF 18GL engine. These studies were part of an on-going program whose intention is to increase the efficiency of this engine from ~42% to 50%, over a ten year period. While reducing mechanical losses is only one of several efficiency-increasing measures to be developed in this time, it is an essential part of reaching the stated goal. Application of optimized lubricant and surface features to the piston ring-pack and cylinder liner is one of many measures that will help the goal efficiency to be achieved.

5.1 The engine

The engine under study is the Waukesha VGF 18GL, a large natural gas engine used for stationary power generation, shown in Figure 5-1. Some engine specifications and operating conditions are given in Table 5-1.

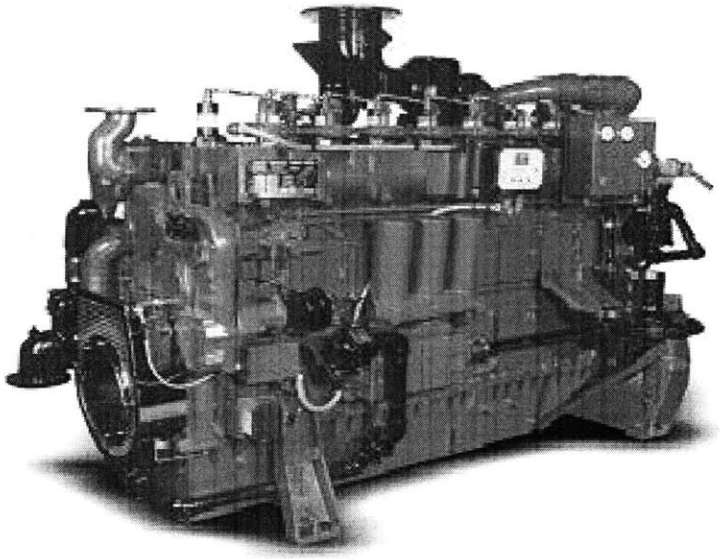

Figure 5-1: The Waukesha VGF 18GL engine

For baseline mechanical and surface roughness parameters, frictional losses in the Waukesha engine ring-pack are dominated by the oil control and top rings, as was shown in Figure 1-5. The OCR is the largest contributor to friction because of its high ring tension. It is required to conform very well to the cylinder liner, while maintaining enough stiffness to resist warping and breakage, so a high tension is necessary. This results in a high ring-liner load throughout the cycle, leading to high friction.

The top ring contribution to friction is also significant, because of the large friction forces associated with boundary friction near the top dead center (TDC) of the combustion stroke. In this region, two factors combine to create high friction: first, the oil supply to the top ring at TDC is very limited, because the oil control ring doesn't reach this high on the liner; second, combustion chamber gas pressure, following compression and combustion, is very high. The combination of high ring load and poor lubrication results in very high asperity contact pressures, and thus high friction (and also high wear). Even though piston speed is very low here, the total frictional power loss from this region is still significant. Figure 5-2 shows this high-friction "spike" for the top ring, compared to the more evenly distributed frictional losses for the OCR.

Table 5-1: Waukesha Engine baseline parameters and operating conditions

Parameter	Value	Unit
Engine type	Natural gas, SI	-
Bore x Stroke	0.152 x 0.165	m x m
Number of cylinders	6	-
Displacement	18	liter
Engine Speed	1800	rev/min
BMEP @ 1800 RPM	1380	kPa
Lubricant grade	SAE 40W	-
Top Ring Type	Skewed barrel	-
Second Ring Type	Napier	-
OCR Type	Twin land	-

Because the majority of top ring friction comes from this dry-region friction spike, however, this ring has not been considered in detail in either of the studies presented here. Top ring friction it is not expected to be strongly affected by lubricant viscosity, because most of the friction is generated in a poorly lubricated regime – if no lubricant is present, its properties cannot matter. A brief study of the effect of lubricant viscosity on oil transport into the dry region was conducted, with results presented in Section 3.8, but the model used to obtain these results had a relatively simple oil transport model, and more research is needed to validate the conclusions.

Also, while top ring friction may be greatly reduced by the addition of surface texturing to the cylinder liner, the mechanism by which this would occur has not been investigated here. The focus of the surface texture study was on the hydrodynamic effects of the surface features, and their ability to reduce friction in a well-lubricated regime. It may be possible to reduce top-ring friction by adding dimples near TDC to act as lubricant reservoirs, and thus increase the lubrication in this area. However, this mechanism has not been studied in the current project.

Because of these considerations, the oil control ring (OCR) was the main focus of both the lubricant and surface texturing studies. The OCR contributes most of the ring-pack friction and is strongly affected by lubricant viscosity and surface texturing. Top ring friction is significant,

but stems mainly from a poorly-lubricated regime in which viscosity and surface effects are expected to be small. The trends observed for the OCR are expected to correspond to viscosity/friction trends for the entire ring-pack.

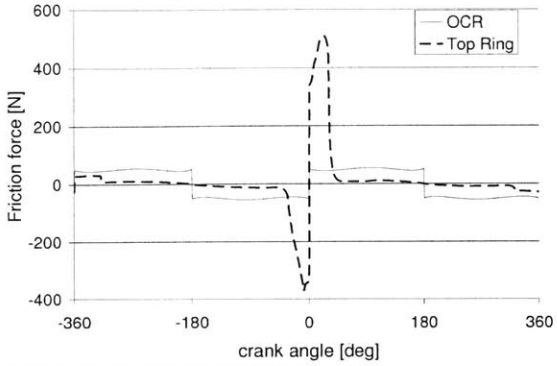

a) Top ring and OCR friction

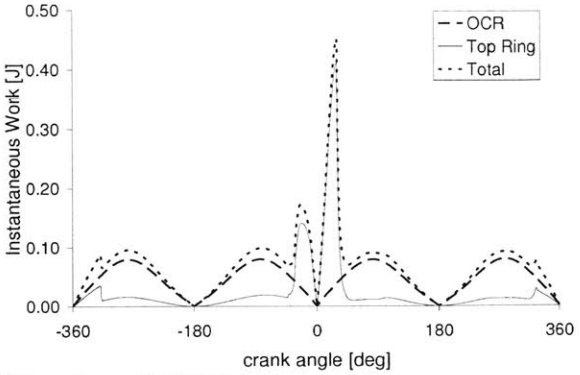

b)Top ring and OCR friction work losses

Figure 5-2: Top ring and OCR contributions to ring-pack friction losses

5.2 Application of lubricant and surface texturing study results to Waukesha engine

Changes in both lubricant viscosity and surface finish can lead to reduced friction in the Waukesha engine ring-pack. Reductions in lubricant viscosity reduce hydrodynamic friction between ring and liner, and if viscosity can be maintained at a higher value near dead-centers, wear in that region can be reduced. Adding an appropriate texture to the cylinder liner may also reduce friction, both hydrodynamic and boundary, by increasing hydrodynamic pressure generation and thus oil film thickness.

In addition to the individual effects of these two parameters, an even greater friction reduction is possible when these two changes are combined. Friction reduction via lubricant viscosity reduction is possible, but not without a concurrent increase in wear. Surface texturing can also be used to reduce friction, but does so by increasing oil film thicknesses, which may cause increased oil consumption. A reduced viscosity lubricant can be combined with a textured liner surface to reduce friction while minimizing these adverse effects.

Fortunately, the side-effects of viscosity reduction and addition of surface texturing are complimentary, so that when these techniques are used concurrently the negative aspects can be minimized. Reducing lubricant viscosity causes a reduction in oil film thickness, which may lead to increased asperity contact, and thus, wear. Adding surface texturing, however, causes an increase in oil film thickness, by increasing hydrodynamic pressure generation. If lubricant and surface texturing parameters can be changed so that oil film thickness remains approximately equal to the baseline case, there should be little effect on wear and oil consumption. Friction will still be reduced, however, because of the reduced lubricant viscosity.

Application of both lubricant viscosity changes and surface texturing to the Waukesha engine power cylinder are discussed below, followed by consideration of the possibility of optimizing lubricant viscosity and surface texturing concurrently. Because the surface texturing

study was a parametric exercise, no specific recommendations or friction reduction estimates can be made for the Waukesha engine, but possible benefits are estimated. Similarly, several examples are given to illustrate the effects of optimizing the lubricant and surface texturing together, but specific recommendations cannot be given. It is hoped that future analysis and testing will take a more in-depth look at the effects of surface texturing, and that an optimized, low-friction surface pattern for the Waukesha engine will be developed.

5.2.1 Optimization of lubricant viscosity

Friction power losses between the piston-rings and liner stem primarily from the mid-stroke region, while wear of the rings and liner is generally concentrated at the end-strokes. Reductions in both friction and end-stroke wear may be possible if lubricant viscosity can be reduced in the mid-stroke region and increased near dead-centers. Such a strategy was applied to the Waukesha engine, described above, and predictions of friction and wear made for an optimized lubricant.

As shown in Figure 5-3, a maximum friction reduction of ~10% is predicted for the OCR, from the baseline case, when viscosity in the mid-stroke region is reduced. An additional reduction of ~1% is possible when dead-center viscosity is held high to reduce boundary friction. For the Waukesha engine, the oil control ring accounts for ~65% of the total ring-pack losses. Then, an OCR friction reduction of 11% leads to a total ring-pack friction reduction of approximately 7%. Cross and Vogel equation parameters for the minimum-friction lubricant are given in Table 5-2 (those that are not given in the table are kept equal to baseline values, for SAE40 weight oil).

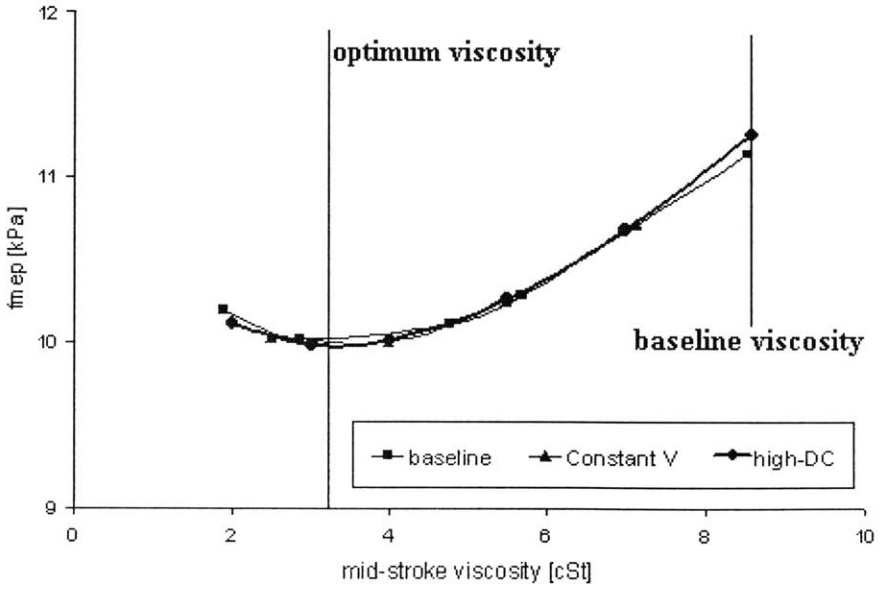

Figure 5-3: Reduction of oil control ring friction with mid-stroke viscosity. Three viscosity variation cases.

The top ring contributes most of the remainder of the ring-pack friction, but experiences most of its losses (~70%) as boundary friction in the poorly-lubricated TDC region of the stroke. Then, viscosity does not have a large direct affect on top ring friction. However, simulations show an indirect effect, where oil transport into the dry region may increase as viscosity decreases. This leads to a decrease in friction of up to 30%, leading to a ring-pack friction reduction of ~9%. However, the mechanism for this reduction is not clear, and a simplified oil-transport model was used which does not include all recognized oil transport mechanisms. Further research is required to investigate this top ring effect.

Ring/liner wear was also briefly considered, in a simple analysis of a wear coefficient related to boundary contact force and ring/liner sliding distance. Wear was found to increase strongly with decreasing viscosity, even as friction remains low. In the interest of keeping wear low, then, it may be necessary to accept a higher-than-minimum level of ring/liner friction. Controlling viscosity variation was shown to have some potential benefit in reducing wear near the end-strokes, because of the reduction in asperity contact forces in these regions, with an integrated wear coefficient reduction of ~25% for an engine cycle.

Table 5-2: Vogel and Cross equation parameters for low-friction lubricant

Parameter	Physical meaning	Current Value	Proposed Value	Ring-pack Friction Reduction
z	viscosity "thickness"	.09	.06	7%
c_1,c2	control critical shear rate	2.3, 0.0225	4.3, 0.0225	
m	controls width of transition region	1 (more gradual transition)	5 (sharper transition)	
μ/μ_0	ratio of high shear to low shear viscosities	1	0.5	

While it may be possible to develop a lubricant with the shear-dependence properties described here, or develop a liner temperature-control system to produce the same viscosity variation with location, the costs of these systems must be balanced against the potential benefits described above. Also, it should be emphasized that the study presented here considered the effects of lubricant viscosity on the piston ring-pack only. The effects of the considered viscosity changes on the other engine components must also be considered before any change in engine lubricant is made.

5.2.2 Optimization of liner surface finish

Surface texturing can be used in many different ways to reduce friction between a piston-ring and the cylinder liner. In this study, the ability of small-scale surface features to act as "micro-hydrodynamic" bearings, and thus increase the hydrodynamic pressure within the lubricant, was evaluated. The action of the micro-features causes an increase in oil film

thickness between the ring and liner, both decreasing asperity contact (if any is present to begin with) and decreasing oil shear rate, which reduces hydrodynamic friction.

The averaged-flow-factor Reynolds analysis method that was used in this study is limited in its ability to model details of the flows and stresses between textured surfaces, and thus the results cannot be used to recommend a specific liner texture for the Waukesha engine, or predict actual reductions in friction resulting from a textured surface. Rather, the trends in friction with changing surface parameters may be used as a starting point for further investigation of the effects of liner texturing, and may be used to estimate the potential for friction reduction in the case of the Waukesha power cylinder.

It has been noted that the surface texture of the Waukesha engine cylinder liner is already well-optimized for low friction, with a low skewness of -2.15 (more plateau surface) and honing grooves with the relatively low honing angle of 45° +/- 5°[10]. Then, further friction reductions for this engine may be relatively small. Figure 5-4 shows the predicted decrease in friction with groove angle for the oil control ring, with a groove depth of ~2μ. The actual depth of the grooves in the existing Waukesha cylinder liner is not known, but known stochastic parameters including roughness and skewness indicate that this is a reasonable estimate.

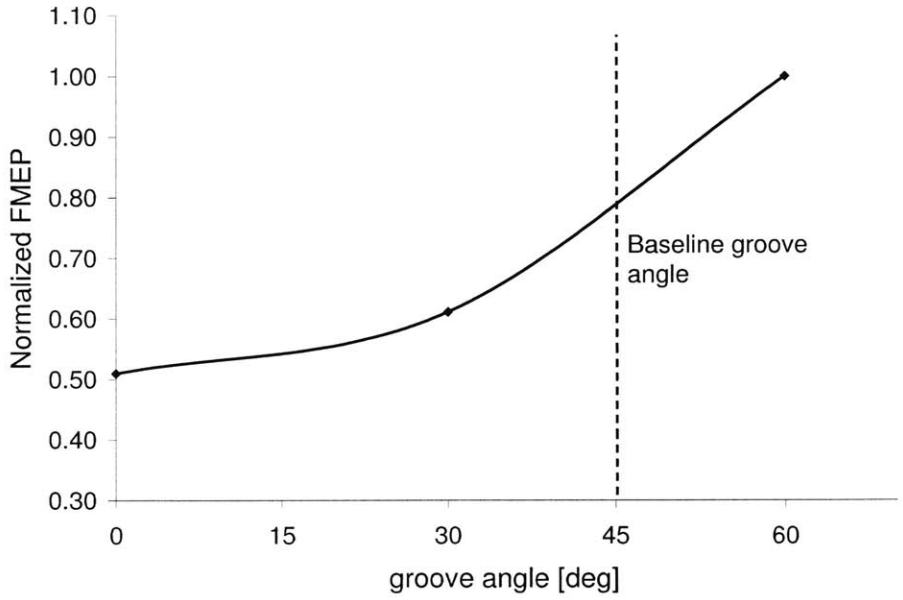

Figure 5-4: Estimate of OCR/liner friction reduction possible with reduced groove angle

Figure 5-4 indicates that, with a decrease in groove angle from 45° to 30°, a friction decrease of ~25% is expected. If the angle is further decreased down to a minimum value of 0°, the total reduction in FMEP is estimated at ~37%. These estimates are for the oil control ring alone. When frictional losses for the top and second rings are added, estimated friction reductions for the ring-pack become 15%, for 30° grooves, and 25% for 0° grooves. Although these numbers seem very promising, the simplifications made in both the surface modeling and the modeling of the ring/liner/lubricant interaction must be considered. Rather than being actual

estimates for FMEP reduction with groove angle, these numbers should be taken as estimates of the magnitude of friction reduction that could be possible.

Although the largest friction reduction is predicted for a very low groove angle, it should be noted that issues of engine wear and scuffing may be associated with honing grooves that are very perpendicular to the cylinder axis (although there is some disagreement over whether this is the case). The reason for this is not well understood. One possibility is that honing grooves at a larger angle allow fluid to flow through them, and thus clean out wear particles that are deposited there, while more perpendicular grooves eventually fill up with particles which then cause increased wear and scuffing. Another possible explanation is that the effect of the textured surface in the high-load, low-speed conditions near TDC of combustion is much different than that in the well-lubricated mid-stroke region. In high-speed, low-load conditions, transverse textures may get "flattened" by contact pressures, while more longitudinal textures survive[51].

The existing Waukesha engine cylinder liner already has a grooved pattern due to the surface honing process. Comparing the relative effectiveness of grooved and dimpled surfaces, it is not recommended that the existing pattern be replaced by a dimpled arrangement, as this would add complications to the finishing process and most likely not incur greater friction-reduction benefits than a grooved surface. It may be useful to add a dimpled or other discrete pattern to the cylinder liner that is on a larger scale than those studied here. Many of the surface textures studied in the literature focus on much larger dimples (with diameters on the order of 100μ and larger, depths on the order of 10μ) that have been shown to reduce friction (see Section 4.1.2 for further detail). However, such large features cannot be studied using the current modeling system.

A parametric study of the effects of surface texturing on ring/liner friction indicates that there is potential for these surfaces to reduce friction by a significant amount. The method of analysis used for this study prevents detailed predictions of friction and oil flow effects from being evaluated, and also limits the size of the surface textures that can be considered. The results from this simple study, however, indicate that appropriate surface texturing may provide a substantial benefit in friction reduction, and that further study, encompassing both more detailed modeling and a larger range of parameters, is justified.

5.2.3 Combined optimization of lubricant and liner surface

Ring/liner friction can be reduced when lubricant viscosity is decreased in the mid-stroke region, but the resulting increase in asperity contact may result in an unacceptable level of wear. A friction reduction is also possible if appropriate surface texturing is added to the cylinder liner, but the accompanying increase in oil film thickness may cause an increase in oil consumption. Alone, each of the friction-reduction techniques studied above can reduce losses but may also have an unwanted side effect. When used together, however, the side effects may be mitigated – the decrease in oil film thickness due to reduced viscosity may be offset by the increase due to the surface texturing – while still achieving a reduction in frictional losses.

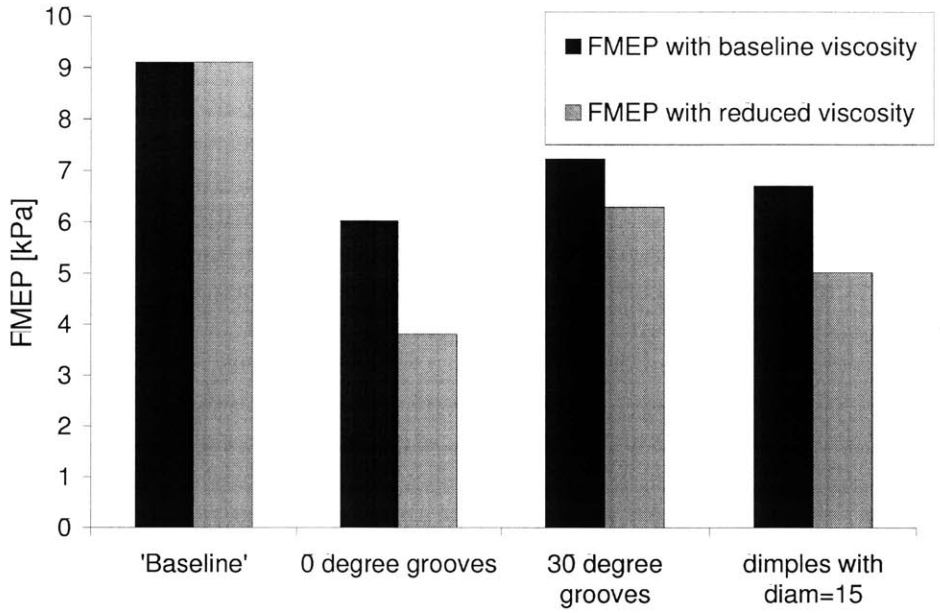

Figure 5-5: FMEP reduction due to combined lubricant and surface texturing effects, example cases

This possibility was studied using several promising surface textures. Because the surface texture study was parametric, and did not use realistic surface roughness in addition to the surface features under study, the results presented here should not be used to design an actual surface/lubricant combination. Rather, they are given as examples to illustrate the possibilities of optimizing the lubricant and surface texturing jointly, and to demonstrate the magnitudes of the possible friction-reduction benefits of doing so.

In each of the example cases, the given surface texturing was applied to the cylinder liner surface, and then the ring-pack simulation was run with varying lubricant viscosities. The viscosity at which oil film thickness and wear were closest to the original baseline case was selected as "ideal." At this viscosity, no net increase in asperity contact or oil film thickness should occur, so that changes in wear and oil consumption should be minimized.

Figure 5-5 shows the friction losses of three example surface textures, as compared to the baseline. For the baseline case the cylinder liner is untextured, and the lubricant is the baseline lubricant for the Waukesha engine (SAE 40). Surface and lubricant parameters for the example cases are given in Table 5-3. Only z, the oil "thickness" parameter from the Vogel equation (Eqn. 3.1) is varied for the lubricant, so that the viscosity temperature dependence remains the same as overall viscosity is changed.

Table 5-3: Surface and lubricant parameters for example cases

Surface texture properties		*Properties of reduced-viscosity lubricant*	
Baseline			
type	none (smooth)	z	.09
0 degree grooves			
type	parallel grooves	z	.025
depth, R_q	0.56 μ		
width	19μ		
groove angle	0 deg.		
area ratio	0.24		
30 degree grooves			
type	parallel grooves	z	.05
depth, R_q	0.56 μ		
width	19μ		
groove angle	30 deg.		
area ratio	0.24		
dimples, diameter = 15			
type	round dimples	z	.04
depth, R_q	0.56 μ		
diameter	19μ		
area ratio	0.25		

As Figure 5-5 shows, adding the surface texturing alone causes friction reduction in all cases, and then additionally reducing the lubricant viscosity causes friction to decrease further. This additional decrease in friction is not as large as that due to texturing alone, but is still a sizable reduction. Also, the reduction due to reduced lubricant viscosity is approximately proportional to that due to the texturing alone. This is because the amount of viscosity decrease that is ideal – that reduces the film thickness back to the baseline value – is directly related to the increase in film thickness that is brought about by the addition of surface texturing. The friction reduction due to the surface texturing is also related to this film thickness, so that the two drops in friction – due to surface features and due to lubricant viscosity reduction – are closely related to each other.

Figure 5-6 and Figure 5-7 show the effects of the combined surface/lubricant optimization on oil film thickness and wear parameter. As was the intention of using a lubricant with reduced viscosity, in cases where the surface and lubricant were optimized together both the oil film thickness and wear parameter are very similar to the baseline case. When surface texturing is used alone, the resulting oil film thicknesses are much higher than in the baseline case, as shown in Figure 5-6. Similarly, as shown in Figure 5-7, if viscosity is reduced without any added surface texturing, a large increase in wear is predicted. Optimizing the liner surface texture and lubricant viscosity concurrently offers the opportunity to mitigate these negative side effects, while still substantially reducing ring/liner friction.

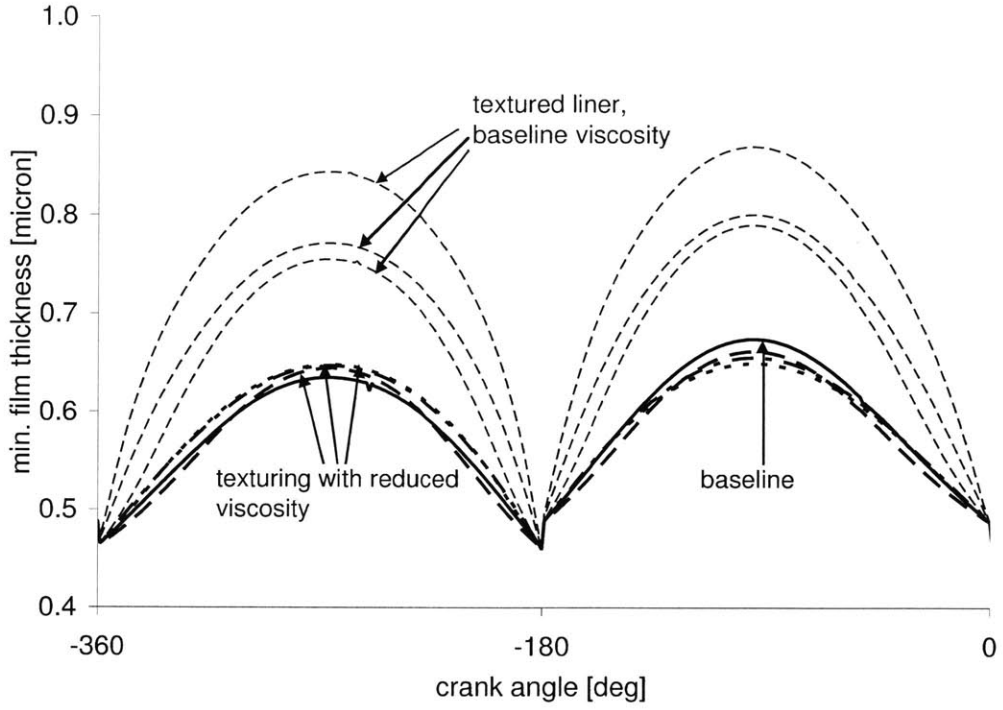

Figure 5-6: Minimum oil film thickness, for combined surface/lubricant effect example cases

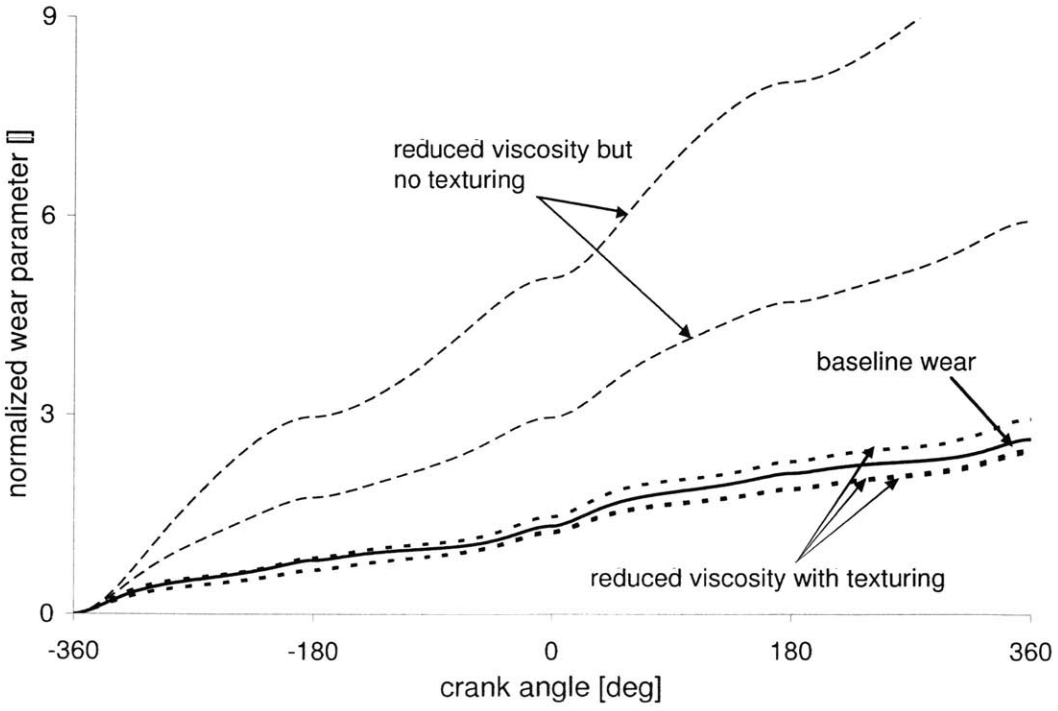

Figure 5-7: Normalized wear parameter, for combined surface/lubricant effect example cases

6. Summary and recommendations

The piston ring-pack is one of the largest contributors to mechanical losses in an internal combustion engine. In this study, the effects of lubricant viscosity and liner surface texturing on ring/liner friction were considered, with the intent of reducing these losses in the Waukesha VGF 18GL engine. An optimized low-friction lubricant was proposed, and a parametric study of surface texturing showed that adding appropriate surface features to the cylinder liner may also significantly reduce ring/liner friction. Also, if the lubricant and surface texturing can be optimized together, an even greater reduction in friction is possible, along with mitigation of undesired side-effects, such as oil consumption and wear, which may accompany changes made to the lubricant viscosity and surface texturing individually.

The ring-pack simulation model used for both the lubricant and surface texturing studies was based on averaged flow factor Reynolds analysis, and was developed at MIT. Inclusion of features such as ring dynamics, gas flows, and different lubrication modes makes this advanced model able to predict ring/liner friction accurately for a variety of conditions. While the lubricants studied in the first phase of this research were certainly unusual, they were not out of the realm of applicability for this model, and results of the lubricant study should be considered to be realistic. However, the textured surfaces considered in the second phase of this study may have been close to the limitations of surface roughness for which this model was intended. Also, the averaged flow-factor method takes into account less detail about fluid flows and asperity contact than is required for an in-depth study of surface texturing. Then, the results of the this study may be used to assess the effects of the various parameter considered, and evaluate the potential of texturing techniques for reducing ring/liner friction, but further, more detailed study is required to predict the effects of specific surface features with good accuracy.

The subject of the initial phase of this research was the potential of changes in the lubricant viscosity to bring about a reduction in ring/liner friction. Lubricant viscosity affects friction both directly, by having a direct affect on hydrodynamic friction, and indirectly, by influencing the oil film thickness and thus the amount of asperity contact that occurs. Increasing viscosity tends to increase oil film thickness, and thus reduce asperity contact, but causes hydrodynamic friction to increase. A viscosity that balances between the hydrodynamic and boundary lubrication modes is required for minimum friction.

Changes in ring speed and load cause the "ideal" viscosity for low friction to change during the engine cycle. The object of the lubricant study was to determine the optimum viscosity for all points in the engine cycle, and evaluate the potential for friction reduction with such an idealized lubricant. Also, the effects of viscosity change on wear were considered.

Because of changes in ring speed, boundary friction becomes large in the dead-center regions of the piston stroke, while hydrodynamic friction dominates in mid-stroke. Thus, for the reduction of ring/liner friction force, a high viscosity is desired near end-strokes and a low viscosity near mid-strokes. However, the purpose of this study was to reduce the power lost to friction, and, because of its dependence on speed, the power lost to friction is much higher near the mid-strokes than at the end-strokes, where piston speed goes to zero. Because of this, the

viscosity of the lubricant in the end-stroke regions was found to have only a small effect on ring/liner FMEP, with the major realm of influence of lubricant viscosity occurring in the mid-stroke region. For the Waukesha engine ring-pack, a friction reduction of ~7% is predicted from reduction of mid-stroke lubricant viscosity.

Although viscosity near the end-strokes has very little effect on friction losses, it does influence ring/liner wear. Slow piston speeds cause asperity contact to be high at the end-strokes, resulting in high wear rates. When viscosity is kept high in these regions asperity contact and thus wear is reduced. Advanced lubricants with appropriate shear-rate dependencies or liner cooling systems that take advantage of the temperature-dependence of the lubricant viscosity may be able to achieve this in practice. A wear parameter analysis predicts that a reduction in wear of ~25% over an engine cycle is possible.

Surface texturing, also, can be used to reduce friction between the ring and liner. Numerous studies have predicted friction reductions with the addition of grooves, dimples, or other features to sliding surfaces. In the second phase of this research, the effect of surface patterns on friction in the hydrodynamic regime was evaluated. Friction reduction was observed when the surface texturing caused an increase in flow resistance, increasing oil film thickness and thus causing a reduction in both asperity contact and hydrodynamic friction. (In the latter case, the increased film thickness causes a reduction in oil shear rate). A parametric analysis of both grooved and dimpled patterns was performed, with the two purposes of studying the effects of various geometrical parameters on this friction reduction, and evaluating the potential of textured surfaces to reduce ring/liner friction and possibly justify further research in this area.

Groove parameters studied included the groove angle, width, depth, and area ratio, while parameters for the round dimples were the dimple depth, diameter, and area ratio. For both types of texturing, friction was found to decrease strongly with the depth of the features, and for grooved surfaces friction dropped substantially as groove angle was reduced (a groove with a lower angle is more perpendicular to the direction of piston travel). Also, for both types of texture, friction decreased with increasing area ratio, although not as strongly as with depth or groove angle. Groove width and dimple diameter had only a minor effect on ring/liner friction, with the dimpled surfaces showing a slight optimum effect (the lowest FMEP was predicted for a mid-range dimple diameter).

The analytical method used in this study did not allow for accurate predictions of ring/liner friction for specific cases, but the trends and orders of magnitude of the friction results can be used to illustrate the effects of textured surfaces and their potential for friction reduction. The study has indicated that even the relatively small-scale (compared to many evaluated in the literature) surface features considered may have a substantial effect on friction power losses. A reduction in oil control ring FMEP of as much as 30%, from a smooth surface case, is predicted for the best case studied. If the results of the parametric study are applied to the Waukesha engine ring-pack, a possible friction reduction of 15-25% is estimated through control of groove angle. While these predictions are approximate and should not be used to design actual friction-reducing surfaces, they indicate that a substantial friction reduction may be possible with the addition of appropriate textures to the cylinder liner.

In addition to studying the lubricant viscosity and liner surface texture independently, the possibility of optimizing these two parameters together was also considered. Not only can concurrent optimization of lubricant viscosity and surface texture cause a greater friction reduction than each individual parameter, the occurrence of unwanted side-effects can also be reduced. A reduction in lubricant viscosity, while reducing friction, also causes an increase in wear because of the reduced oil film thickness. Adding a surface texture to the liner may also reduce friction, but does so by causing an increase in oil film thickness which may in turn cause an increase in oil consumption. Fortunately, the effects of the two changes are opposed: reducing viscosity reduces oil film thickness, whereas adding surface texturing increases it. If the viscosity and texturing effects are considered together, the lubricant and liner surface can be designed so that oil film thickness remains constant, thus eliminating the wear and oil consumption increases, while still reducing friction.

The nature of the combined optimization of lubricant viscosity and surface texturing is essentially to use the increase in hydrodynamic pressure brought about by the texture to allow lubricant viscosity to be reduced. Then, the source of the friction reduction is purely hydrodynamic, and stems from the reduced viscosity. This study has indicated that the amount of friction reduction possible using a combined method is proportional to that possible from surface texturing alone. For the best combination of surface and lubricant studied, compared to a smooth surface with the lubricant currently used in the Waukesha engine, a reduction in FMEP of greater than 50% is predicted for the oil control ring, translating into a reduction of ~30% for the ring-pack. While friction reduction will likely be less than this when applied in real situations (particularly as many surfaces and lubricants are already well-optimized compared to the smooth surface case used as the baseline in this comparison,) this prediction indicates that there is significant potential for friction reduction via concurrent optimization of lubricant and surface properties.

The results presented above are believed to be as realistic as possible given the scope and constraints of this study. However, several approximations and simplifications have been made, and some factors not considered. Several recommendations for further study, both analytical and experimental, can be made, to both advance the state of knowledge on the topics studied here and to move towards an integrated, low-friction system for the Waukesha engine.

Several recommendations are made for further study in the area of surface texturing, as this is a promising field that is far from being well-understood at this time. As mentioned above, the ring-pack model used in this study is intended to be applied in cases where the ring and liner textures are relatively simple and can be well-described stochastically. It is recommended that further studies of surface effects be carried out with a deterministic model that can take more details of fluid flow and asperity contact into account, and has a wider range of application, both with respect to surface features and running conditions. For example, such a model should be able account for flows into and around specific surface features, such as flow within grooves, and cope with cases where oil does not entirely fill the gap between the sliding surfaces. Such a model would also allow a larger range of surface textures to be considered than can currently be studied. The averaged flow factor method is limited to surface features that are much smaller than the wetted are between ring and liner, whereas a deterministic model would not be constrained in this respect.

Also, for a more complete understanding of the benefits of surface texturing in the engine, study should be made of other possible surface texture benefits in addition to the hydrodynamic effects described here. Surface dimples or grooves may act as lubricant reservoirs or as wear particle traps, and possibly in other capacities as well. Study of these phenomena would help answer questions as to what textures are appropriate for the cylinder liner, where they should be placed, etc. For example, it has been suggested that dimples be placed on the liner near TDC to act as lubricant reservoirs for the top ring. Modeling the effectiveness of such dimples would inform the choice of using these or other textures.

It is also important to consider the effects of the various changes recommended in this study on other engine components. The results presented above are based on analysis of the piston ring-pack only. However, changes in both liner surface texture and particularly lubricant properties will have wider ranging effects. The surface texture of the liner will affect the friction and lubrication of the piston, which is thought to account for as much of the engine mechanical losses as the ring-pack. Changes in the lubricant will have an even broader effect, as the lubricant is used throughout the engine. A reduction in lubricant viscosity may cause unsustainable wear in other engine components, for example. It may be possible to mitigate such an effect by adding coatings or appropriate surface texturing to these components, but a thorough a investigation of these and other possibilities should be performed. The influence of the recommended changes on the entire system must be considered before recommendations for the Waukesha engine can be made.

The effects of the optimizations recommended above should be considered with respect to not only the performance of the engine, but also the financial costs associated with them. If surface textures that cannot be created with small adjustments to the standard honing process are required, the additional cost of new manufacturing techniques must be considered. Also, lubricants with the properties recommended above, which have high viscosity near end-strokes and low near mid-strokes, are not currently available. The costs of either developing such a lubricant or designing an appropriate liner cooling system should be evaluated against the projected benefits.

In addition to analytical work, it is recommended that experimental investigation be used to validate and inform the analytical models. Testing in a full-scale Waukesha engine has been performed in the past, and is recommended for use in the future when specific recommendations for this engine have been made. However, it will also be very useful to use a smaller-scale testing device, such as a bench-top tribometer or single-cylinder engine, for more general testing and model validation. Such a test set-up would allow the measurement of parameters such as the oil film thickness and instantaneous friction coefficient, which are essential for confirmation of model predictions and calibration of analytical simulations, as well as the overall frictional reductions which are the eventual goal of this research.

References

1. Class notes for course GEO 3005: Earth resources, at University of Minnesota. Data source: USEIA, MN Energy Data Book, 1997. http://talc.geo.umn.edu/courses/3005/resource.html

2. http://cdiac.esd.ornl.gov/trends/emis/usa.htm, from Carbon Dioxide Information Analysis Center at Oak Ridge National Laboratory.

3. Brook, E.J., "Tiny Bubbles Tell All," Science, vol. 310, pp.1285-1287, 2005.

4. Richardson, D.E., "Review of Power Cylinder Friction for Diesel Engines", Internal Report, Cummins Engine Company

5. Heywood, J.B., "Internal Combustion Engine Fundamentals", McGraw-Hill Inc., 1988

6. McGeehan, J.A., "A Literature Review of the Effects of Piston and Ring Friction and Lubricating Oil Viscosity on Fuel Economy", SAE Paper 780673, 1978

7. Wakuda, M., et al. "Effect of surface texturing on friction reduction between ceramic and steel materials under lubricated sliding contact," Wear vol. 254, pp. 356-363, 2003.

8. Hegemier, T., Stewart, M., "Some Effects of Liner Finish on Diesel Engine Operating Characteristics," SAE paper 930716, 1996.

9. Jeng, Y., "Impact of Plateaued Surface on Tribological Performance," Tribology Transactions, vol . 29, pp. 354-361, 1996.

10. Jocsak, Jeffrey "The Effects of Surface Finish on Piston Ring-Pack Performance in Advanced Reciprocating Engine Systems," Master's Thesis, Massachusetts Institute of Technology, Cambridge, MA, June 2005

11. Water, Fred, Fundamentals of Manufacturing for Engineers, UCL Press, London, 1996.

12. Rohde, S.M., "A Mixed Friction Model for Dynamically Loaded Contacts with Application to Piston Ring Lubrication," Proc. of the 7th Leeds-Lyon Symposium on Tribology, Westbury House, pp. 19-50, 1980.

13. Liu, J.J., et. al., "Current and Future Approaches for Laser Texturing of Thin Film Media," IEEE Transactions on Magnetics, vol. 36, pp. 125-132, 2000.

14. Etsion, I., "State of the Art in Laser Surface Texturing," ASME Journal of Tribology, vol. 127, pp. 248-253, 2005.

15. see: "The Future of the Surface: Optimum Tribosystems Through Functionally Optimized Surfaces," www.Gehring.de/enpdf/LaserHoning.pdf

16. Economou, P.N., Dowson, D. and Baker, A.J.S., "Piston Ring Lubrication – Part I: The Historical Development of Piston Ring Technology," ASME Journal of Lubrication Technology, vol. 104, pp. 118-126, 1982.

17. Dowson, D., et. al., "Piston Ring Lubrication – Part II: Theoretical Analysis of a Single Ring and a Complete Ring Pack," Energy Conservation Through Fluid Film Lubrication Technology, Winter Annual Meeting of ASME, NY, pp.23-52, 1979.

18. Michail, S.K. and Barber, G.C., "The Effects of Roughness on Piston Ring Lubrication Part I: Model Development," Tribology Transactions, vol. 38, pp. 19-26, 1995.

19. Tian, T., "Modeling the Performance of the Piston Ring Pack in Internal Combustion Engines", PhD Thesis, Department of Mechanical Engineering, Massachusetts Institute of Technology, June 1997

20. Greenwood, J.A., Tripp, J., "The Contact of Two Nominally Flat Surfaces," Proc. Inst. Mech. Engrs., vol. 185, pp. 625-633, 1971.

21. Hu, Y., et. al., "Numerical Simulation of Piston Ring in Mixed Lubrication – A Non-Axisymmetrical Analysis," ASME Journal of Tribology, 1993.

22. Elderton, P.E. and Johnson, L.J., Systems of Frequency Curves, London: Cambridge University Press, 1969.

23. Chung, Y., Schock, H.J. and Brombolich, L.J., "Fire Ring Wear Analysis for a Piston Engine," SAE Paper # 930797, 1997.

24. Patir, N. and Cheng, H.S., "Application of Average Flow Model to Lubrication Between Rough Sliding Surfaces," ASME Journal of Lubrication Technology, vol. 101, pp. 220-230, 1979.

25. Tian, T., et.al., "A Piston Ring-Pack Film Thickness and Friction Model for Multigrade Oils and Rough Surfaces," SAE paper 962032, 1996.

26. Arghir, et. al., "Theoretical Analysis of the Incompressible Laminar Flow in a Macro-Roughness Cell," ASME Journal of Tribology, vol. 125, pp. 309-318, 2003.

27. Taylor, R.I. and Mainwaring, R., "Trends in Fluid Lubrication," in Total Tribology, Sherrington, Rowe & Wood, eds., London, Professional Engineering, 2002.

28. Taylor, R.I., et. al., "Lubricants & Energy Efficiency: Life-Cycle Analysis," Leeds-Lyon Symposium on Tribology, 2004.

29. Hoult, D.P., et. al., "Direct Observation of the Friction Reduction of Multigrade Lubricants," SAE Paper # 910742, 1991.

30. Tian, T. "Dynamic behaviors of piston rings and their practical impact, Part2: Oil Transport, Friction, and Wear of Ring/Liner Interface and the Effects of Piston and Ring Dynamics," Proc. Inst. Mech. Engrs. Part J: Engineering Tribology (216) 2002, pp. 229-247

31. Amoser, M., Schnellman, L., and Werner, T., "Sulzer TriboPak: Service Experience Report," Wartsila, Inc., 2003., http://www.wartsila.com/Wartsila/docs/en/ship_power/media_publications/technical_papers/sulzer/tribopack_servexp.pdf

32. Hamilton, D.B., Walowit, J.A. and Allen, C.M., "A Theory of Lubrication by Microasperities", ASME J. Basic Eng., vol. 88, pp. 177-185, 1966.

33. Anno, J.N., Walowit, J.A. and Allen, C.M., "Microasperity Lubrication", ASME Journal of Lubrication Technology, vol. 90, pp. 351-355, 1968.

34. Anno, J.N., Walowit, J.A., and Allen, C.M., "Load Support and leakage from Microasperity-Lubricated Face Seals", ASME Journal of Lubrication Technology, vol. 91, pp. 726-731, 1969.

35. Tian, H., Saka, N., Suh, N., "Boundary Lubrication Studies on Undulated Titanium Surfaces", Tribology Transactions, vol. 32, pp. 289-296, 1989.

36. Tønder, K., "Inlet Roughness Tribodevices: Dynamic Coefficients and Leakage", Tribology International, vol. 34, pp. 847-852, 2001.

37. Suh, N., Tribophysics, Englewood Cliffs, NJ: Prentice-Hall, Inc., 1986.

38. Petterson, U. and Jacobson, S., "Influence of Surface Texture on Boundary Lubricated Sliding Contacts", Tribology International, vol. 36, pp. 857-864, 2003.

39. Blatter, A., et. al., "Lubricated Sliding Performance of Laser-Patterned Sapphire," Wear, vol. 232, pp. 226-230, 1999.

40. Kovalchenko, A., Ajayi, O., Erdemir, A., Fenske, G., Etsion, I., "The Effect of Laser Surface Texturing on Transitions in Lubrication Regimes During Unidirectional Sliding Contact", Tribology International, vol. 38, pp. 219-225, 2005.

41. Sadeghi, F., et. al., "Advanced Natural Gas Reciprocating Engine: Parasitic Loss Control Through Surface Modification," presented at ARES/ARICE Low Engine Friction Alliance Workshop, Cambridge, MA, Dec. 1, 2005.

42. Etsion, I., et. al., "Analytical and Experimental Investigation of Laser-Textured Mechanical Seal Faces," Tribology Transactions, vol. 42, pp. 511-516, 1999.

43. Ronen, A., Etsion, I., Kligerman, Y., "Friction-Reducing Surface-Texturing in Reciprocating Automotive Components," Tribology Transactions, vol. 44, pp. 359-366, 2001.

44. Ryk, G., Kligerman, Y., Etsion, I., "Experimental Investigation of Laser Surface Texturing for Reciprocating Automotive Components," Tribology Transactions, vol. 45, pp. 444-449, 2002.

45. Siripuram, R. and Stephens, L., "Effect of Deterministic Asperity Geometry on Hydrodynamic Lubrication", ASME Journal of Tribology, vol. 126, pp. 527-534, 2004.

46. Hsu, S., "Integrated Surface Modification Technology Development," presented Sept. 15, 2005.

47. Kotwal, C. and Bhushan, B., "Contact Analysis of Non-Gaussian Surfaces for Minimum Static and Kinetic Friction and Wear," Tribology Transactions vol. 39, pp. 890-898, 1996.

48. Pinkus, O., Theory of Hydrodynamic Lubrication, New York:, McGraw-Hill Book Co., 1961.

49. Etsion, I., et. al., "Analytical and Experimental Investigation of Laser-Textured Mechanical Seal faces," Tribology Transactions vol. 42, pp. 511-516, 1999.

50. Ronen, A., Etsion, I., and Kligerman, Y., "Friction-Reducing Surface-Texturing in Reciprocating Automotive Components," Tribology Transactions vol. 44, pp. 359-366, 2001.

51. Kweh, et. al., "Micro-Elastohydrodynamic Lubrication of an Elliptical Contact with Transverse and Three-Dimensional Sinusoidal Roughness," ASME Journal of Tribology, vol. 111, pp. 577-584, 1989.

Appendix A: Derivation of Fundamental Equations

A.1. Reynolds Equation

The Reynolds equation is used to model the behavior of the lubricant between ring and liner. A derivation of the Reynolds equation for smooth surfaces (surface roughness not taken into account) is given below. It is a simplification of the fundamental conservation of momentum relationships of the Navier-Strokes equations (A.1) and conservation of mass, or continuity (A.2):

x-direction:

$$\rho\left(\frac{\partial u}{\partial t}+u\frac{\partial u}{\partial x}+v\frac{\partial u}{\partial y}+w\frac{\partial u}{\partial z}\right)=-\frac{\partial p}{\partial x}+\mu\left(\frac{\partial^2 u}{\partial x^2}+\frac{\partial^2 u}{\partial y^2}+\frac{\partial^2 u}{\partial z^2}\right)+\rho X$$

y-direction:

$$\rho\left(\frac{\partial v}{\partial t}+u\frac{\partial v}{\partial x}+v\frac{\partial v}{\partial y}+w\frac{\partial v}{\partial z}\right)=-\frac{\partial p}{\partial y}+\mu\left(\frac{\partial^2 v}{\partial x^2}+\frac{\partial^2 v}{\partial y^2}+\frac{\partial^2 v}{\partial z^2}\right)+\rho Y \tag{A.1}$$

z-direction:

$$\rho\left(\frac{\partial w}{\partial t}+u\frac{\partial w}{\partial x}+v\frac{\partial w}{\partial y}+w\frac{\partial w}{\partial z}\right)=-\frac{\partial p}{\partial z}+\mu\left(\frac{\partial^2 w}{\partial x^2}+\frac{\partial^2 w}{\partial y^2}+\frac{\partial^2 w}{\partial z^2}\right)+\rho Z$$

$$\frac{d\rho}{dt}+\frac{\partial}{\partial x}(\rho u)+\frac{\partial}{\partial y}(\rho v)+\frac{\partial}{\partial z}(\rho w)=0 \tag{A.2}$$

where ρ is the lubricant density, u, v and w are the flow speeds in the x, y and z directions, respectively, μ is the lubricant dynamic viscosity, and X, Y and Z are external forces acting on the lubricant in the x, y and z directions. Since the film thickness, h, is much smaller than the curvature of the cylinder, rectangular coordinates can be used. In application to the ring/liner interface, the x-axis is taken along the axis of the cylinder, the y-axis is in the radial direction and the z-axis in the tangential direction.

Several simplifying assumptions can be made for the case of lubricant between ring and liner. First, it is assumed that there are no external forces, so that the X, Y and Z terms disappear. Other simplifications can be more clearly justified using a non-dimensionalized Navier-Stokes relationship[26], (A.6). In these relations, non-dimensionalized length variables:

$$x^*=\frac{x}{L}, y^*=\frac{y}{h}, z^*=\frac{z}{L} \tag{A.3}$$

and velocity terms:

$$u^* = \frac{u}{V}, v^* = \frac{v}{V}\frac{L}{h}, w^* = \frac{w}{V} \tag{A.4}$$

are used, where L is a characteristic length scale in the plane of the oil film, h is a length scale in the radial direction, and V is a characteristic speed in the plane of the film. For the ring/liner system, L is taken to be the ring axial width, h a typical oil film thickness, and V the piston speed. A characteristic velocity in the radial direction is taken to be proportional to V via a ratio of length scales. Characteristic time τ =L/V and pressure, P can also be chosen to non-dimensionalize the time and pressure variables:

$$p^* = \frac{p}{P}, t^* = t\frac{V}{L} \tag{A.5}$$

Then, the Navier-Stokes equations become:

$$\mathrm{Re}\frac{h}{L}\left(\frac{\partial u^*}{\partial t^*} + u^*\frac{\partial u^*}{\partial x^*} + v^*\frac{\partial u^*}{\partial y^*} + w^*\frac{\partial u^*}{\partial z^*}\right) = -\frac{\partial p^*}{\partial x^*}\frac{Ph^2}{L\mu V} + \frac{\partial^2 u^*}{\partial y^{*2}} + \left(\frac{h}{L}\right)^2\left(\frac{\partial^2 u^*}{\partial x^{*2}} + \frac{\partial^2 u^*}{\partial z^{*2}}\right)$$

$$\mathrm{Re}\left(\frac{h}{L}\right)^3\left(L\frac{\partial u^*}{\partial t} + u^*\frac{\partial v^*}{\partial x^*} + v^*\frac{\partial v^*}{\partial y^*} + w^*\frac{\partial v^*}{\partial z^*}\right) = \tag{A.6}$$

$$-\frac{\partial p^*}{\partial y^*}\frac{Ph^2}{L\mu V} + \left(\frac{h}{L}\right)^2\frac{\partial^2 v^*}{\partial y^{*2}} + \left(\frac{h}{L}\right)^4\left(\frac{\partial^2 v^*}{\partial x^{*2}} + \frac{\partial^2 v^*}{\partial z^{*2}}\right)$$

$$\mathrm{Re}\frac{h}{L}\left(\frac{\partial w^*}{\partial t^*} + u^*\frac{\partial w^*}{\partial x^*} + v^*\frac{\partial w^*}{\partial y^*} + w^*\frac{\partial w^*}{\partial z^*}\right) = -\frac{\partial p^*}{\partial z^*}\frac{Ph^2}{L\mu V} + \frac{\partial^2 w^*}{\partial y^{*2}} + \left(\frac{h}{L}\right)^2\left(\frac{\partial^2 w^*}{\partial x^{*2}} + \frac{\partial^2 w^*}{\partial z^{*2}}\right)$$

Typical values for the characteristic parameters are given in Table A-1. These values are typical for the ARES engine geometry and running conditions, near mid-stroke. In particular, it should be noted that the Reynolds number for the flow is small compared to the transition to turbulence for internal flow, while the ratio of length scales, h/L, is very small. These parameters imply that some simplifications can be made based on the physical state of the flow: the small Re indicates that the flow is laminar and viscosity terms should be more important than inertial terms, while the very small h/L ratio indicates that the film is very thin compared to its extent, and so the pressure drop across the film is expected to be negligible. When the values in Table A-1 are substituted in to A.6 and "small" terms eliminated, these expected simplifications appear. Eqns. A.7 give the final form of the simplified Navier-Stokes relations.

It should be noted that, for the case of the piston rings, parameters such as the piston speed and ring load change by several orders of magnitude over the course of an engine cycle. The parameters given in Table A-1 are typical in the mid-stroke range where Reynolds equation is expected to be applicable. Near end-strokes where piston speeds are low and the ring load may be high, care should be taken to ensure applicability of the Reynolds approximations resulting in Eqns. A.7.

Table A-1: Typical values of parameters in non-dimensionalized Navier-Stokes relations (mid-stroke)

h	10^{-6} m
L	10^{-3} m
ρ	10^{3} kg/m^3
V	10 m/s
μ	10^{-3} kg/ms
P	10^{6} Pa
Re = ρ Vh/ μ	10
Ph^2/ μVL	10^{-1}
h/L	10^{-3}

$$\frac{1}{\mu}\frac{\partial p}{\partial x} = \frac{\partial^2 u}{\partial y^2}$$
$$0 = \frac{\partial^2 v}{\partial y^2} \qquad \text{(A.7)}$$
$$\frac{1}{\mu}\frac{\partial p}{\partial z} = \frac{\partial^2 w}{\partial y^2}$$

The equations A.7 are used, along with boundary conditions, to model the flow between ring and liner. A no-slip condition is specified for all surfaces (U is the relative speed between the two translating surfaces, assumed to be entirely axial, h is the separation between the surfaces):

$$u(y=0) = 0$$
$$u(y=h) = U$$
$$v(y=0) = 0$$
$$v(y=h) = \frac{\partial h}{\partial t} \qquad \text{(A.8)}$$
$$w(y=0) = 0$$
$$w(y=h) = 0$$

Then, integration of Eq. (A.7) with application of the above boundary conditions yields the following result:

$$u = \frac{1}{2\mu}\frac{\partial p}{\partial x}y(y-h) + \frac{Uy}{h}$$
$$v = \frac{\partial h}{\partial t}\left(\frac{y}{h}\right) \qquad \text{(A.9)}$$
$$w = \frac{1}{2\mu}\frac{\partial p}{\partial z}y(y-h)$$

Assuming that the fluid is incompressible, continuity (conservation of mass, A.2) becomes:

$$\frac{\partial u}{\partial x} + \frac{\partial v}{\partial y} + \frac{\partial w}{\partial z} = 0 \qquad \text{(A.10)}$$

Substituting the expressions from A.9 into A.10, and integrating across the oil film thickness, (from 0 to h) yields:

$$\frac{\partial}{\partial x}\left(\frac{h^3}{\mu}\frac{\partial p}{\partial x}\right) + \frac{\partial}{\partial z}\left(\frac{h^3}{\mu}\frac{\partial p}{\partial z}\right) = -6U\frac{\partial h}{\partial x} + 12\frac{\partial h}{\partial t} \qquad \text{(A.12)}$$

This is the two-dimensional Reynolds Equation for incompressible lubricants. In piston analysis the full 2-D equation must be used to account for fluid distribution between the piston skirt and liner. For the rings, however, a simplified relationship can be used.

A.1.1. 1-D Reynolds Equation

In the case of the piston rings, the two-dimensional Reynolds equation can be further simplified to a 1-D case, if it is assumed that there is a negligible change in pressures around the circumference of the ring. Then, Eq. A.12 can be simplified to:

$$\frac{\partial}{\partial x}\left(\frac{h^3}{\mu}\frac{\partial p}{\partial x}\right) = -6U\frac{\partial h}{\partial x} + 12\frac{\partial h}{\partial t} \qquad \text{(A.13)}$$

where the x direction is axial direction. This relationship can be used to study lubrication conditions on one part of the ring.

A.2. Shear Stress and Volumetric Flow Rate of Oil

The same relationships given above in equations A.1 and A.2 are used to derive the shear stress and volumetric flow rate of the oil. The derivation given below is the 1-D case, based on Eq. A.13, for simplicity in demonstrating the concepts. However, the method of derivation is applicable to multi-dimensional cases.

Beginning again with Eqs. A.7, and the boundary conditions given in A.8, an expression for the axial velocity of lubricant flow is obtained:

$$u = \frac{1}{2\mu}\frac{\partial p}{\partial x} y(y-h) + \frac{Uy}{h} \tag{A.14}$$

It should be noted that it has been assumed, in this derivation, that the viscosity is does not change across the oil film thickness (in the y-direction). This may be valid in reality if the oil temperature is approximately constant across the film thickness, or if the oil is not shear-thinning. For shear-thinning oils, the shear rate will change across the film thickness, as will the oil viscosity. It has been shown by Tian[19], however, that even in the case of shear-thinning fluids, reasonably accurate results can be obtained by approximating the viscosity as that obtained with an average, nominal shear rate.

Shear stress is given by:

$$\tau(x) = \mu \left.\frac{\partial u}{\partial y}\right|_{y=0} \tag{A.15}$$

Then, using Eq. (A.14):

$$\tau(x) = \frac{\mu U}{h} - \frac{h}{2}\frac{dp}{dx} \tag{A.16}$$

The volumetric flow rate can also be derived using the above results:

$$Q(x) = \int_0^h u(y)dy \tag{A.17}$$

Using Eq. (A.14):

$$Q(x) = -\frac{h^3}{12\mu}\frac{dp}{dx} + \frac{Uh}{2} \tag{A.18}$$

(This page was intentionally left blank)

Appendix B: Complete flow factor results for surface analysis

Calculated flow factors for all parametric cases studied are given below. Pressure flow factor, shear flow factor, pressure stress factor and shear stress factor are shown. Geometric factors are not shown because they exhibit no change in the cases of the surfaces used in the parametric study. This is because the surfaces are assumed to be smooth except for the added features, so that contact will not occur and the nominal and mean surface separations will always be equal.

B.1 Grooves

Flow factors were obtained for several different groove geometries. The parameters studied were: groove angle, groove width, groove depth and area ratio. Also, cross-hatch patterned grooves were compared with single grooves (grooves parallel to each other, with no cross-over). Comparing cross-hatch and parallel grooves, with all other parameters equal, showed no effect from the pattern change. That is, the effect of the cross-hatch grooves on the flow factors appears to be exactly the same as the effect of the parallel grooves. Therefore only results from the parallel pattern of grooves is shown here, and the "groove angle" indicated is the cross-hatch angle, or twice the angle of the groove from the horizontal (see Figure 4-8).

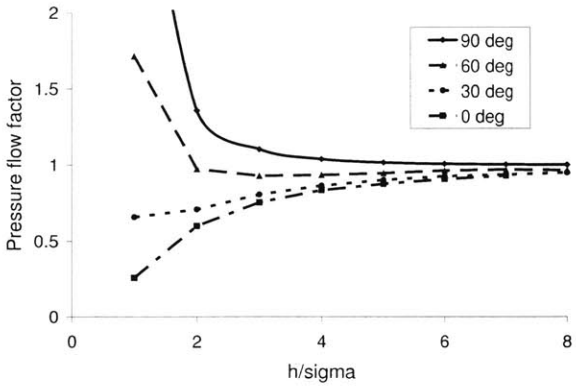

a) pressure flow factor

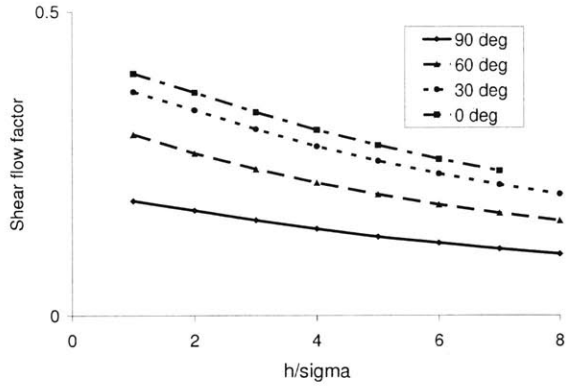

b) shear flow factor

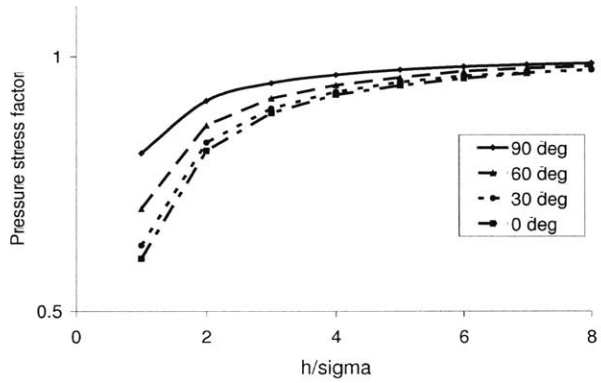

c) pressure stress factor

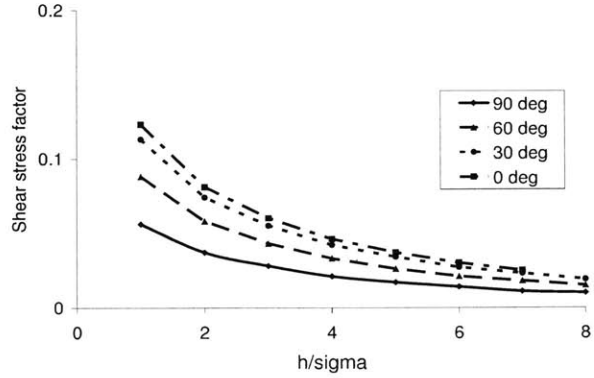

d) shear stress factor

Figure B-1: Flow and stress factors for changing groove angle, depth = 3 micron, width = 19 micron, area ratio=0.24.

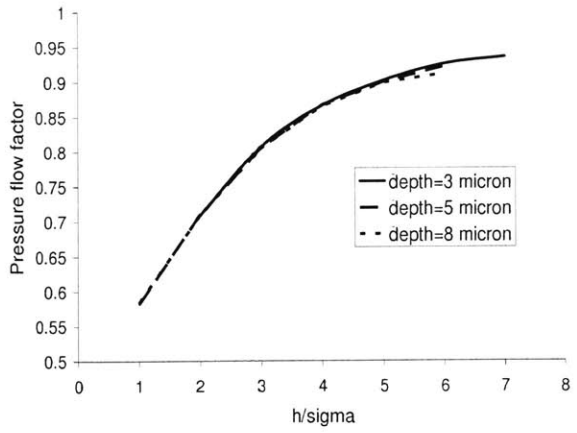

a) pressure flow factor

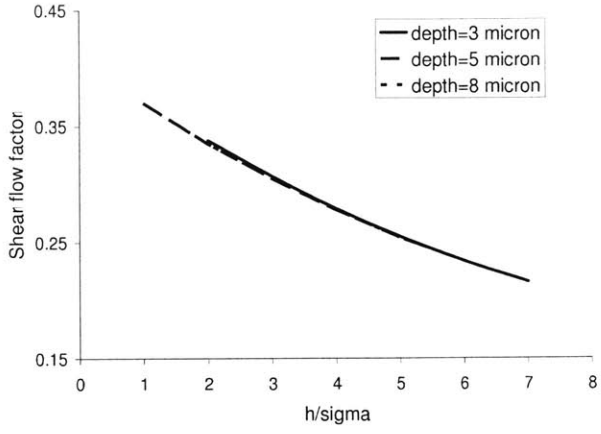

b) shear flow factor

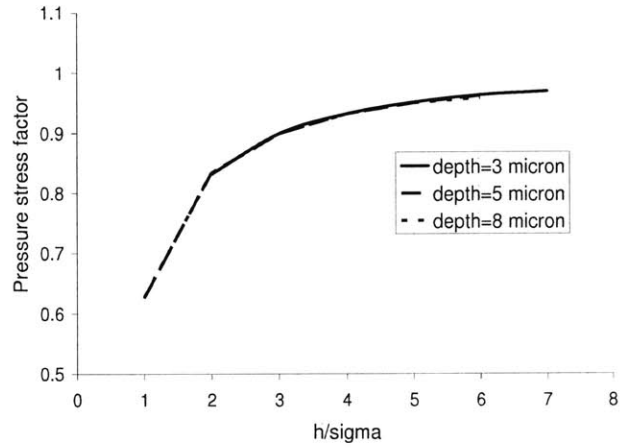

c) pressure stress factor

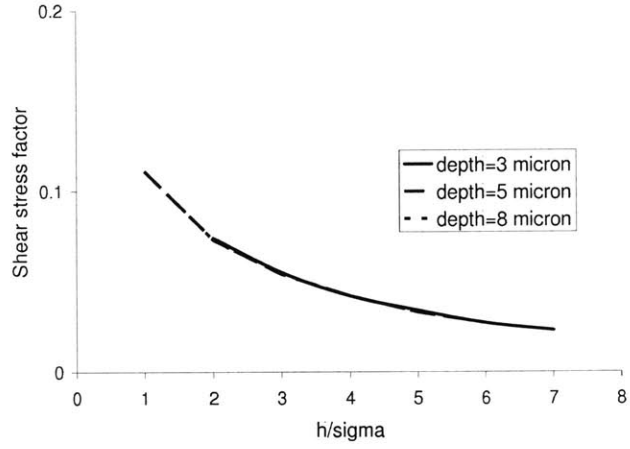

d) shear stress factor

Figure B-2: Flow and stress factors for changing groove depth, 15 deg. angle, width=19 micron, area ratio=0.24

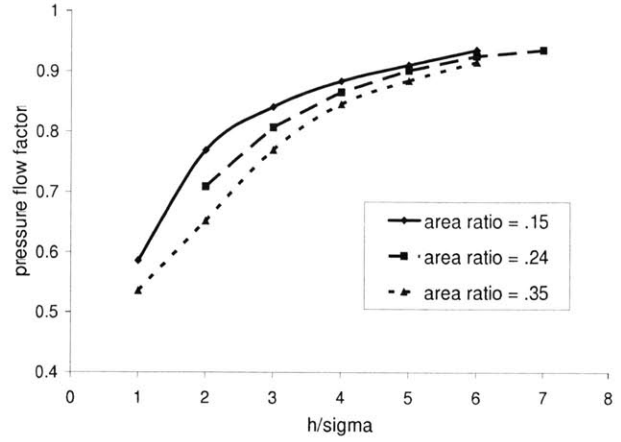

a) pressure flow factor

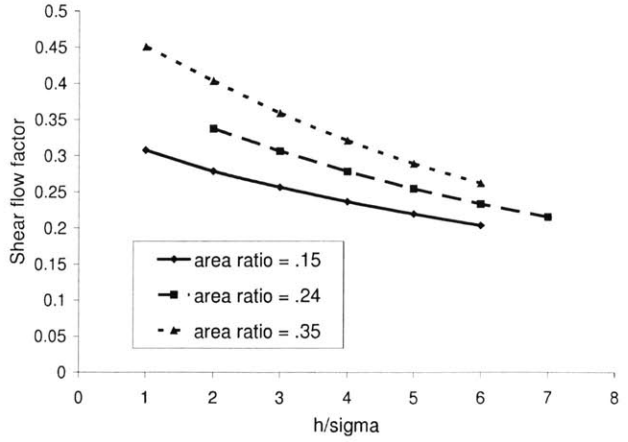

b) shear flow factor

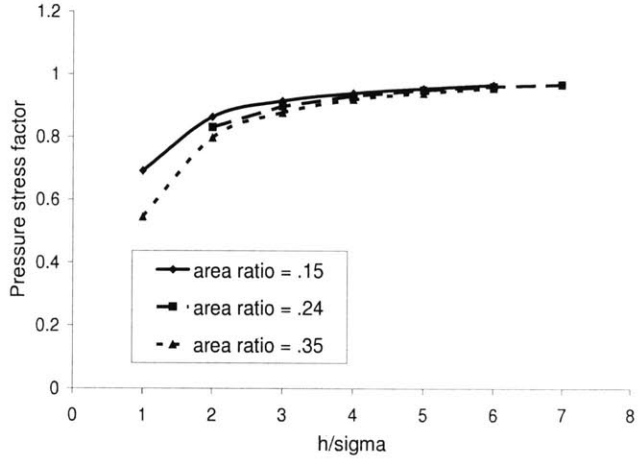

c) pressure stress factor

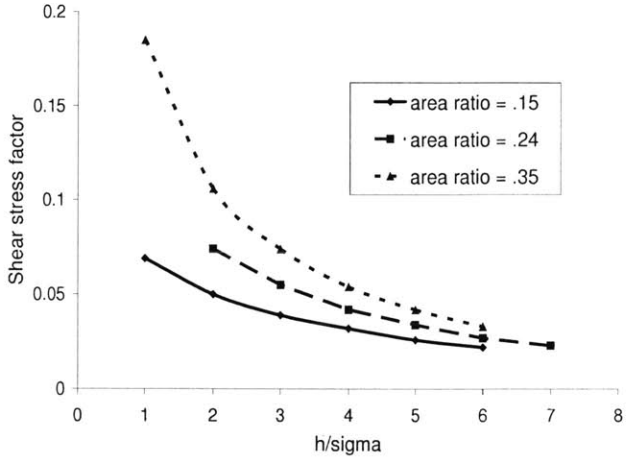

d) shear stress factor

Figure B-3: Flow and stress factors for changing groove area ratio, 15 deg. angle, width=19 micron, depth=3micron.

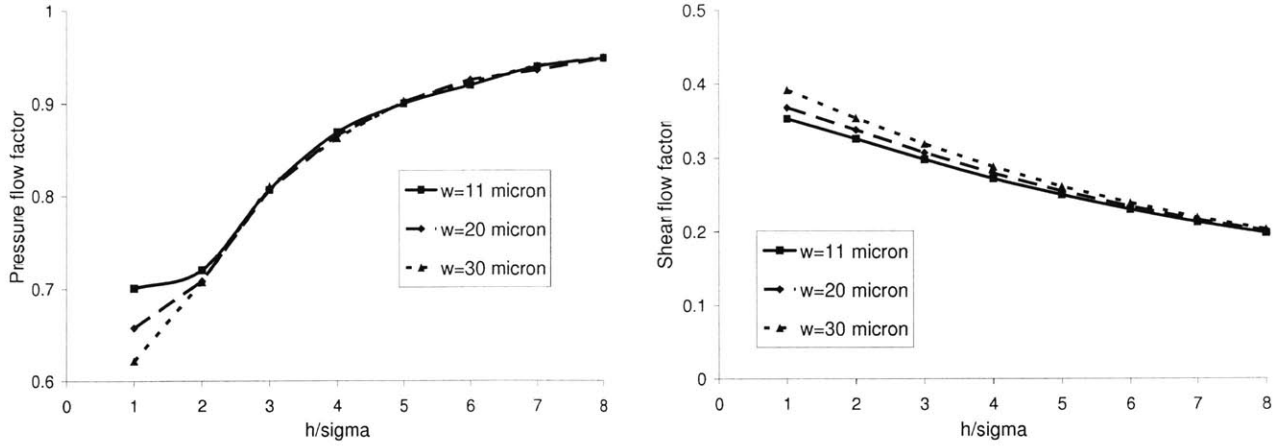

a) pressure flow factor

b) shear flow factor

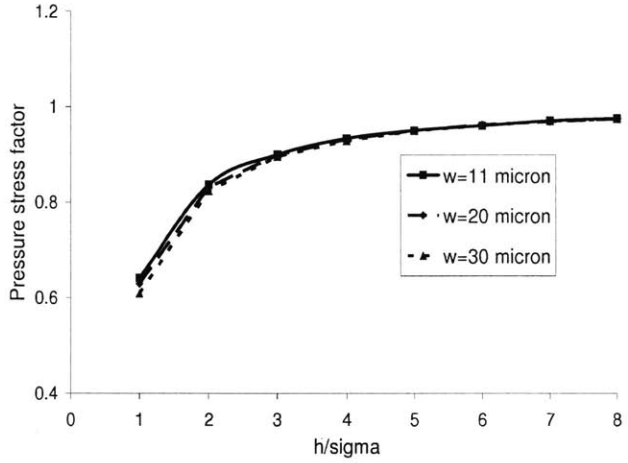

c) pressure stress factor

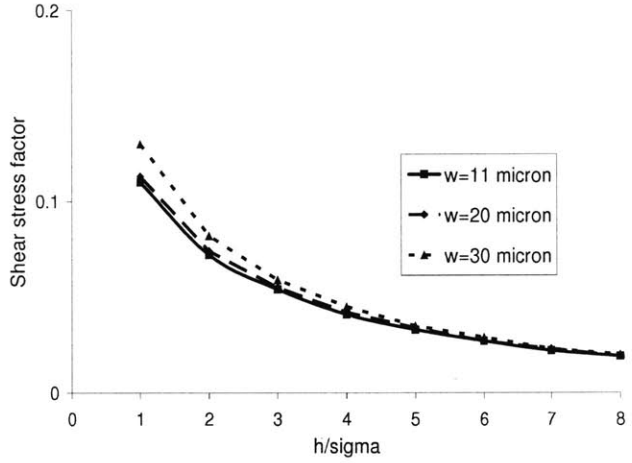

d) shear stress factor

Figure B-4: Flow and stress factors for changing groove width, 15 deg. angle, depth=3 micron, area ratio=0.24.

B.2 Dimples

Flow factors were also calculated for several different round dimple geometries. Parameters considered were dimple diameter, depth, and area ratio. A comparison of dimple patterns between a rectangular and hexagonal arrangement was also made, and no effect of changing the arrangement was seen on the factors. Therefore, only results for the hexagonal arrangement are shown, it can be assumed that results for a rectangular dimple arrangement would be the same as those given for a hexagonal arrangement with the same dimple depth, diameter and area ratio.

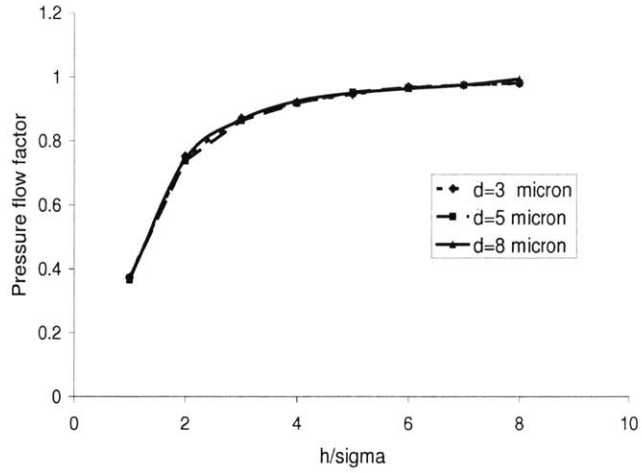

a) pressure flow factor

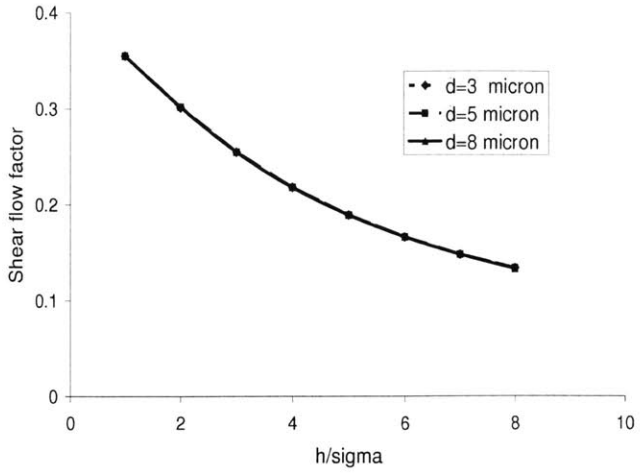

b) shear flow factor

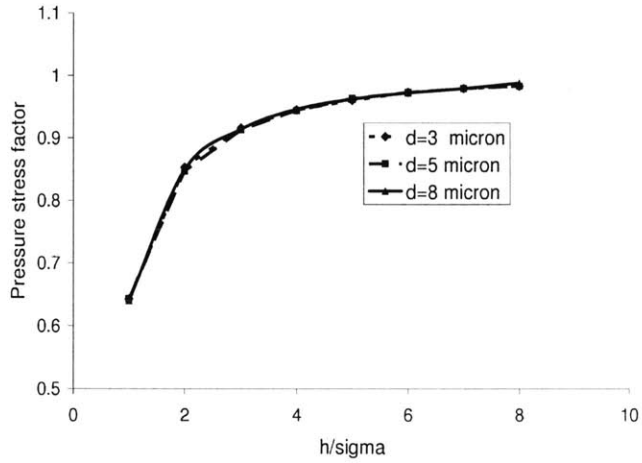

c) pressure stress factor

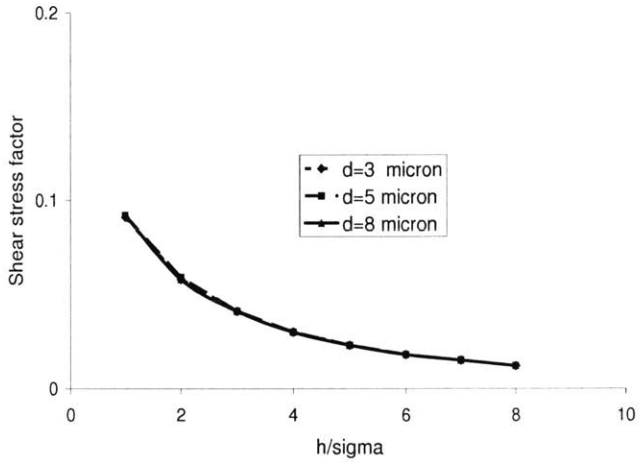

d) shear stress factor

Figure B-5: Flow and stress factors for changing dimple depth, diameter = 19 micron, area ratio=0.25

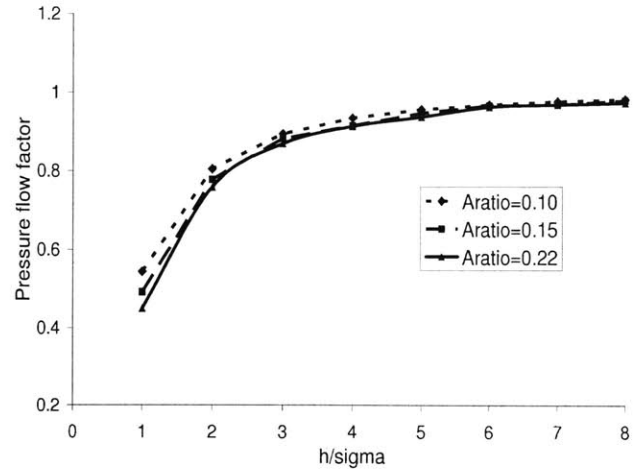

a) pressure flow factor

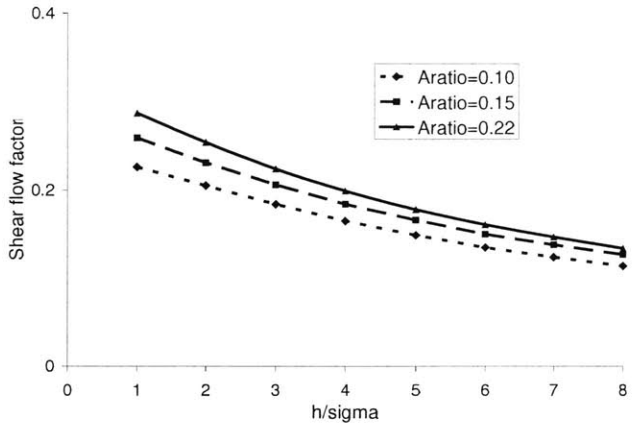

b) shear flow factor

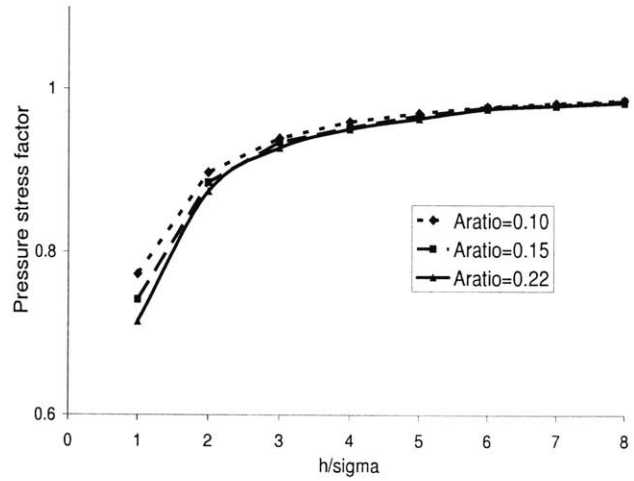

c) pressure stress factor

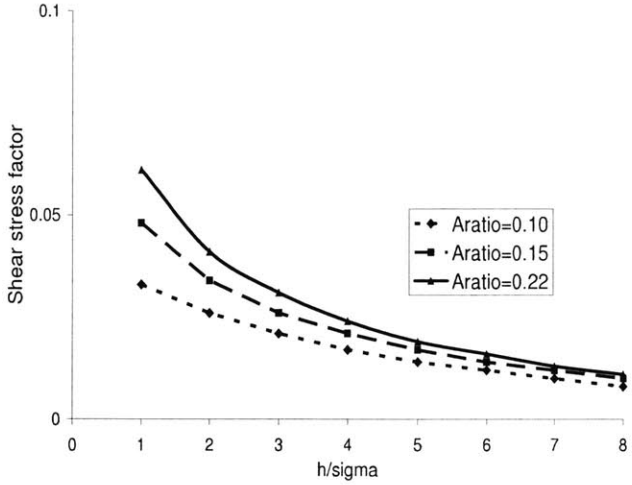

d) shear stress factor

Figure B-6 Flow and stress factors for changing dimple area ratio, diameter = 19 micron , depth=3micron.

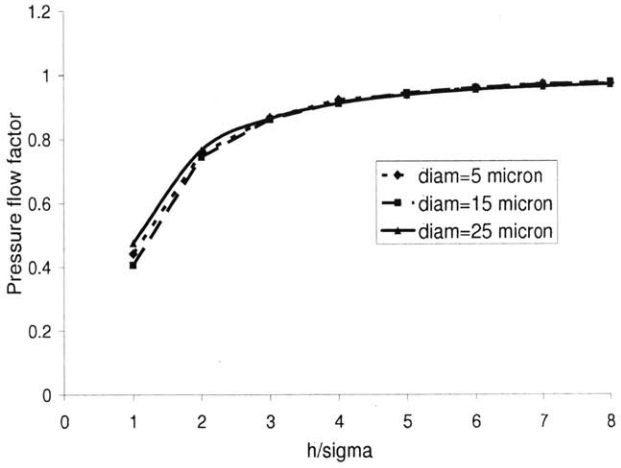

a) pressure flow factor

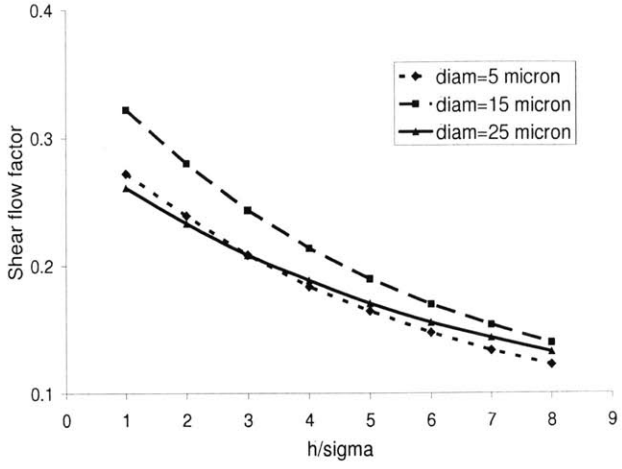

b) shear flow factor

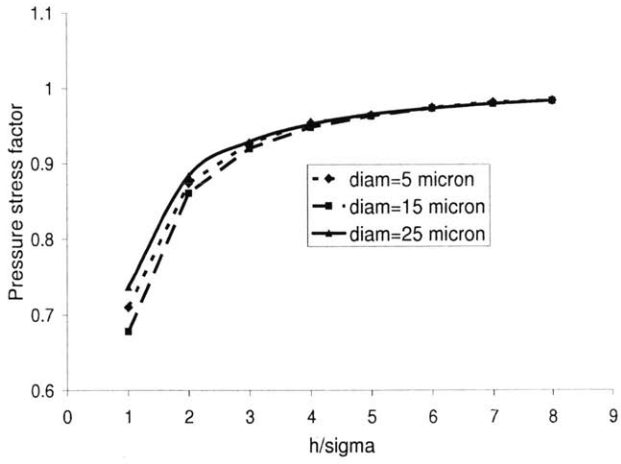

c) pressure stress factor

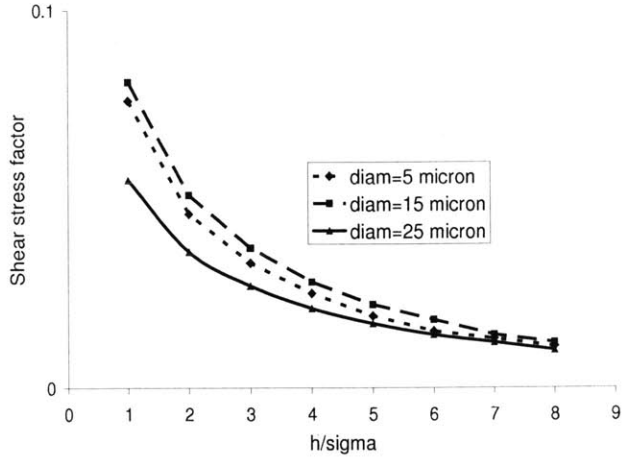

d) shear stress factor

Figure B-7: Flow and stress factors for changing dimple diameter, depth = 3 micron , area ratio=0.25